THE OHIO STATE UNIVERSITY

Three Dimensional Scattering Center Imaging Techniques

P.R. Younger and W.D. Burnside

The Ohio State University
ElectroScience Laboratory
Department of Electrical Engineering
Columbus, Ohio 43212

Technical Report 722780-2
Grant No. NAG 2-542, Supp. No. 2
March 1991

National Aeronautics and Space Administration
Ames Research Center
Moffett Field, CA 94035

and

Pacific Missile Test Center
Point Mugu, CA 93042

NOTICES

When Government drawings, specifications, or other data are used for any purpose other than in connection with a definitely related Government procurement operation, the United States Government thereby incurs no responsibility nor any obligation whatsoever, and the fact that the Government may have formulated, furnished, or in any way supplied the said drawings, specifications, or other data, is not to be regarded by implication or otherwise as in any manner licensing the holder or any other person or corporation, or conveying any rights or permission to manufacture, use, or sell any patented invention that may in any way be related thereto.

50272-101

REPORT DOCUMENTATION PAGE	1. REPORT NO.	2.	3. Recipient's Accession No.
4. Title and Subtitle Three Dimensional Scattering Center Imaging Techniques			5. Report Date March 1991 6.
7. Author(s) P.R. Younger and W.D. Burnside			8. Performing Org. Rept. No. 722780-2
9. Performing Organization Name and Address The Ohio State University ElectroScience Laboratory 1320 Kinnear Road Columbus, OH 43212			10. Project/Task/Work Unit No. 11. Contract(C) or Grant(G) No. (C) (G) NAG 2-542, Supp. No. 2
12. Sponsoring Organization Name and Address NASA Ames Research Center Moffett Field, CA 94035 Pacific Missile Test Center Point Mugu, CA 93042			13. Report Type/Period Covered Technical Report 14.

15. Supplementary Notes

16. Abstract (Limit: 200 words)

Two methods to image scattering centers in three dimensions are presented. The first method uses two dimensional images generated from ISAR measurements taken by two vertically offset antennas. This technique is shown to provide accurate three dimensional imaging capability which can be added to an existing ISAR measurement system, requiring only the addition of a second antenna. The second technique uses target impulse responses generated from wide-band radar measurements from three slightly offset antennas. This technique is shown to identify the dominant scattering centers on a target in nearly real time. The number of measurements required to image a target using this technique is very small relative to traditional imaging techniques.

17. Document Analysis a. Descriptors

IMAGING
SCATTERING
3-D
MEASUREMENT
SIGNAL PROCESSING
ELECTROMAGNETIC

b. Identifiers/Open-Ended Terms

c. COSATI Field/Group

18. Availability Statement	19. Security Class (This Report)	21. No. of Pages
A. Approved for public release; Distribution is unlimited.	Unclassified	143
	20. Security Class (This Page) Unclassified	22. Price

(See ANSI-Z39.18) *See Instructions on Reverse* OPTIONAL FORM 272 (4-77)
Department of Commerce

Contents

List of Figures

Chapter 1

Introduction

If a target is illuminated by a plane wave whose wavelength is small relative to the size of the target, the target's electromagnetic scattering can be considered to originate from distinct features called scattering centers. The object of this research is to locate these scattering centers in three dimensions using swept frequency backscatter measurements resulting from plane wave illumination. Two methods will be presented to accomplish this task. The first method uses the impulse responses of the target as seen from three slightly different look angles. The second method uses images generated from inverse synthetic aperture radar (ISAR) measurements taken by two vertically offset antennas.

For purposes of target identification and radar cross section (RCS) analysis, it is advantageous to know the locations of the scattering centers associated with a target under test. Traditional imaging techniques are used to determine the down range and cross range positions as well as the relative magnitudes of the scattering centers composing a target. A technique is presented in this report which expands the capability of the traditional two dimensional imaging techniques to three dimensions. This is accomplished by generating images from backscatter measurements of a target taken from two slightly different angles of illumination in the vertical plane. The di-

rection of propagation corresponding to these two look angles are the same except for a small difference in their vertical displacements. The images from these two look angles should be identical except that the images of the individual scattering centers will be slightly shifted along the down range direction by an amount proportional to their vertical offset. By calculating the down range offset for a particular scattering center, its position can be determined in all three dimensions.

Despite the effectiveness of traditional imaging techniques in locating scattering centers, a drawback inherent in them is the large amount of time required to obtain the measurements necessary to generate an image. A technique is presented in Chapter 5 which identifies the major scattering centers of a target in three dimensions and does it in nearly real time. If one takes backscatter measurements of a target over a wide frequency bandwidth, the target's impulse response along the direction of propagation can be obtained by performing an inverse Fourier transform on the frequency domain measurements. If a scattering center on the target is separated sufficiently from other mechanisms along the direction of propagation, its down range position can be determined accurately. If a scattering center's position is determined for three different directions of propagation, which are not coplanar, its three dimensional position can be determined by simple triangulation. This technique is shown to work well for point scatterers with sufficient down range separation. A problem encountered when applying this technique though, is that a scattering center on a target may experience interference from other scattering mechanisms on the target, making it difficult to determine the scattering center's exact down range position. A method is proposed which solves this problem by analyzing images from several different look angles. By doing this a scattering center can be tracked through a range of look angles and identified even when it

suffers from interference.

This report is organized as follows: Chapter 2 includes the assumptions made about a target's scattering characteristics as well as a review of its impulse response. A review of the techniques used to generate traditional images is found in Chapter 3. Chapter 4 describes the method used to generate the necessary offset plane waves in the OSU compact range. A presentation of the imaging technique using impulse responses is given in Chapter 5. Chapter 6 contains a description of the method used to determine the three dimensional positions of scattering centers from two dimensional images. Finally, the results of applying these two imaging techniques to a complex real-world target are given in Chapter 7.

Chapter 2

One Dimensional Target Images

2.1 Scattering Center Location in Three Dimensions

When an object is illuminated by an electromagnetic wave, currents are induced on the structure which reradiate and produce scattered fields. The induced currents are not uniform, and if the object is electrically large, the scattering tends to be concentrated at distinct locations, which are referred to as scattering centers. In fact, the total scattered field from an electrically large radar target can, in most cases, be approximated by a linear superposition of these scattering center responses.

For purposes of target identification and radar cross section analysis, it is advantageous to know the locations of the scattering centers associated with a target under test. In this paper, a method is proposed to identify these scattering center locations using swept frequency backscatter measurements of a target, resulting from plane wave illumination. The method is conceptually very simple and is presented here in terms of an example. First, assume that a scattering center is placed in a fixed coordinate system as shown in Figure 1. Next, place a radar at a distance of R_r from the ori-

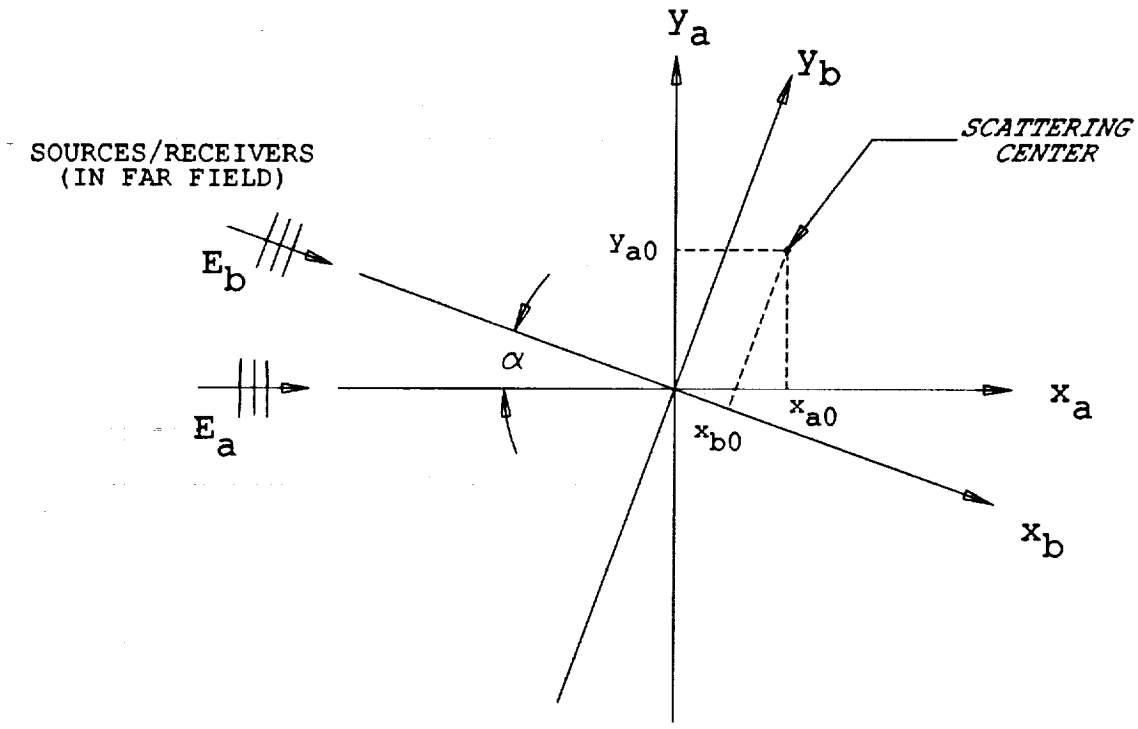

Figure 1: Determination of cross range position from down range measurements.

gin of the coordinate system and illuminate the target zone with the radar. Note that R_r is considered to be large enough so that far field assumptions can be made. The down range distance of the scattering center, R_0, is the distance from the radar to the projection of the scattering center's position onto the down range axis of the radar. The down range distance of the scattering center can be determined from swept frequency radar measurements. The distance R_0 is measured with respect to the radar. It will be convenient for later sections of this report to move the phase center to the origin of the fixed coordinate system. Upon moving the phase center to the origin, the down range position of the scattering center is x_{a0}, where it is understood that $R_0 = R_r + x_{a0}$. To obtain the information needed to calculate the cross range position y_{a0}, the radar is then moved to a second position which is equidistant from the origin, but rotated by an angle α with respect to the first look angle. A second measurement is then taken to determine x_{b0}, the distance from the radar to the scattering center, at the second look angle. Once x_{b0} is determined, it is a simple matter to calculate the cross range position from the following formula:

$$y_{a0} = \frac{x_{b0} - x_{a0}\cos\alpha}{\sin\alpha}. \tag{2.1}$$

For small α, Equation (2.1) becomes

$$y_{a0} = \frac{x_{b0} - x_{a0}}{\alpha} \tag{2.2}$$

where

y_{a0} = cross range position with respect to antenna A

x_{a0} = down range position with respect to antenna A

x_{b0} = down range position with respect to antenna B, and

α = separation between plane waves in azimuth angle.

This result is used to determine the location of the scattering center in the $x - y$ plane. To obtain its third dimension, the vertical offset, this process can be repeated using a plane wave with a small vertical propagation component. With this approach, the initial measurement is taken using the desired plane wave illumination. The second measurement is taken by rotating the plane wave a small angle in the horizontal direction. A third measurement is then taken by scanning the plane wave a small angle in the vertical direction. From these measurements, the scattering center is located in all three dimensions.

In a realistic application where many scattering centers are encountered in close proximity to one another, locating the scattering centers is a much more difficult task. The two problems which impede identification and location of scattering centers are

1. the complexity and composition of the target, and

2. the limitations of the measurement system.

Section 2.2 presents the assumptions made about the target and how the target is characterized. Section 2.3 shows the method for determining the distance from the radar to the scattering centers and the effects of system limitations on this determination.

2.2 Target Scattering Characterization

The identification scheme to be presented later in this report, requires two assumptions about the target. First, it assumes that the target is electrically large, and second, it assumes that the target is composed of a finite set of point scatterers. If one assumes that a target is electrically large, it can be treated, in most cases, as a linear superposition of scattering center responses. The backscatter behavior of each of the scattering center

responses is dependent on the frequency of the incident wave and the position of the radar with respect to the target. The total scattering from a target composed of N such mechanisms, at a given frequency of illumination and look angle, can be defined as

$$E^s(\omega,\theta,\phi) = \sum_{n=1}^{N} E_n^s(\omega,\theta,\phi) \tag{2.3}$$

where

E^s = the total scattered field

E_n^s = the complex scattered field of the n^{th} scattering center including the relative phase due to propagation

ω = angular frequency in radians

θ = elevation angle, and

ϕ = azimuth angle.

Obviously, E^s and E_n^s are dependent on the illumination direction (θ,ϕ) of the target. In this paper, the scattered fields will often be discussed for an arbitrary look angle. However for convenience of notation, the dependence of the target scattering on the look angle will be implicit, except where the explicit referencing of θ and ϕ is required.

The second assumption made about the target is that each of the scattering centers can be represented as point scatterers. In defining point scatterers, it is first assumed that they are line-of-sight scatterers. The term "line-of-sight" implies that the signal path is a direct path from the radar to the point scatterer and back again. On many realistic targets the first order terms are basically line-of-sight, but the higher-order ones, such as multiple reflections, creeping waves, or edge waves, are not. By assuming a direct path from the radar to the target and back, some scattering mechanisms may be incorrectly located. This problem is acceptable because

the consideration of multiple path scattering would introduce ambiguities which cannot currently be evaluated.

The assumption made above also dictates that a point scatterer's phase is a linear function of its distance from the phase center. The frequency response of such a point scatterer, as seen by the radar, is

$$E_n^s(\omega) = A_n(\omega)e^{j\psi_n}e^{-j\omega T_n} \tag{2.4}$$

where

$$A_n(\omega) = A_n(-\omega).$$

$A_n(\omega)$ is a positive real function and is the amplitude of the backscatter signal of the target which is dependent on frequency. Note that $e^{j\psi_n}$ represents any phase shift introduced by the individual target scattering mechanisms. The time required for the radar signal to propagate from the radar to the n^{th} scattering center of the target and back is denoted as T_n. If the distance from the radar to the point scatterer is R_n, then one obtains

$$T_n = \frac{2R_n}{c}. \tag{2.5}$$

Again, for convenience, the phase center is moved from the radar to the origin. If the down range distance of the scattering center is $R_n = R_c + x_n$, the point scatterer's frequency response is written as

$$E_n^s(\omega) = A_n(\omega)e^{j\psi_n}e^{-j\omega t_n} \tag{2.6}$$

where

$$t_n = \frac{2x_n}{c}. \tag{2.7}$$

Therefore, by substituting (2.6) into (2.3), one finds that

$$E^s(\omega) = \sum_{n=1}^{N} A_n(\omega)e^{j\psi_n}e^{-j\omega t_n} \tag{2.8}$$

which represents the complete target scattering characterization as assumed in this report.

2.3 Scattering Center Down Range Position Determination

A scattering center's position in three dimensions can be determined by knowing its down range position with respect to three offset plane waves. This section reviews the method by which the down range distance x_n is determined from measured data and the impact of measurement limitations on the accuracy of x_n. To determine the down range positions of each scattering center, the impulse response of the target is needed. Note that the impulse response and the frequency response of a target form a Fourier transform pair. If the target is composed of linear scattering centers, the transform pair is

$$E^s(\omega) = \int_{-\infty}^{\infty} e^s(t) \cdot e^{-\jmath\omega t} dt \tag{2.9}$$

and

$$e^s(t) = \frac{1}{2\pi} \int_{-\infty}^{\infty} E^s(\omega) \cdot e^{\jmath\omega t} d\omega \tag{2.10}$$

where the impulse response is $e^s(t)$ [4].

The impulse response is by definition causal, and therefore its frequency spectrum is infinite in extent. Clearly, no radar system has the capacity to represent $E^s(\omega)$ completely. The measured data used in this paper consists of backscatter measurements of a target taken from 2-18 GHz at 10 MHz steps. This information yields a discretely sampled version of the frequency response of the target given in Equation (2.3).

The scattering mechanisms treated in this paper have impulse responses which are exclusively real. For a real impulse response $e_n^s(t)$, its frequency response must satisfy the following:

$$E_n^s(\omega) = [E_n^s(-\omega)]^*. \tag{2.11}$$

If E_n^s is measured over a limited bandwidth, the resultant frequency response can be represented as

$$E_{nb}^s(\omega) = A_{nb}(\omega)e^{\jmath\psi_n}e^{-\jmath\omega t_n} \tag{2.12}$$

where

$$A_{nb}(\omega) = \begin{cases} A_n(\omega) & \omega_0 - \omega_b \leq \mid \omega \mid \leq \omega_0 + \omega_b, \text{ and} \\ 0 & \text{elsewhere.} \end{cases} \tag{2.13}$$

In general, the amplitude term of the positive spectrum of $E_{nb}^s(\omega)$ from $\omega_0 - \omega_b$ to $\omega_0 + \omega_b$, is not symmetric about its mid-frequency ω_0. The same is true for the negative spectrum. In [11], it is shown that such a spectrum yields an impulse response which is both phase and amplitude modulated, such that

$$a_{nb}(t) = 2\sqrt{a_{np}^2(t) + a_{nq}^2(t)}\cos\left(\omega_0(t) - \tan^{-1}\frac{a_{nq}(t)}{a_{np}(t)}\right) \tag{2.14}$$

which yields an impulse response for the scattering center given by

$$e_{nb}^s(t) = 2\sqrt{a_{np}^2(t - t_n) + a_{nq}^2(t - t_n)}\cos\left(\omega_0(t - t_n) - tan^{-1}\frac{a_{nq}(t - t_n)}{a_{np}(t - t_n)}\right). \tag{2.15}$$

Note that a_{np} and a_{nq} are the in phase and quadrature components, respectively, of $a_{nb}(t)$ as defined in [11]. The amplitude modulated term of (2.15) is given by

$$e_{nenv}^s(t) = \sqrt{a_{np}^2(t - t_n) + a_{nq}^2(t - t_n)} \tag{2.16}$$

The maximum of this term occurs at $t = t_n$, the down range location of the scattering center. The scattering center's position can therefore be

determined by locating the peak of this amplitude modulated term. In this paper, the amplitude modulated term of a target is referred to as its envelope.

2.4 Band Limited Discretely Sampled Spectra

Since the down range positions of the scattering centers are determined from the envelope of the impulse response of the target, it is now necessary to study the impact of limited bandwidth on the envelope. To illustrate the effect of limited bandwidth, return to the band limited frequency response of a point scatterer in (2.12). One can reformulate its response as the product of an ideal band pass filter and the original point scatterer frequency response of (2.4) such that

$$E_b^s(\omega) = W(\omega) \cdot E^s(\omega) \tag{2.17}$$

where

$$W(\omega) = \begin{cases} 1 & \omega_0 - \omega_b \leq \mid \omega \mid \leq \omega_0 + \omega_b, \text{ and} \\ 0 & \text{elsewhere} \end{cases} \tag{2.18}$$

or

$$W(\omega) = \mathcal{F}[w(t)].$$

Multiplication in the frequency domain transforms to a convolution in the time domain such that

$$e_b^s(t) = \int_{-\infty}^{\infty} e^s(\tau) w(t-\tau) d\tau. \tag{2.19}$$

Since the impulse response of a target is the superposition of the impulse responses from the individual scattering centers, the band limited response of a target composed of N scattering centers is

$$e_b^s(t) = \sum_{n=1}^{N} \int_{-\infty}^{\infty} e_n^s(\tau - t_n) w(t - \tau) d\tau. \tag{2.20}$$

The band limited impulse response is therefore a sum of convolutions: the convolutions of the impulse responses of the individual scattering centers with the impulse response of the band pass filter. The result of the convolutions is a distorted version of the actual impulse response. The distortions introduced are dependent on the impulse response of the ideal band pass filter which can be expressed as

$$w(t) = \frac{\omega_b}{\pi} \text{sinc}(\omega_b t) \cos(\omega_0 t). \tag{2.21}$$

This function and its envelope are pictured in Figure 2 for a bandwidth of 2-18 GHz. Note the high side lobes and ringing which are due to Gibb's phenomenon. The high side lobe levels cause two problems which are detrimental to identifying scattering centers. Every peak in the envelope of the impulse response of the target is considered to correspond to a scattering center. The high side lobe levels of Figure 2 limit the dynamic range of peaks which can be identified as scattering centers. The first side lobes of the envelope for the ideal band pass filter are only 13 dB down from the peak of the main beam. This implies that peaks whose magnitudes are more than 13 db down from the largest peak in a target's envelope might have to be discarded since actual scattering centers at these levels could not be distinguished from side lobes of adjacent scattering centers.

A second problem which high side lobe levels cause is distortion of the estimated down range positions of scattering centers. The position of the maximum of a peak is assumed to correspond to the down range position of a scattering center. To obtain an accurate estimate of a scattering center's cross range position, its down range position must be estimated very

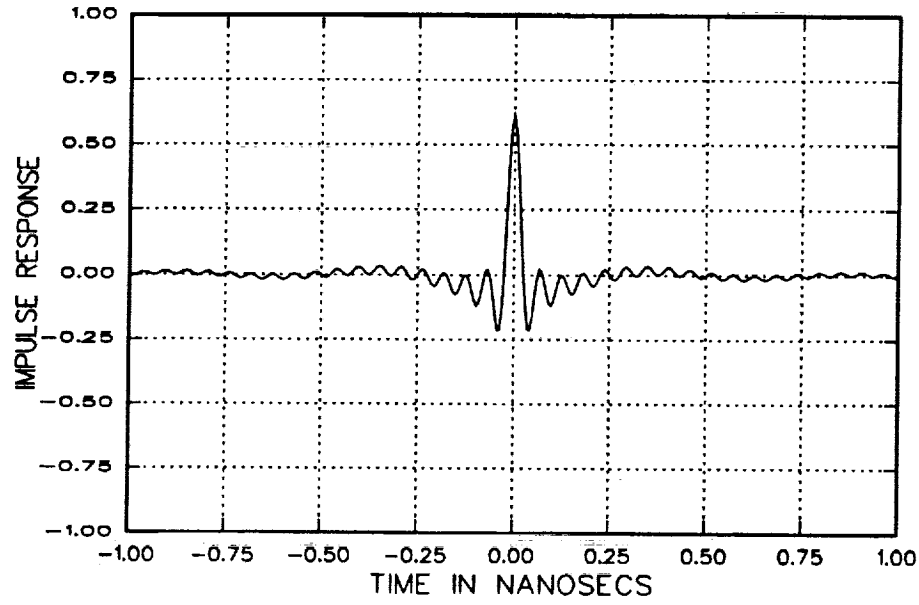

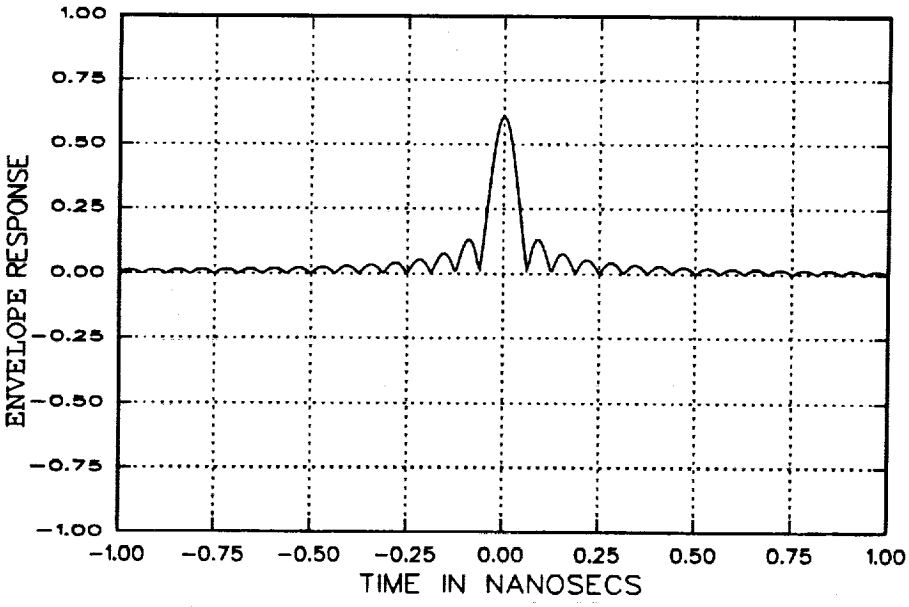

Figure 2: Impulse response and envelope for an ideal band pass filter.

accurately. For the case where two scattering centers are located in close proximity, the presence of high side lobe levels can cause a shift in the positions of the peaks in the envelope response relative to the actual down range positions of the scattering centers. This shift in down range position can result in significant errors in the estimated cross range position of a scattering center.

In order to reduce the impact of these problems, the classical approach of windowing in the frequency domain is taken. Windowing is the process of altering the frequency dependence of $W(\omega)$ in Equation (2.17) so that the function $w(t)$ has the desired properties for a particular application. Harris discusses this topic thoroughly in [9]. Windowing is used to decrease the impact of the discontinuities of a band limited spectrum. The window used in this work was chosen such that it had relatively low side lobe levels without making its main lobe so wide that the impulse response lost its physical significance. The Kaiser-Bessel window was chosen as a reasonable compromise. The Kaiser-Bessel window used in this paper has the form

$$W(\omega) = \frac{I_0\left[\pi\alpha\sqrt{1-\left(\frac{\omega-\omega_0}{\omega_b}\right)^2}\right]}{I_0[\pi\alpha]} \tag{2.22}$$

where I_0 is the modified Bessel function of the first kind, order zero, with $\alpha = 2$.

Figure 3 shows the envelope response of the rectangular and Kaiser-Bessel windows for a uniform signal from 2-18 GHz. Note that the first side lobe of the envelope resulting from a K-B windowed spectrum is 46 dB down from its peak. Also recognize that the main lobe of the K-B transfer function is much wider. The drawback of having a wider main lobe is that the distance of separation required between scattering centers to resolve them increases. Resolution, as it is traditionally defined, is not applicable

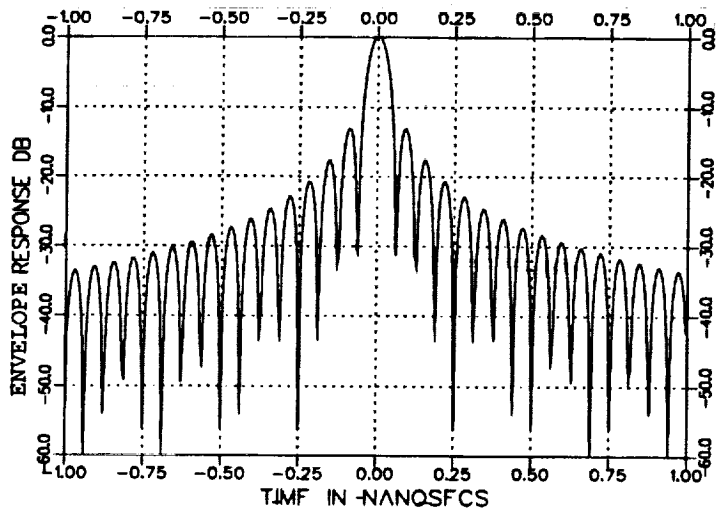

a) Rectangular window

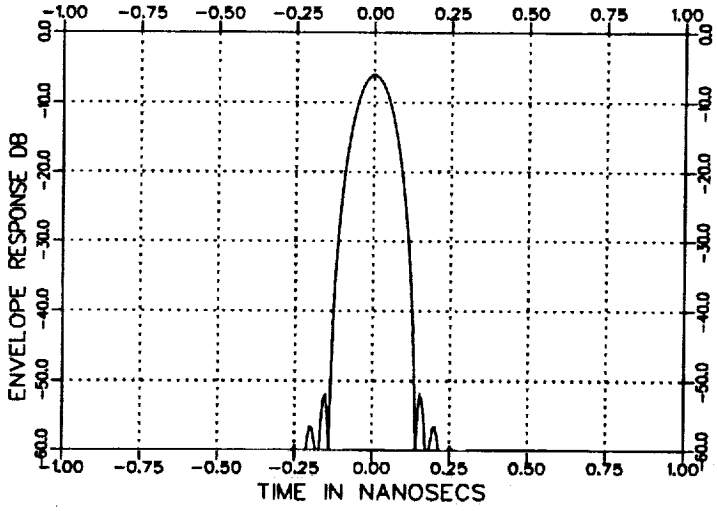

b) Kaiser-Bessel window

Figure 3: Envelopes for various windows

to the problem presented above and will be discussed in Chapter 5 of this report.

The measurements taken for this work, as well as being band limited, are discretely sampled in frequency. Shannon's sampling theorem states that given a function $f(t)$ where

$$f(t) = 0 \qquad \text{for } \mid t \mid > T \tag{2.23}$$

its Fourier transform $F(\omega)$ can be uniquely determined from its values $F(\frac{\pi n}{T})$ at a sequence of equidistant points, a distance $\frac{\pi}{T}$ apart [11]. To illustrate this theorem, consider the time limited function $f(t)$ and its transform $F(\omega)$ as shown in Figure 4. $F(\omega)$ is sampled at regular intervals in ω such that the sampled version of $F(\omega)$ is given by

$$F_s(\omega) = \sum_{n=-\infty}^{\infty} F(n2\pi\Delta f). \tag{2.24}$$

This function can also be represented as the product of $F(\omega)$ and a periodic train of impulses. The sampled version of $F(\omega)$ can be expressed as

$$F_s(\omega) = F(\omega) \cdot S(\omega) \tag{2.25}$$

where

$$S(\omega) = \sum_{n=-\infty}^{n=\infty} \delta(\omega - n2\pi\Delta f). \tag{2.26}$$

Since multiplication in the frequency domain transforms to convolution in the time domain, the inverse Fourier transform of $F_s(\omega)$ is

$$f_s(t) = f(t) \otimes s(t) \tag{2.27}$$

where

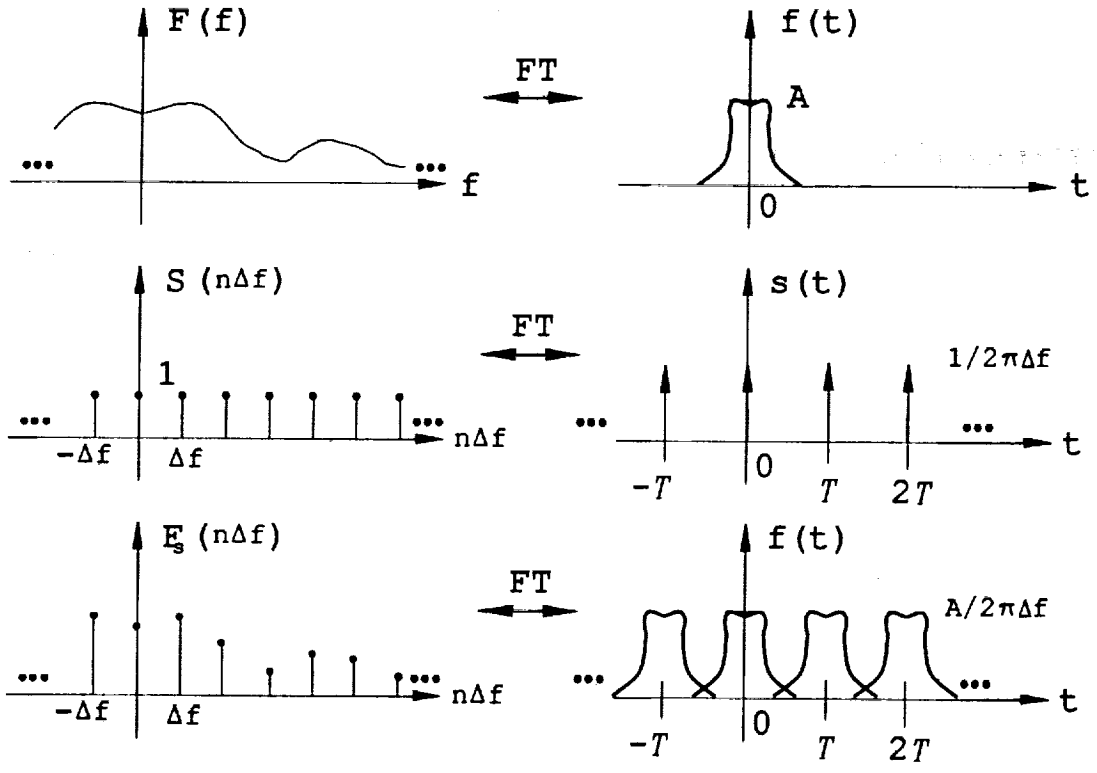

Figure 4: Impulse response of a discretely sampled spectrum.

$$s(t) = \frac{1}{2\pi\Delta f} \sum_{n=-\infty}^{\infty} \delta(t - \frac{n}{\Delta f}). \tag{2.28}$$

The convolution of $s(t)$ and $f(t)$ is a superposition of scaled versions of $f(t)$ shifted in time as shown in Figure 4. Sampling in frequency therefore implies periodicity in time. Figure 4 illustrates Shannon's sampling theorem. If Δf is not chosen such that

$$f(t) = 0 \qquad \text{for } \mid t \mid > \frac{1}{\Delta f} \tag{2.29}$$

then the problem of aliasing is encountered. Aliasing is the overlapping of periodic versions of $f(t)$.

When dealing with a target of maximum dimension, D, the time that it takes a radar impulse to travel the length of the aircraft and back is $\frac{2D}{c}$, where c is the velocity of light. This value can be considered to be the minimum extent of the signal if a target's scattering centers are point targets. The maximum frequency sampling step for such a target is

$$\Delta f \leq \frac{c}{2D} \tag{2.30}$$

where c is the speed of light and the factor of 2 accounts for the two way trip from the radar to the scattering center and back. When dealing with a realistic target one often encounters higher order mechanisms which appear beyond the physical body of the target, as well as clutter from the radar range. An additional factor of k is introduced to accomodate these additional sources of scattering [10]; thus, one finds that

$$\Delta f \leq \frac{c}{2(1+k)D}. \tag{2.31}$$

In this work, Δf is chosen to be 10 MHz, which means that the frequency response function for an 8 foot target is highly oversampled.

Chapter 3

Two Dimensional Target Images

At the beginning of the last chapter, a method was presented to identify the position of a scattering center in three dimensions. The method uses the envelope of the impulse response of the scattering center from three different look angles. A second approach is presented in this chapter which also determines the positions of scattering centers in three dimensions; however, it uses two dimensional images of the target produced from ISAR measurements taken by two antennas which are offset vertically. The two dimensional images are created using Computerized Axial Tomography (CAT). A CAT image is a two dimensional function of reflectivity. In the case presented in this report, the two dimensions are defined by the down range and cross range relative to the radar look angles. These images are widely used as tools for RCS analysis of targets and for identifying the positions of scattering centers on a target. A review of the mathematics of CAT follows. Also discussed are the aspects of the image which are most important to identifying the scattering centers in three dimensions, and the distortions introduced into the images due to the limitations of the measuring system.

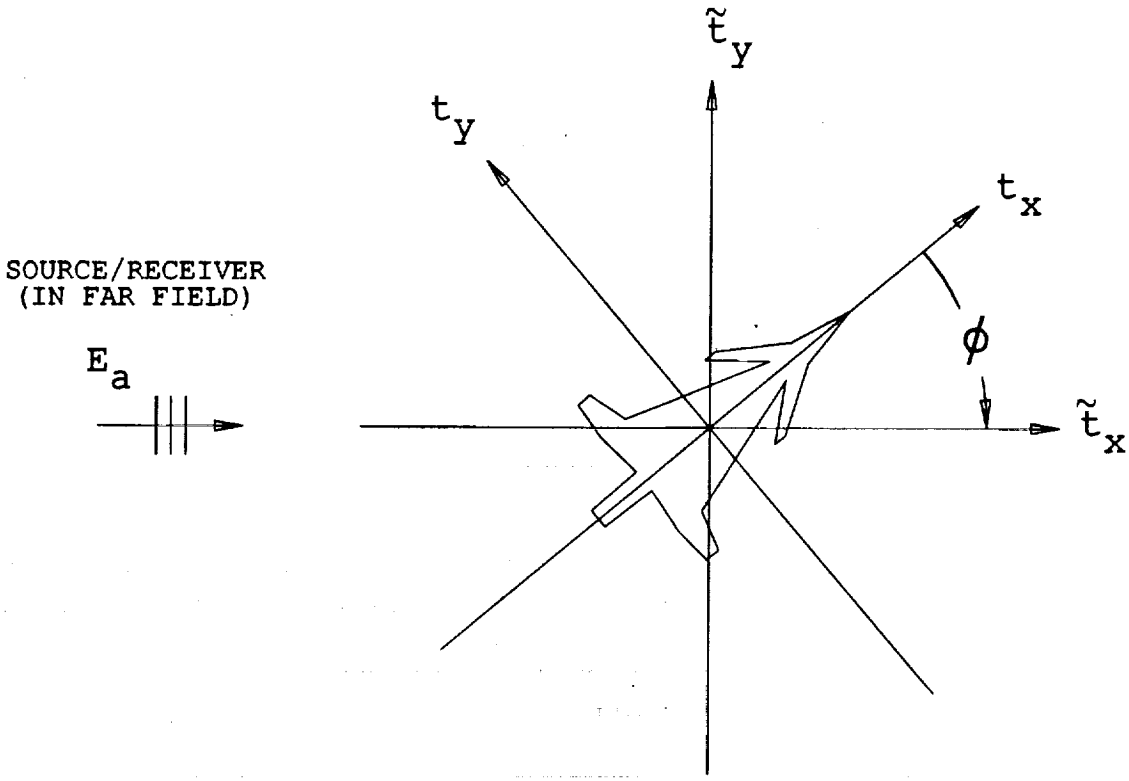

Figure 5: CAT imaging geometry.

3.1 Image Construction

CAT was introduced by EMI Ltd. of England in 1973 as a way of imaging cross sections of the human body in two dimensions. Although our application is different, the mathematics used to derive the image are the same. Articles on CAT are available in [5],[6],[7], and [12]. The mathematics of CAT are used in this report to establish the relationship between swept frequency measurements of a target taken at consecutive look angles and its reflectivity density function [12].

The measurements used to produce the CAT images in this report are swept frequency ISAR measurements. The imaging geometry used to obtain these measurements is shown in Figure 5. The target is located on a

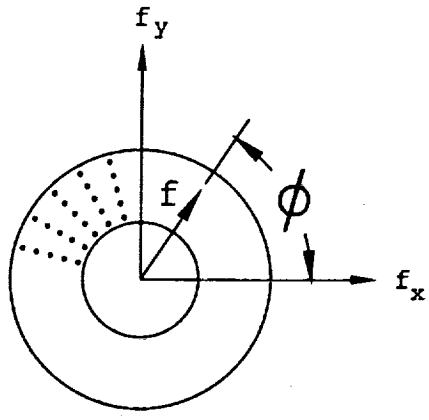

Figure 6: Polar sampling format.

platform which rotates about the origin of the coordinate system fixed to the radar. The down range direction of the radar corresponds to the $\tilde{t}_x$ axis of this system. Thus, $\tilde{t}_x$ represents the two way trip time to the scattering center and back. The backscattered field is measured by a stationary radar in the far field. At a look angle ϕ, measurements are taken of the target across the system bandwidth at discrete intervals. These measurements produce a sampled version of $E^s(f, \theta_0, \phi)$, where θ_0 is a fixed angle. For notational convenience, it is assumed that $\theta_0 = \frac{\pi}{2}$, so that the (x, y) plane of the target corresponds to the (t_x, t_y) plane of the radar. The target is then rotated by $\Delta\phi$ and measurements are taken again, yielding a second version of the transfer function $E^s(f, \theta_0, \phi + \Delta\phi)$. This process is repeated until a total angle of 2ψ has been swept.

To visualize the two dimensional space defined by f and ϕ, refer to the polar coordinate system of Figure 6. The coordinate f corresponds to the radial component, and ϕ corresponds to the angular one. The amplitude and phase of the backscattered field at a particular f_m and ϕ_n correspond to a discrete sample of $E^s(f, \theta_0, \phi)$. For notational convenience, a two dimensional complex function Λ is defined as $\Lambda(f, \phi) = E^s(f, \theta_0, \phi)$ for

$\theta_0 = \frac{\pi}{2}$. From $\Lambda(f, \phi)$, one can obtain the reflectivity density function $\mu_a(t_x, t_y)$.

The reflectivity density function of a target is its spatial distribution of reflectivity [12]. It can be expressed as the real function $\mu(t_x, t_y, t_z)$. At the beginning of the previous chapter, it was stated that the backscatter from an electrically large target can be considered to originate from distinct features on the target called scattering centers. The reflectivity of the scattering centers and their locations determine $\mu(t_x, t_y, t_z)$ for a target. The reflectivity function which CAT produces, $\mu_a(t_x, t_y)$, is a two dimensional function. In this work, $\mu_a(t_x, t_y)$ is simply the projection of $\mu(t_x, t_y, t_z)$ onto the plane defined by the down range and cross range axes of the radar. Note that $\mu_a(t_x, t_y)$ is obtained by taking the line integral along the t_z coordinate at (t_x, t_y), such that

$$\mu_a(t_x, t_y) = \int_{-\infty}^{\infty} \mu(t_x, t_y, t_z) dt_z. \tag{3.1}$$

Having defined $\mu_a(t_x, t_y)$ and $\Lambda(f, \phi)$, the relationship between them must now be established. Since $\mu_a(t_x, t_y)$ is a two dimensional function, one can perform a two dimensional Fourier transform to the (f_x, f_y) space. Let $\tilde{\Lambda}(f_x, f_y)$ be the transfer function for $\mu_a(t_x, t_y)$ which is given by

$$\tilde{\Lambda}(f_x, f_y) = \int_{-\infty}^{\infty} \int_{-\infty}^{\infty} \mu_a(t_x, t_y) e^{-j2\pi(f_x t_x + f_y t_y)} \, dt_x \, dt_y. \tag{3.2}$$

The inverse Fourier transform of $\tilde{\Lambda}$ is

$$\mu_a(t_x, t_y) = \int_{-\infty}^{\infty} \int_{-\infty}^{\infty} \tilde{\Lambda}(f_x, f_y) e^{j2\pi(t_x f_x + t_y f_y)} \, df_x \, df_y. \tag{3.3}$$

Now define a function which is equivalent to $\tilde{\Lambda}$ but is defined in polar coordinates. It is expressed as follows:

$$\tilde{\Lambda}(f_x, f_y) = \Lambda(f, \phi). \tag{3.4}$$

Equation (3.3) can be converted to a polar Fourier transform by substituting Λ for $\bar{\Lambda}$, $f_x = f\sin\phi$, $f_y = f\cos\phi$, and $df_x df_y = f\,df\,d\phi$; thus, one finds that

$$\mu_a(t_x, t_y) = \int_0^{2\pi}\int_0^{\infty} \Lambda(f,\phi) e^{j2\pi f(t_x\cos\phi + t_y\sin\phi)} f\ df\ d\phi. \tag{3.5}$$

Separating the integral into two parts, one finds that

$$\begin{aligned}\mu_a(t_x, t_y) = &\int_0^{\pi}\int_0^{\infty} \Lambda(f,\phi) e^{j2\pi f(t_x\cos\phi + t_y\sin\phi)} f\ df\ d\phi \\ &+ \int_{\pi}^{2\pi}\int_0^{\infty} \Lambda(f,\phi) e^{j2\pi f(t_x\cos\phi + t_y\sin\phi)} f\ df\ d\phi.\end{aligned} \tag{3.6}$$

Recognize that

$$\begin{aligned}\cos(\phi+\pi) &= -\cos(\phi) \\ \sin(\phi+\pi) &= -\sin(\phi), \text{ and} \\ \Lambda(f,\phi+\pi) &= \Lambda(-f,\phi).\end{aligned}$$

Then, one obtains the following expression:

$$\mu_a(t_x, t_y) = \int_0^{\pi}\int_{-\infty}^{\infty} \Lambda(f,\phi) e^{j2\pi f(t_x\cos\phi + t_y\sin\phi)} \mid f \mid\ df\ d\phi. \tag{3.7}$$

Note that $\mu_a(t_x, t_y)$ is referenced to the coordinate system of the target. The offset angle between the target's coordinate system and the radar's coordinate system is ϕ. The relationship between the coordinate system fixed to the radar and the coordinate system fixed to the target is

$$\tilde{t}_x = t_x\cos\phi + t_y\sin\phi, \text{ and} \tag{3.8}$$

$$\tilde{t}_y = -t_x\sin\phi + t_y\cos\phi. \tag{3.9}$$

One can therefore express the exponent of (3.7) as given in (3.8) as the down range coordinate with respect to the radar. Now consider the integration on f after making this substitution:

$$I(\tilde{t}_x, \phi) = \int_{-\infty}^{\infty} \Lambda(f,\phi) e^{j2\pi f\tilde{t}_x} \mid f \mid df. \tag{3.10}$$

By substituting $\omega = 2\pi f$ and $d\omega = 2\pi df$, one finds that

$$I(\tilde{t}_x, \phi) = \frac{1}{(2\pi)^2} \int_{-\infty}^{\infty} \Lambda(\omega, \phi) e^{j\omega \tilde{t}_x} \mid \omega \mid d\omega. \tag{3.11}$$

Equation (3.11) is simply the inverse Fourier transform of the swept frequency measurements at a given angle ϕ multiplied by $\mid \omega \mid$ and a constant. $I(\tilde{t}_x, \phi)$ is also known as the back projection for look angle ϕ. It is called a back projection because the down range image, which is the projection of $\mu_a(t_x, t_y)$ onto the down range axis $\tilde{t}_x$, is projected back onto the (t_x, t_y) plane. The value of the back projection at (t_x, t_y) is determined by the value of the down range image at $\tilde{t}_x$, the look angle ϕ, and the relationship $\tilde{t}_x = t_x \cos\phi + t_y \sin\phi$. The back projection can then be substituted into (3.7) to obtain

$$\mu_a(t_x, t_y) = \int_0^{\pi} I(\tilde{t}_x, \phi)\, d\phi. \tag{3.12}$$

From Equation (3.12) the image construction technique is shown to be an integration of the back projections over a set of look angles. Since $\Lambda(f, \phi)$ is sampled discretely over angle, the image construction technique consists of simply summing the back projections of the target obtained at each look angle.

3.2 Image Interpretation

To arrive at (3.12), it was assumed that $\Lambda(f, \phi + \pi) = \Lambda(-f, \phi)$. In order for this assumption to be correct, the transfer function of a target E^s, would have to satisfy the condition

$$E^s(f, \frac{\pi}{2}, \phi + \pi) = [E^s(f, \frac{\pi}{2}, \phi)]^*. \tag{3.13}$$

In general, this is not the case. Of the scattering centers making up a target, many have transfer functions which are dependent on azimuth angle, and

on most realistic targets, scattering centers are often shadowed by other parts of the target, making (3.13) invalid.

To justify the assumption $\Lambda(f, \phi + \pi) = \Lambda(-f, \phi)$, the way in which the image will be used must be considered. The section of this work which uses the CAT images is concerned with identifying the three dimensional positions of scattering centers on a target at a particular look angle. Since it is desired to determine the scattering characteristics of the target at one look angle, a reflectivity density function is needed which reflects contributions from only the specified look angle. The reflectivity density function $\mu_a(t_x, t_y)$ of Equation (3.11) includes contributions from scattering centers through an angular sweep of 180 degrees. On a realistic target a scattering center may contribute significantly to the backscatter of a target over only a limited number of look angles. If these look angles do not coincide with the desired look angle, the image which results from a sweep of π radians will not accurately reflect the scattering at the desired look angle. In order to eliminate these corrupting contributions, this work has used the approach of creating a reflectivity density function, $\mu_{a0}(t_x, t_y)$, which is limited in angular extent as expressed by

$$\mu_{a0}(t_x, t_y) = \int_{\phi_0 - \psi}^{\phi_0 + \psi} I(\tilde{t}_x, \phi)\, d\phi. \tag{3.14}$$

By choosing ψ relatively small, it is assumed that only those scattering centers which are present in the backscatter at ϕ_0 will contribute to $\mu_{a0}(t_x, t_y)$. In addition, since $\mu_{a0}(t_x, t_y)$ is designed to reflect only contributions from a look angle of ϕ_0, the actual value of $\Lambda(f, \phi + \pi)$ is of no concern. It can therefore be arbitrarily set to satisfy the requirement $\Lambda(f, \phi + \pi) = \Lambda(-f, \phi)$.

3.3 Sampling Effects For Two Dimensional Spectra

A practical target's reflectivity function is limited in space. This implies that to reproduce $\mu_a(t_x, t_y)$ exactly, one would have to sample $\Lambda(f, \phi)$ over all f and ϕ. Since Λ is discretely sampled in f and ϕ and over limited bandwidth and limited angular extent, the target's image may suffer from limited resolution, aliasing, and truncation effects.

The backscatter measurements used to generate the CAT images for this report are taken in the format shown in Figure 7. In order to determine the impact this sampling scheme has on a target's image, first consider the transform pair of Equation (3.3). In this transform, there is a direct transform from coordinate f_x to t_x, and from coordinate f_y to t_y. If the target's spectrum is sampled as shown in Figure 8, the effects of sampling along f_x are manifested along the t_x coordinate and the effects of sampling along f_y are manifested along the t_y coordinate.

Although there is no such direct relation between (f, ϕ) and (t_x, t_y) the observations of the previous paragraph can be used to determine the impact of the polar sampling scheme on the target's image. First note that each radial slice of Figure 7 corresponds to a frequency sweep at a particular look angle. Consider the projection of each of these slices onto the f_x axis. The projection of each sample is expressed by $f_x = f \cos\phi$, which for small ϕ is $f_x = f$. This implies that if ψ is small enough, the behavior of the image along t_x is determined by the sampling parameters in f. The problems of limited resolution, aliasing, and truncation effects along t_x can therefore be treated in the same manner that they were treated for t in Chapter 2.

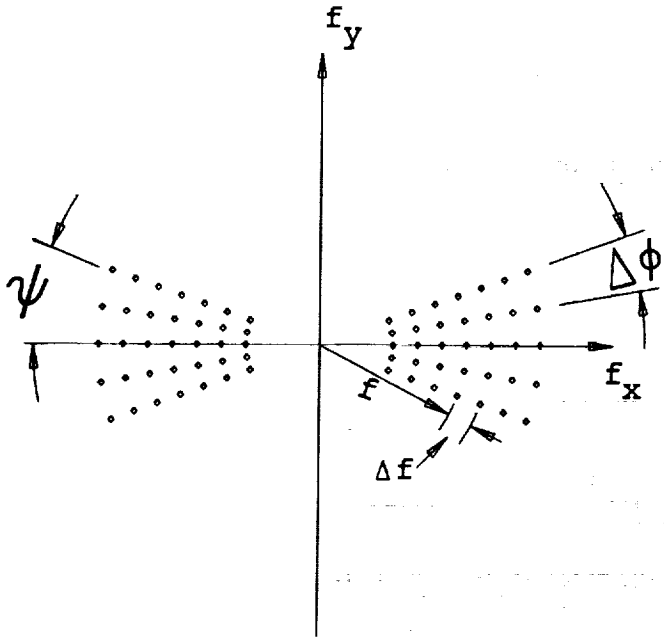

Figure 7: Polar sampling scheme.

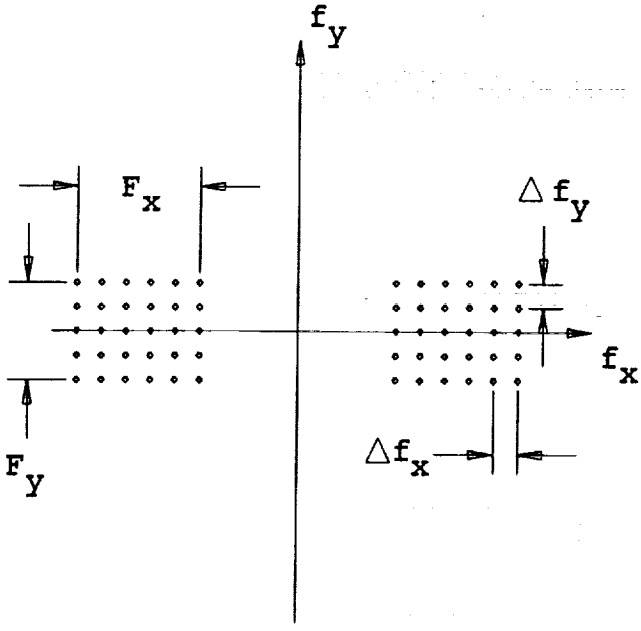

Figure 8: Rectangular sampling scheme.

The behavior of the image along the cross range coordinate t_y is a result of sampling in both f and ϕ. First consider a slice from Figure 7 along an arc defined by a constant frequency. The projection of such an arc onto the f_y axis is expressed by $f_y = f \sin\phi$, which for small ϕ is $f_y = f \cdot \phi$. The sampling step size along f_y is therefore $f\Delta\phi$. To prevent aliasing in cross range, $\Delta\phi$ must be chosen small enough so that the Nyquist criterion is satisfied. In Chapter 2, it was shown that the Nyquist criterion was satisfied if a target's spectrum was sampled in steps of

$$\Delta f \leq \frac{c}{2D}. \tag{3.15}$$

The analogous situation for sampling in the angular domain is

$$\Delta\phi \cdot f \leq \frac{c}{4\rho_{max}} \tag{3.16}$$

where ρ_{max} is the distance from the origin to the point on the target furthest from the origin [12]. To satisfy the Nyquist criterion over the entire bandwidth, f must be chosen to be f_{max}, such that

$$\Delta\phi \leq \frac{\lambda_{min}}{4\rho_{max}}. \tag{3.17}$$

The resolution in cross range along t_y is determined by the bandwidth along f_y. By projecting the angular slices onto the f_y axis, the bandwidth at a particular value of f is $2f\psi$. The bandwidth computed in this fashion though, varies by a factor of 9 for a spectrum spanning 2-18 Ghz. Since no direct method is available to determine resolution in cross range, it is done empirically by allowing two point scatterers to approach each other in cross range until their positions become distorted. The resolution using this technique is approximately 3 inches.

In Chapter 2 the effects of abruptly truncating a scattering center's spectrum were discussed. Similar problems are encountered in images along t_y when $\Lambda(f,\phi)$ is truncated abruptly with respect to ϕ. These effects

consist mostly of high side lobes in cross range, which are unacceptable for the processing in which the images are to be used. To reduce the impact of truncation a cosine squared window is applied to the sampled data with respect to angle.

Chapter 4

Plane Wave Illumination

4.1 Plane Wave Illumination in Target Zone

At the beginning of Chapter 2, the radar used to illuminate the target was placed in the far field. This placement was necessary so that the wave front incident on the target could be considered planar. Also, it was stated that a scattering center must be illuminated from three different look angles in order to determine its position in three dimensions. The following chapter briefly explains the method used for generating the plane waves for the three required look angles.

At the OSU ElectroScience Laboratory the required planar wave front is generated in a compact range which is pictured in Figure 9. This picture shows the large parabolic reflector which is central to the range's function. Via reflection, the parabolic reflector transforms the spherical wave front emitted by the feed antenna at the reflector's focus into a plane wave which illuminates the target zone. A schematic of this measurement range is given in Figure 10. Note that the dimensions of the usable target zone for this application are also shown.

The interested reader is referred to [3] in order to learn more about the use and design of a compact range. What is essential to this work is that the wave front generated in the compact range remain planar throughout

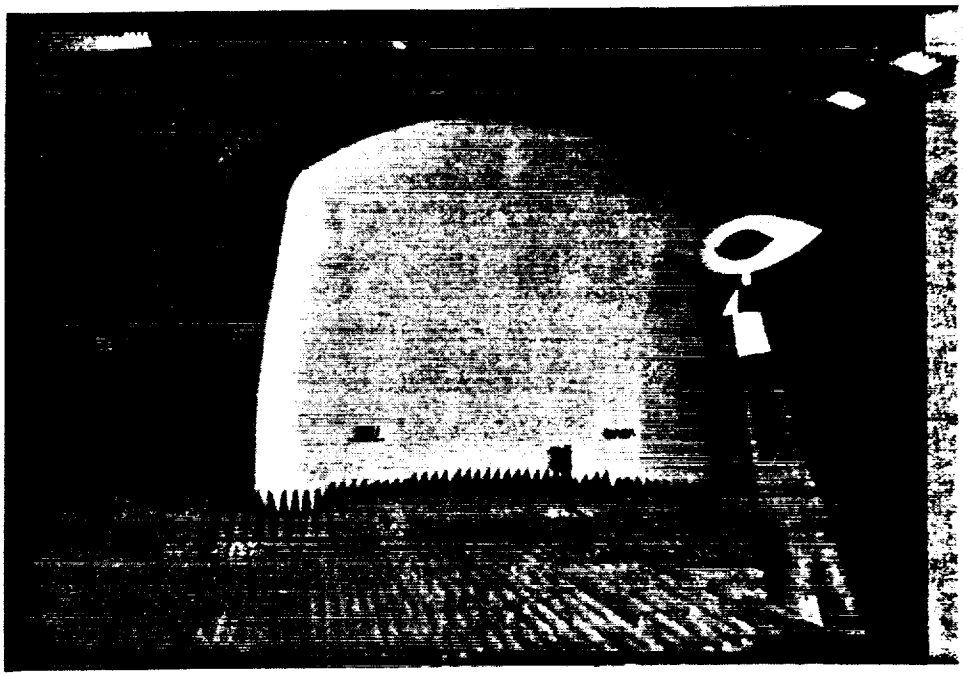

Figure 9: Compact range at Ohio State University ElectroScience Laboratory.

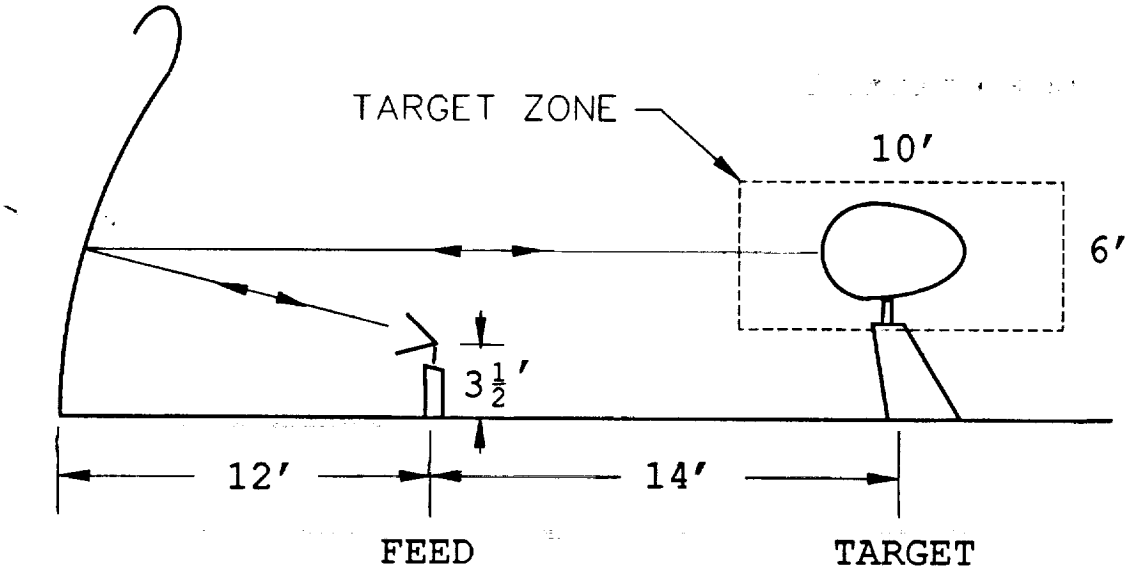

Figure 10: Schematic of compact range at Ohio State University ElectroScience Laboratory.

the target zone for each of the three look angles. In order to generate the wave fronts for the three required look angles, an antenna configuration as shown in Figure 11 is used. This antenna mounting system is set at the focal point of the parabolic reflector such that the central antenna is located at the focal point, one is offset horizontally from the focal point, and one is offset vertically from the focal point.

The NEC-REF code [14], created at the OSU ElectroScience Laboratory, is used here to show that the wave fronts generated from the antennas meet the requirements of the three distinct look angles. This code calculates the phase and amplitude of the electric field in the target zone of the compact range as a result of an antenna placed near the focal point of the parabolic reflector. The electric fields are calculated for linear cuts through the target zone, and for this work the cuts will all be taken in a plane across the chamber. The plane that the cuts are taken from is located at a down range position of 288 inches, and the cuts from the test plane are referenced

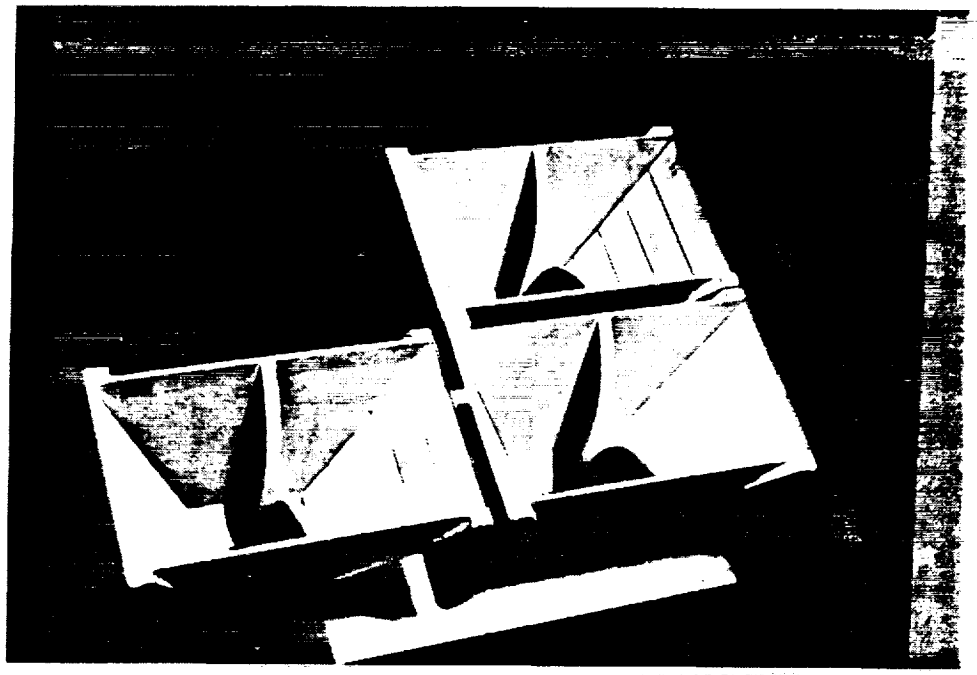

Figure 11: Antenna configuration to generate the three planar wave fronts.

to a point centered in cross range and offset vertically 102 inches from the floor. This corresponds to the center of the target zone. For each case to be presented a vertical cut perpendicular to the floor of the range and a horizontal cut parallel to the floor of the compact range are displayed. The frequency of illumination for the cuts is chosen to be the upper end of the bandwidth used, 18 GHz. This frequency is chosen because the higher frequencies have a greater potential for phase distortion. The plane from which the cuts are taken will be referred to as the test plane.

The wave front for the horn at the focus of the parabola will be considered first. This wave front should be parallel to the test plane. The phase

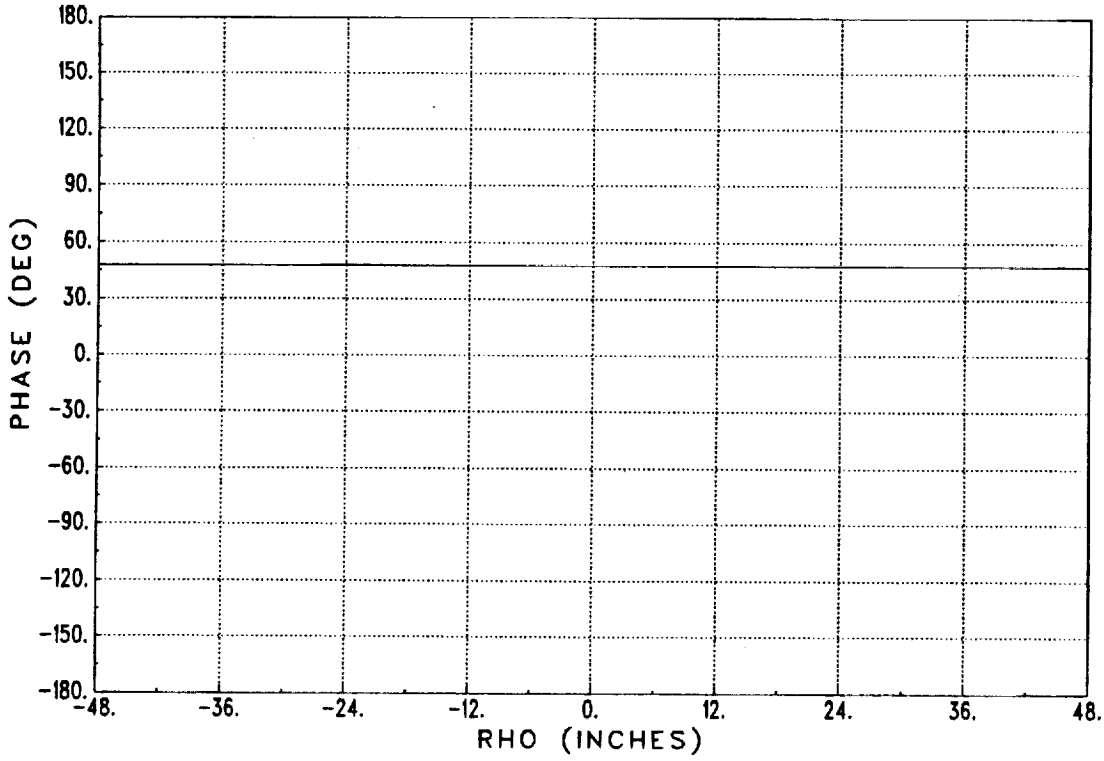

Figure 12: Phase of the electric field along a vertical cut due to the antenna at the focus of the parabolic reflector.

of the electric field at any point in the test plane is proportional to the distance ρ from the antenna to that point. The phase due to propagation in free space is $\frac{2\pi\rho}{\lambda}$. If the wave front is planar, the phase of the electric field will remain constant throughout the test plane. The phase of the electric field along the vertical and horizontal cuts are shown in Figures 12 and 13, respectively. In both cases the phase remains constant along the entire cut as anticipated.

The next set of cuts to be analyzed is associated with the antenna which is offset horizontally by $5\frac{1}{8}$ inches from the focal point of the parabolic reflector. The measurements from this antenna are intended to provide the information necessary to determine the horizontal cross range position of a scattering center. The wave front generated from this antenna should be

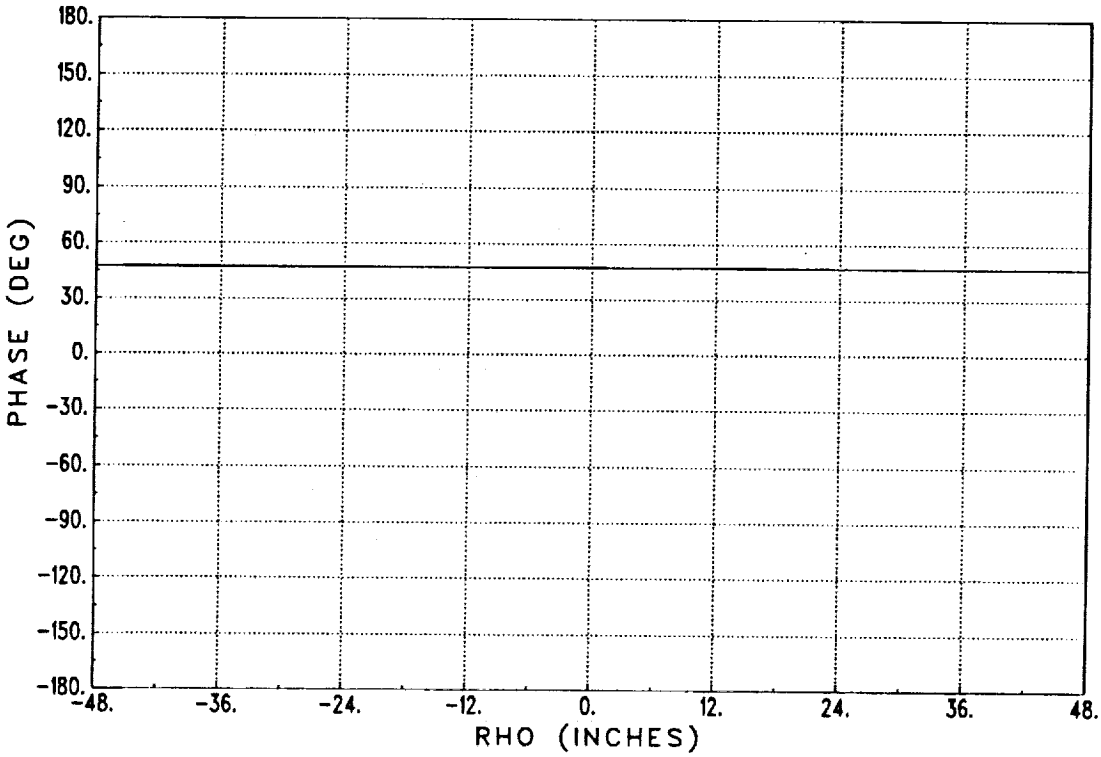

Figure 13: Phase of the electric field along a horizontal cut due to the antenna at the focus of the parabolic reflector.

offset in angle horizontally from the wave front of the antenna at the focus. Any vertical offset in angle in the plane wave's direction of propagation introduces an error into the estimated cross range position of a scattering center. If the wave front possesses these properties the phase of the electric field due to the offset antenna will vary linearly along a horizontal cut and remain constant along a vertical cut. Figures 14 and 15 show, respectively, plots of the phase of the electric field along both a horizontal cut and a vertical cut. The phase along the horizontal cut varies nearly linearly with respect to cross range offset and yields a calculated angle of separation between the plane waves of 1.92 degrees. From Figure 15, one can see that the phase is not constant with respect to the vertical cut. The deviation shown introduces an error into the cross range position determination for a scattering center which has a non-zero vertical offset. For instance, the estimated cross range location of a scattering center has an error of 0.5 inches if its vertical offset is 18 inches. This error though is relatively small and can be compensated for to give the necessary plane wave illumination.

The third set of cuts to be considered are for the vertically offset antenna, which is offset by $-4\frac{7}{8}$ inches. The wave fronts generated from this antenna should be offset in angle vertically from the wave front of the antenna at the focus. The phase of the electric field along a vertical cut should therefore vary linearly with a vertical offset and the phase should remain constant along the horizontal cut. Figure 16 shows that the phase variation with respect to the vertical cut is nearly linear. The calculated angle of separation resulting from this plot is -1.85 degrees. Figure 17 shows the change in phase of the electric field with respect to the horizontal cross range. Although the phase does not vary considerably, especially in the center of the target zone, one can see that this phase is not constant and will introduce some error in the vertical offset estimation. For example, a

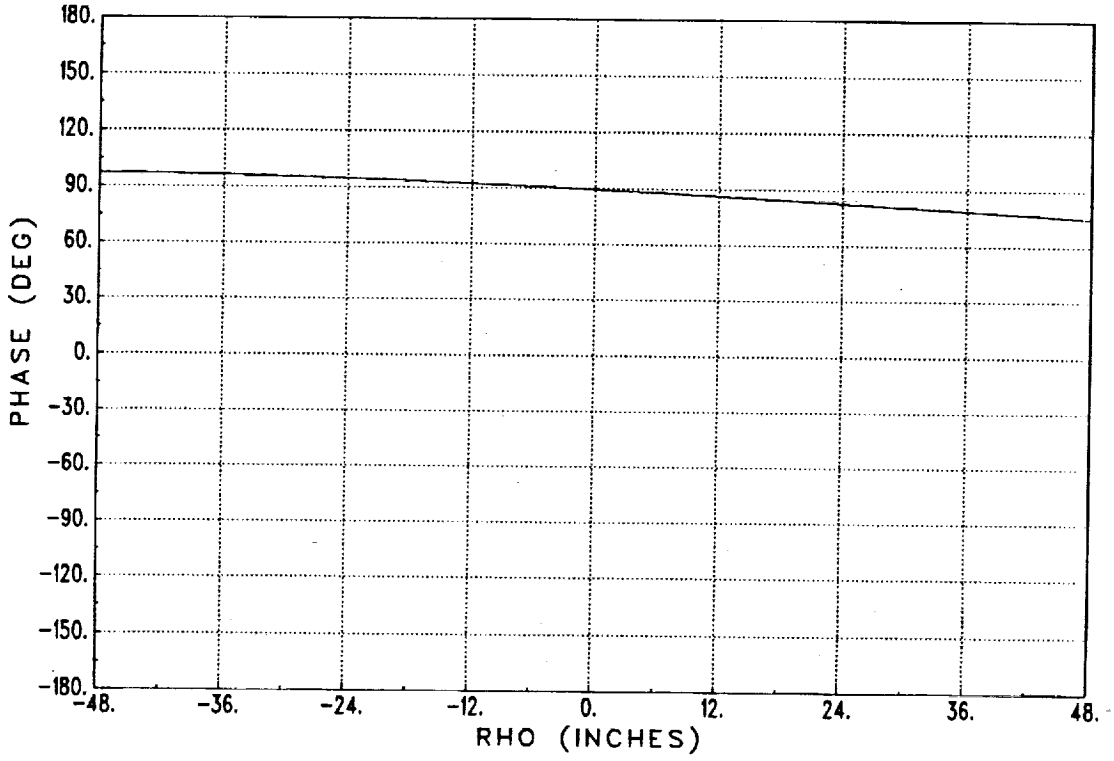

Figure 14: Phase of the electric field along a vertical cut due to the horizontally offset antenna.

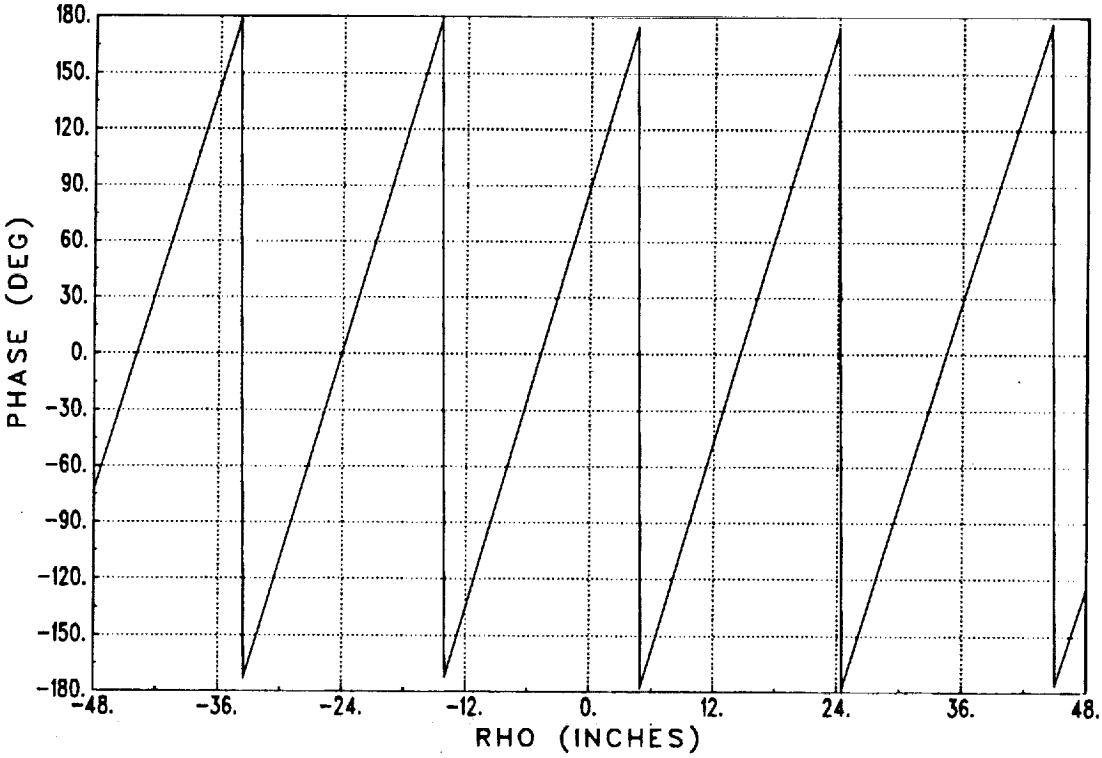

Figure 15: Phase of the electric field along a horizontal cut due to the horizontally offset antenna.

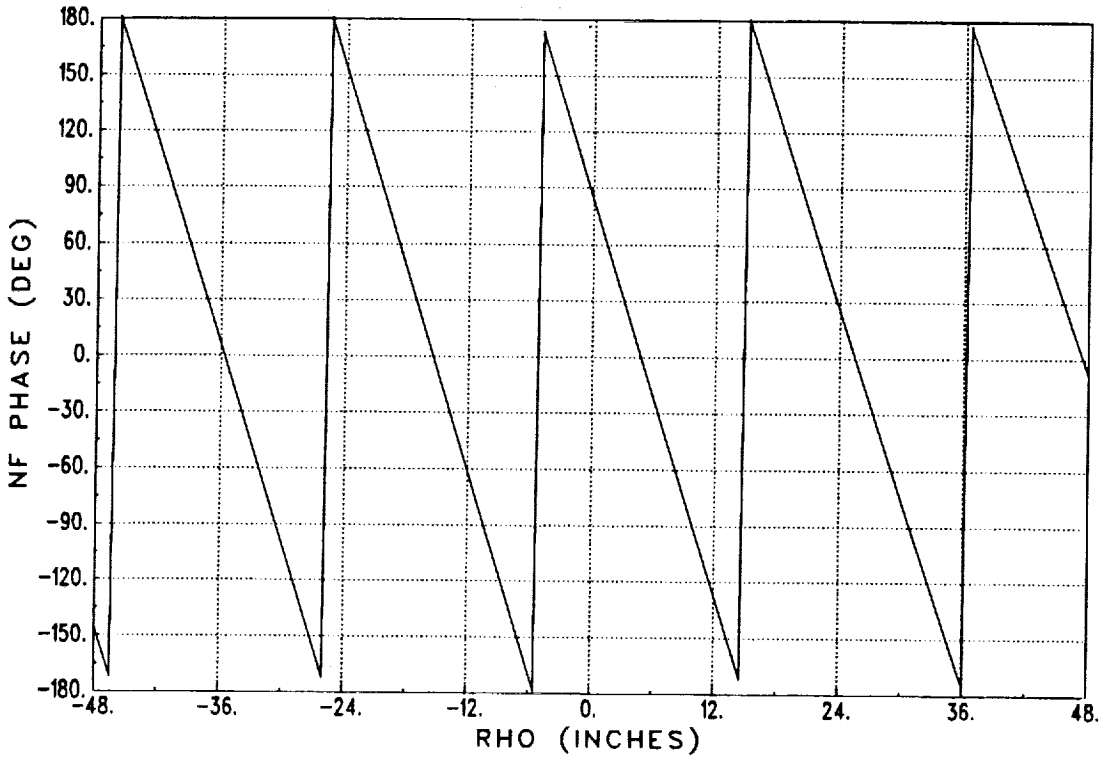

Figure 16: Phase of the electric field along a vertical cut due to the vertically offset antenna.

scattering center which is offset by 24 inches horizontally will have an error of -0.6 inches in its estimated vertical offset. This error though can be accomodated for so that the necessary plane wave illumination is achieved.

In the preceeding discussion, the electromagnetic waves illuminating the target and the backscatter from the target are transmitted and received by the same antenna. The data for this paper was generated by transmitting from the antenna at the focus of the reflector and receiving backscatter signals on all three antennas. The measurement system is therefore composed of one monostatic radar and two bistatic radars. The bistatic equivalence theorem states that the results from a bistatic radar operating at a wavelength of λ can be replicated using a monostatic radar placed midway between the transmit and receive antennas of the bistatic radar, operating

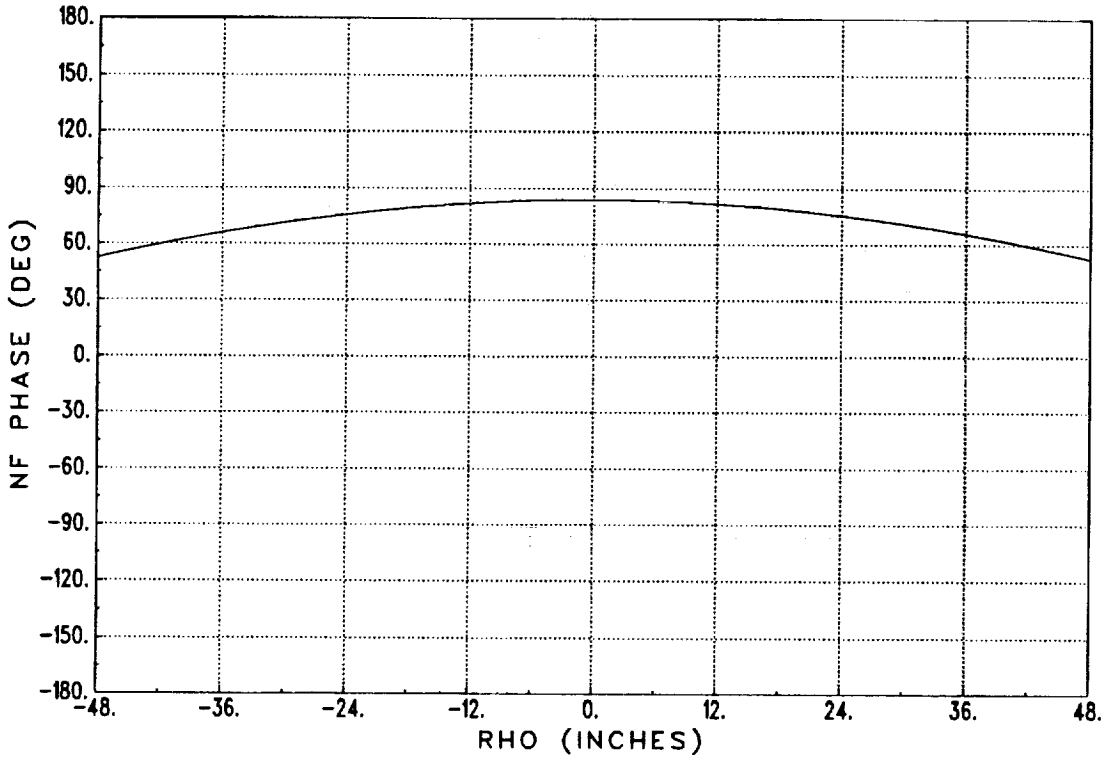

Figure 17: Phase of the electric field along a horizontal cut due to the vertically offset antenna.

at a wavelength of $\lambda \sec(\frac{\alpha}{2})$ [8]. The angle of separation of the antennas used to collect data for this paper was approximately two degrees. The wavelength of the virtual monostatic radar is therefore almost identical to the wavelength used by the bistatic system. One can therefore treat the bistatic radar, composed of the antenna at the focus and the offset antenna, as a monostatic radar located at the angle bisector.

4.2 Measured Angular Offset

It is desirable to be able to determine the angle of separation between the three wave fronts experimentally. The following procedure can be used to determine the angle of separation between wave front A, due to the antenna at the focus of the reflector, and wave front B, due to the horizontally offset antenna. The two antennas are first calibrated with respect to a six inch sphere in the center of the target zone. After calibration the sphere is offset in cross range by a known distance y_0 and swept frequency backscatter measurements are taken for both A and B. These spectrums are transformed into the time domain where the envelope of the impulse response for each is extracted. From the envelopes, the down range position of the specular responses for each can be determined: x_{a0} for A and x_{b0} for B as shown in Figure 1. These values can then be inserted into the following equation to determine the angle of separation such that

$$\alpha = \frac{x_{b0} - x_{a0}}{y_0}. \tag{4.1}$$

A plot of the envelopes for a sphere horizontally offset by 16 inches is shown in Figure 18. Applying the method just presented, the angle of separation between A and B is 0.98 degrees. This compares favorably with the value of 0.96 degrees obtained after applying the bistatic equivalence theorem to the calculated results.

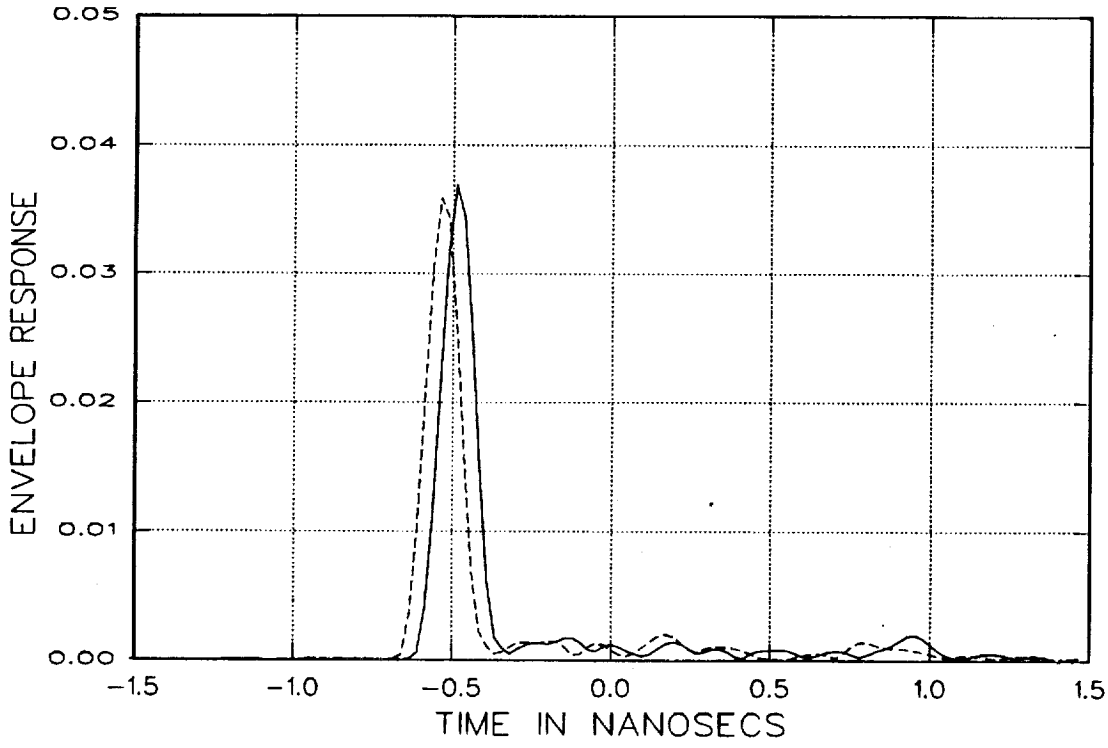

Figure 18: Envelopes for a horizontally offset sphere using horizontally offset antennas.

The separation in angle between plane wave C, due to the vertically offset antenna, and plane wave A is determined in a similar fashion. In this case, the sphere is offset vertically by a known amount z_1. The necessary measurements are taken to determine the down range position of the specular responses for A and C which are, respectively, denoted as x_{a1} and x_{c1}. The angle of separation is then determined by

$$\gamma = \frac{x_{c1} - x_{a1}}{z_1}. \tag{4.2}$$

The measured angle of separation between A and C is 0.97 degrees. This result compares well with the calculated result of 0.93 degrees.

Chapter 5

Scattering Center Location in Three Dimensions Using Target Impulse Responses

At the beginning of Chapter 2, a simple technique was presented to locate the position of a scattering center using radar measurements taken from three slightly offset antennas. The measurements were processed to yield the envelopes of the impulse response of the target from which the down range position of the scattering center was determined with respect to each antenna. Then, knowing the configuration of the antennas, the three dimensional position of the scattering center was determined. This technique is applied here to a target with multiple scattering centers.

It was previously shown that the envelope of the impulse response of a scattering center, whose spectrum was band limited and windowed, was a single large peak with negligible side lobe levels. In addition, if the scattering center is linear, its down range position corresponds exactly to the location of the maximum of its peak in the envelope. A realistic target generally consists of many scattering centers; thus, its envelope response is composed of several peaks of differing amplitudes, shapes, and locations. Since the scattering characteristics of a target are taken to be unknown, it is assumed that every peak in the envelope of a target's impulse response

corresponds to a distinct scattering center. Upon obtaining the envelopes of the impulse responses of the target for the three offset plane waves, it is hoped that the positions of all the scattering centers on the target could be determined. In order to estimate the position of a given scattering center, it is necessary to identify the peak corresponding to it in each of the three envelopes. This identification process is the fundamental obstacle in applying this technique to a realistic target.

When dealing with a realistic target, one encounters basically two impediments to correctly identifying and locating scattering centers. The first is grouping three peaks together which do not all correspond to the same scattering center. If the three peaks do not all correspond to the same scattering center, a scattering center is generated which does not actually exist on the target. The second problem results from distortion of the peaks defining a given scattering center. In this case, the peaks which are grouped together all correspond to the same scattering center; the distortion present in the individual peaks though, causes an error in the estimated down range position of the scattering center. Consequently, the horizontal and vertical offsets may be incorrectly estimated, and the scattering center is again placed at the wrong position.

In the sections which follow, some of the impediments to correctly grouping peaks to form a scattering center, and correctly estimating its position, are discussed. A method is proposed to evaluate the validity of a scattering center and the accuracy of its position. Finally, a technique using information from several look angles is presented which tracks scattering centers to confirm whether a scattering center exists or is an anomaly.

5.1 Defining Possible Scattering Centers

The first step in scattering center identification is choosing three peaks which correspond to the same scattering center. This task is simplified by knowing the dimensions of the target and the angles of separation between the offset plane waves. Recall that a target is characterized as a linear superposition of point scatterers. By definition these point scatterers lie on the physical body of the target. It will be shown shortly that it is necessary for the target to rotate with respect to the antennas to obtain scattering information from different look angles. The geometry used for obtaining measurements at different look angles is identical to the imaging geometry used for the CAT imaging discussed in Chapter 3, except that a second antenna is added at a position offset by α degrees. This geometry is shown in Figure 19. Note that there exists a distance ρ_{max} from the axis of rotation to the point on the target which is farthest from the axis of rotation. Since the scattering centers are assumed to be point scatterers confined to the body of the target, ρ_{max} and the axis of rotation can be used to define a circle within which all scattering centers on the target must lie, regardless of look angle.

Now consider an envelope generated from measurements resulting from plane wave A. Assume a peak in this envelope is located at a distance x_{a0} from the axis of rotation as shown in Figure 20. As discussed in Chapter 2, the down range distance of a scattering center is the projection of its position onto the down range axis of the illuminating plane wave. The down range distance, coupled with the circle defined by ρ_{max}, confines the scattering center's location to somewhere along the line $\overline{a_0 a_1}$. A second envelope is generated from measurements resulting from plane wave B. In order to calculate the offset of the scattering center giving rise to the peak

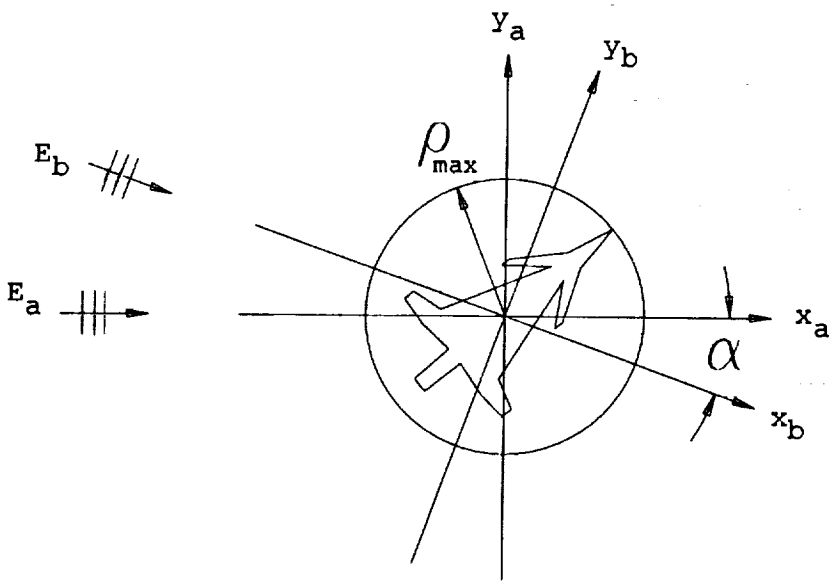

Figure 19: Imaging geometry.

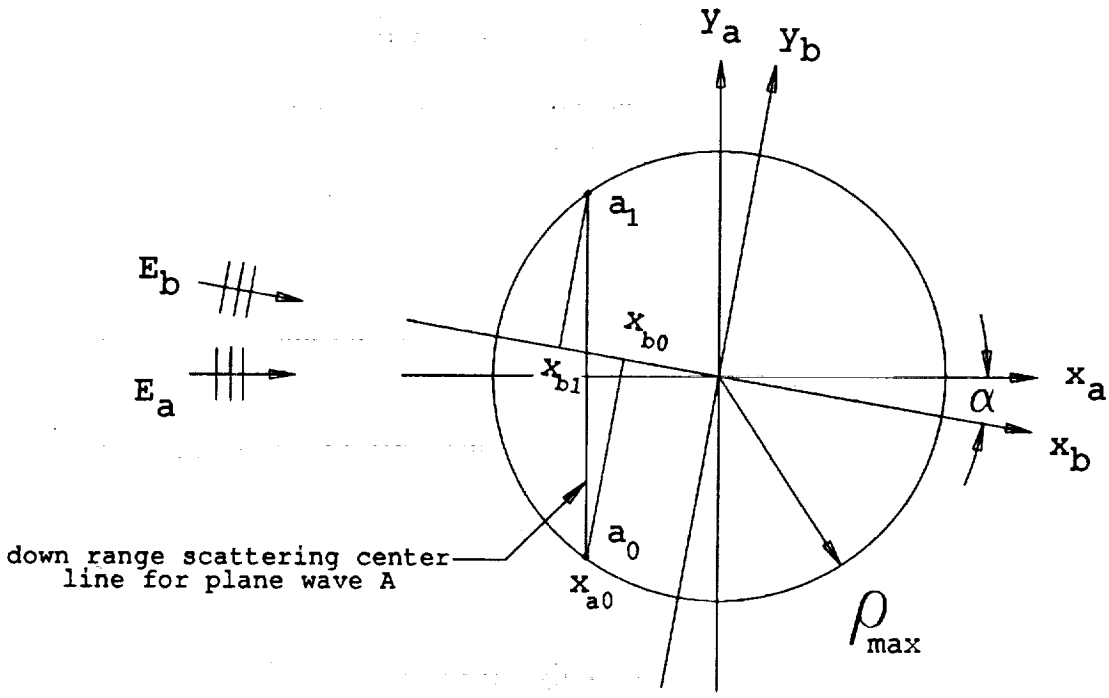

Figure 20: Possible scattering center locations based on maximum extent of target.

at x_{a0}, the peak corresponding to the scattering center must be identified in the envelope of plane wave B. Since the scattering center is known to be confined to $\overline{a_0 a_1}$, its corresponding peak in the envelope of B must lie between x_{b0} and x_{b1} as shown in Figure 20. Note that

$$\begin{aligned} x_{b0} &= \rho_{max} \cos(\beta - \alpha) \\ x_{b1} &= \rho_{max} \cos(\beta + \alpha) \\ \alpha &= \text{separation between plane waves in azimuth angle} \\ \beta &= \cos^{-1}\left(\tfrac{x_{a0}}{\rho_{max}}\right). \end{aligned} \tag{5.1}$$

Any peak positioned between x_{b0} and x_{b1} in the envelope for plane wave B can be considered a possible match to the peak located at x_{a0} in the envelope for plane wave A. The matches in this case are termed "possible" because the offset in down range between them defines a position within the ρ_{max} circle. The two peaks making up the match though, do not necessarily correspond to the same scattering center.

A possible match from the envelopes of A and B defines a scattering center in two dimensions, down range and cross range. In order to find a scattering center's position in all three dimensions its vertical offset must also be obtained. In order to obtain the information necessary to determine a scattering center's vertical offset, it was shown previously that a plane wave must be offset in a direction perpendicular to the plane defined in Figure 20. Such a configuration is shown in Figure 21. A peak must now be found in the envelope of plane wave C which corresponds to the peak at x_{a0}. To determine the number of possible matches in the envelope of C with the peak at x_{a0}, refer to Figure 21. Note that the target rotates in a plane perpendicular to the page. This implies that in the plane defined by the page, the scattering centers move only with respect to down range as the target is rotated; their vertical offsets remain unchanged. There exists then a pair of distances, V_{max} and V_{min}, which equal the maximum and minimum vertical offsets of the body of the target with respect to the down range axis. The possible matches for the peak at x_{a0} in the envelope of plane wave C therefore lie between x_{c0} and x_{c1} where

$$
\begin{aligned}
x_{c0} &= x_{a0}\cos\gamma + V_{max}\sin\delta \\
x_{c1} &= x_{a0}\cos\gamma + V_{min}\sin\delta \\
\delta &= \cos^{-1}\left(\frac{x_{a0}}{\rho_{max}}\right), \text{ and} \\
\gamma &= \text{separation between plane waves in elevation angle.}
\end{aligned}
$$

A possible scattering center is formed from grouping a possible match from A and B and a possible match from A and C which share a common peak in the envelope of plane wave A. Again, the adjective "possible" is used here because the scattering center lies within the extent of the volume swept by the target, but it may not actually exist.

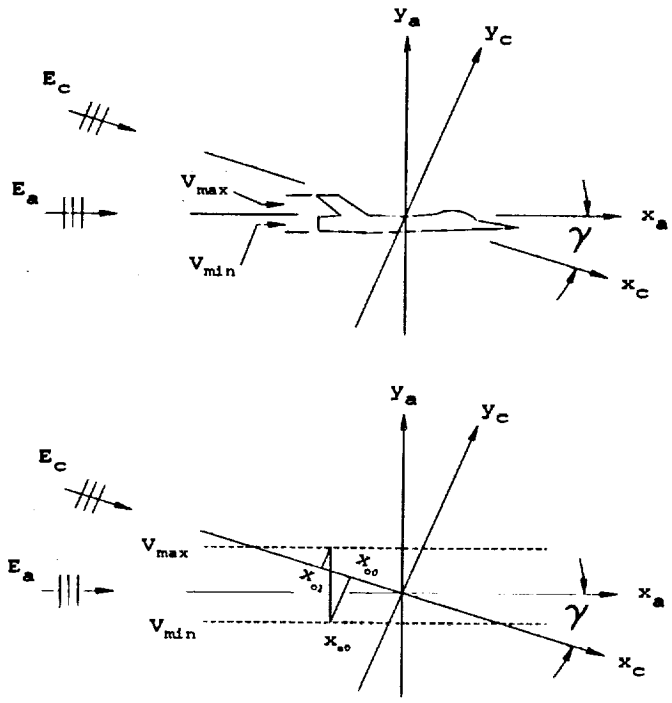

Figure 21: Imaging geometry for vertical offset determination.

5.2 Validity of Individual Peaks

Once a possible scattering center is defined, the validity or probability that it actually exists, must be evaluated. The validity of a possible scattering center is based on two criteria:

1. Do the peaks defining the possible scattering center all correspond to the same actual scattering center?
2. If the peaks do correspond to the same scattering center, is the estimated position equivalent to the actual position of the scattering center?

The information used to answer these questions is gleaned from the envelopes of the impulse responses from each plane wave. It is assumed that the down range position of a scattering center is equivalent to the location of the maximum of its envelope. Any corruption in the envelope which

violates this assumption degrades the validity of the predicted location of the scattering center.

The validity of an individual peak is based exclusively on the degree to which its corresponding scattering center is free of interference from other scattering mechanisms. When a scattering center is free of interference from other scattering mechanisms its down range position can be determined very accurately. As an example of such a case consider the target pictured in Figure 22. It is composed of corner reflectors whose specular response satisfies the definition of the point scatterer defined in Chapter 2. The envelopes of Figures 23 are a result of taking backscatter measurements of the target at the look angle pictured in Figure 24. By applying the maximum dimension restrictions discussed in the last section, the major peaks of the envelope can each only belong to one possible scattering center. The resultant possible scattering centers and their positions with respect to the target are pictured in Figures 24 and 25. These figures demonstrate that when there is little interference between scattering centers their locations can be estimated accurately.

It is only when scattering centers interfere with each other that inaccuracies are introduced into the location estimation. If other scattering mechanisms are introduced at a similar down range position, the peak corresponding to the scattering center is distorted. To demonstrate the resultant distortion consider first an alternate expression for the point scatterers of Chapter 2 such that

$$E^s_{n_b}(\omega) = H_n(\omega)e^{-\jmath\omega t_n} \tag{5.2}$$

where

$$H_n(\omega) = A_{nb}(\omega)e^{\jmath\psi_n}. \tag{5.3}$$

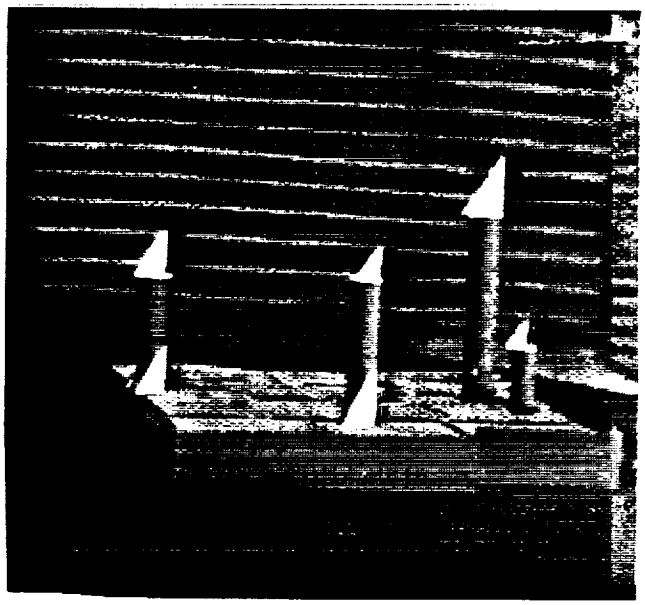

Figure 22: Target composed of corner reflectors.

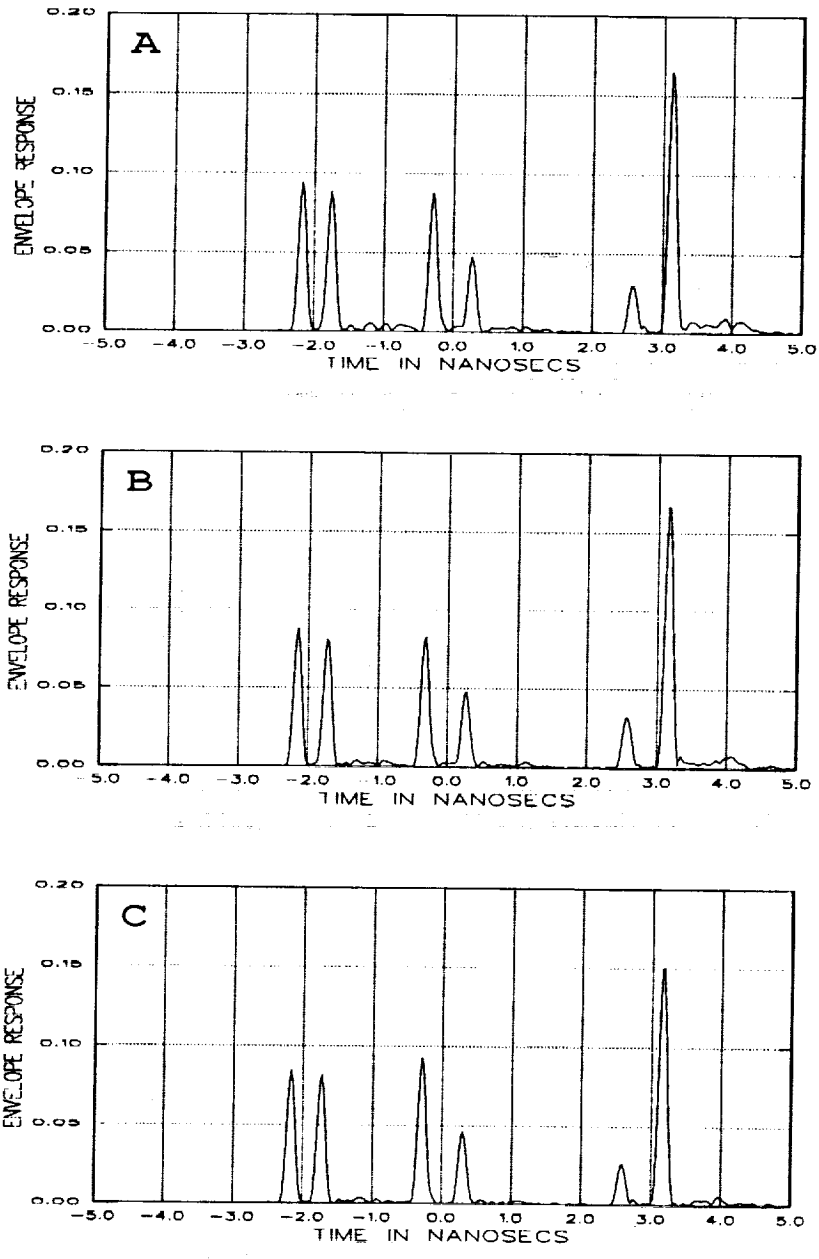

Figure 23: Envelope of each plane wave for corner reflectors at $\phi = 10°$.

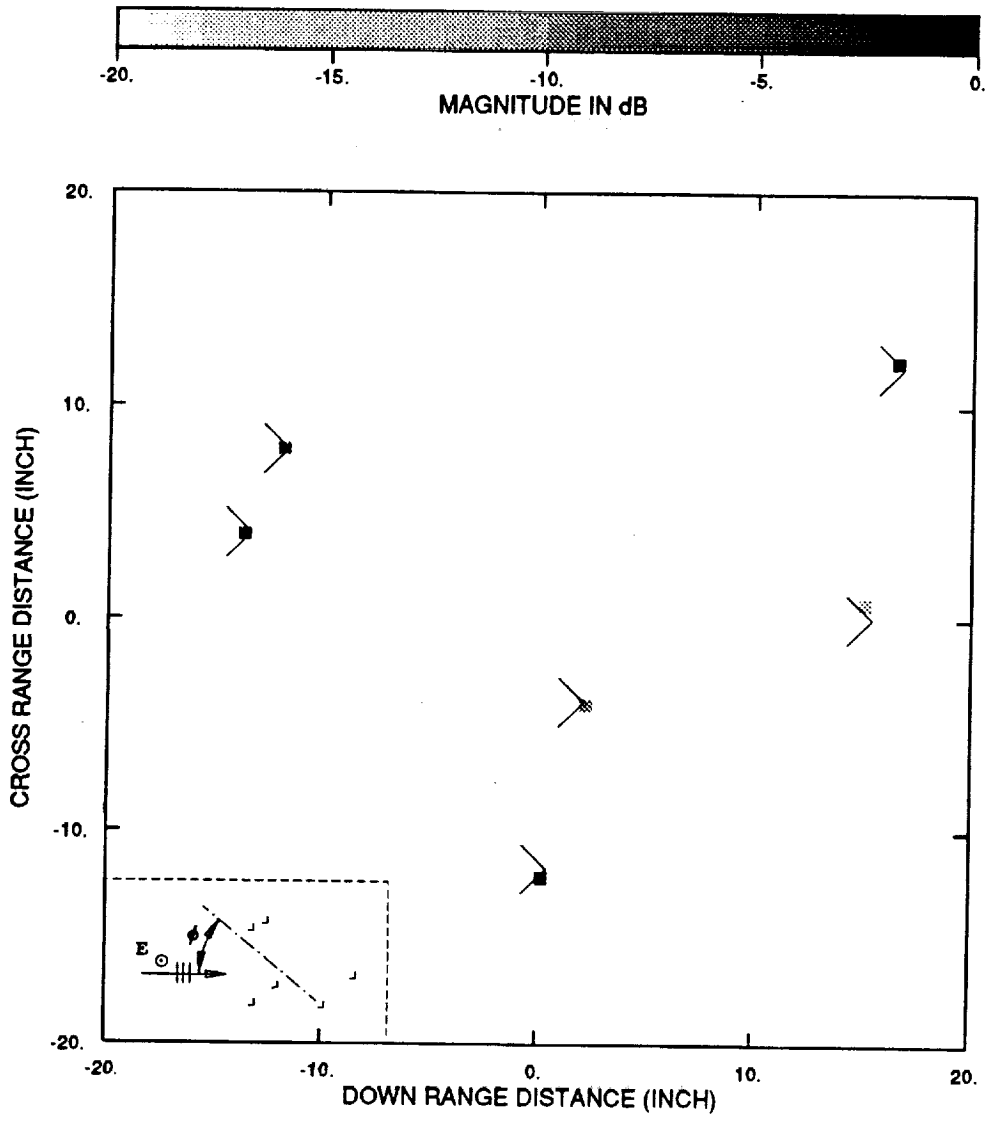

Figure 24: Top view of scattering centers resulting from measurements at $\phi = 10°$.

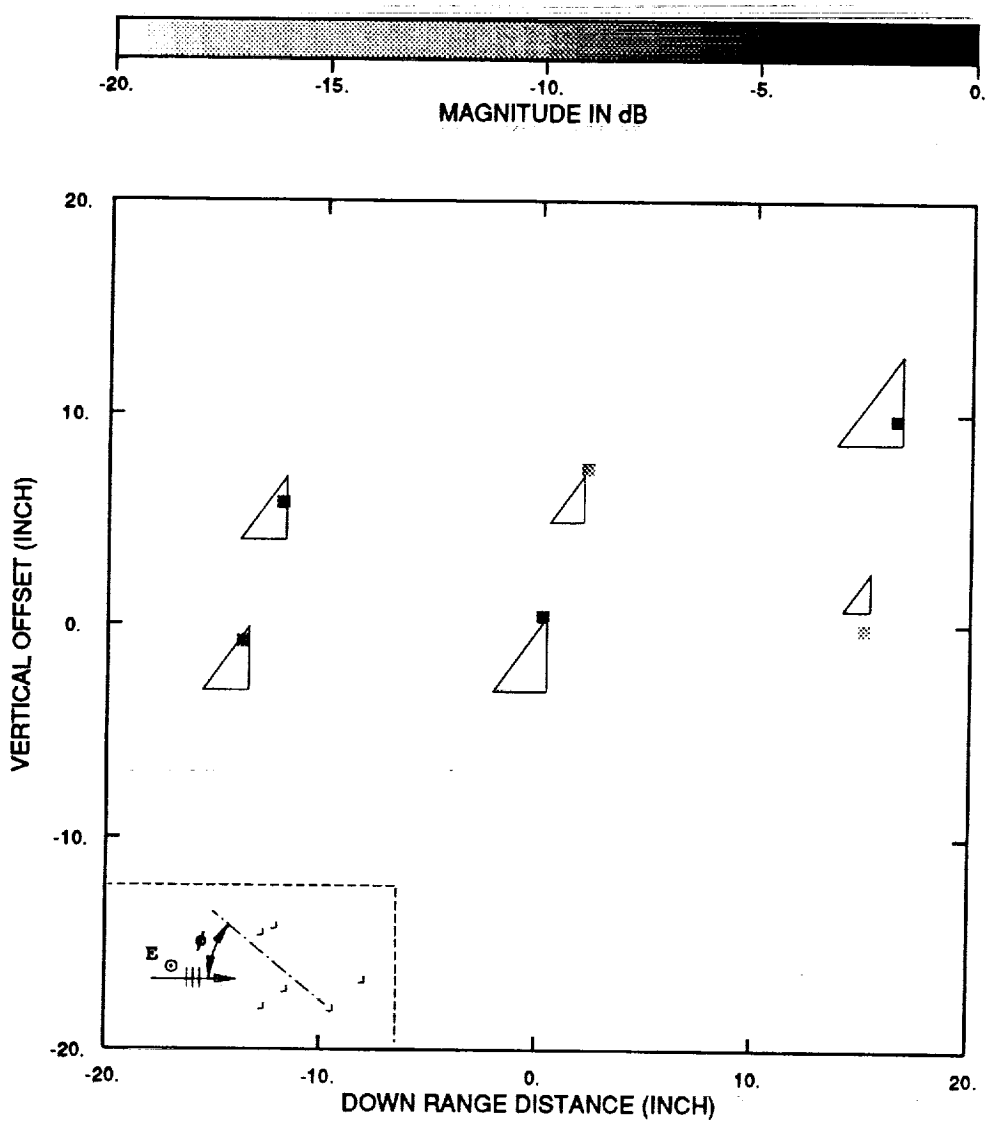

Figure 25: Side view of scattering centers resulting from measurements at $\phi = 10°$.

The H_n term is the amplitude and phase of the scattering center dependent on its characteristics. Its inverse Fourier transform $h_n(t)$ can be expressed in terms of its in-phase and quadrature terms as follows:

$$h_n(t) = h_{n_p}(t)cos\omega_0 t \; + \; h_{n_q}(t)sin\omega_0 t. \tag{5.4}$$

With this definition, the impulse response of the target can be expressed by

$$\begin{aligned} e_b^s(t) = 2\left[\sum_{n=1}^{N} h_{n_p}(t-t_n)\cos\omega_0 t_n - h_{n_q}(t-t_n)\sin\omega_0 t_n\right]\cos\omega_0 t \\ + 2\left[\sum_{n=1}^{N} h_{n_q}(t-t_n)\cos\omega_0 t_n - h_{n_p}(t-t_n)\sin\omega_0 t_n\right]\sin\omega_0 t \end{aligned} \tag{5.5}$$

which yields an envelope that is given by

$$e_{env}^s(t) = \sqrt{\begin{array}{l}\left[\sum_{n=1}^{N} h_{n_p}(t-t_n)\cos\omega_0 t_n - h_{n_q}(t-t_n)\sin\omega_0 t_n\right]^2 \\ + \left[\sum_{n=1}^{N} h_{n_q}(t-t_n)\cos\omega_0 t_n - h_{n_p}(t-t_n)\sin\omega_0 t_n\right]^2\end{array}}. \tag{5.6}$$

To determine the effect of interference between scattering centers when they approach the same down range position, let $N = 2$. The expression for the envelope of two scattering centers is

$$e_{env}^s(t) = \sqrt{\begin{array}{l}\left[h_{1_p}^2(t-t_1) + h_{1_q}^2(t-t_1)\right] + \left[h_{2_p}^2(t-t_2) + h_{2_q}^2(t-t_2)\right] \\ +2\left[h_{1_p}(t-t_1)h_{2_p}(t-t_2) + h_{1_q}(t-t_1)h_{2_q}(t-t_2)\right]\cos\omega_0(t_1-t_2).\end{array}} \tag{5.7}$$

The first two bracketed terms are the squares of the envelopes of the individual scattering centers. The third bracketed term is the result of the interaction between the two scattering centers. The third term results in a distortion between the peaks. In order to visualize the distortion introduced by interference refer to Figure 26. It is a plot of the difference

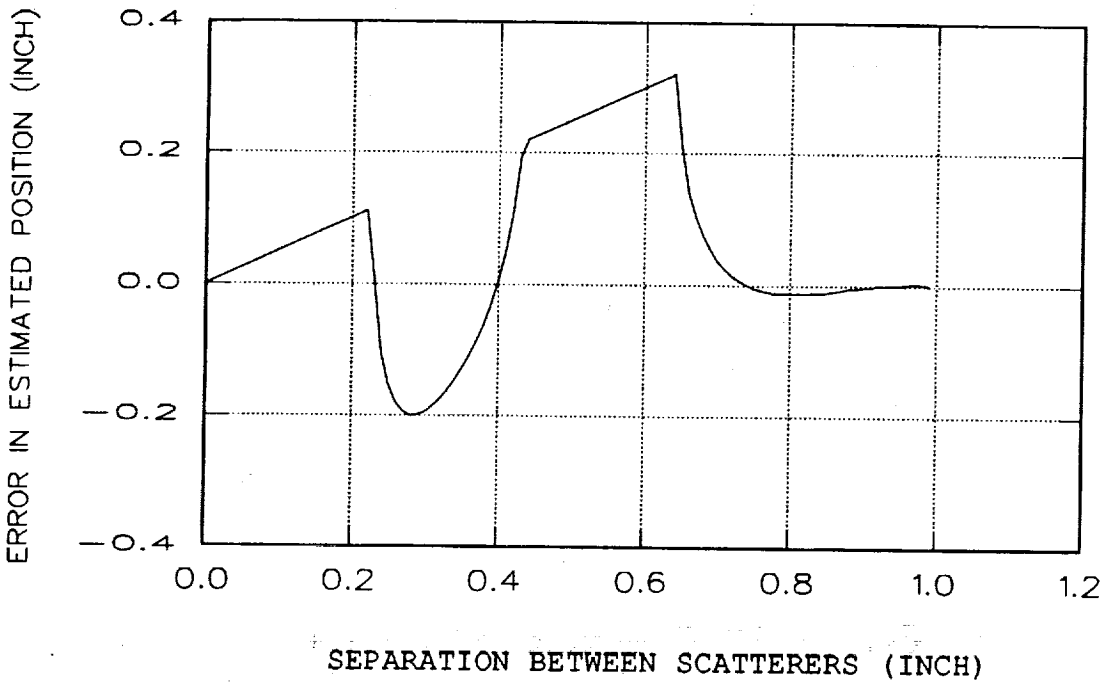

Figure 26: Error in estimated position versus separation distance between point scatterers.

between the estimated position of a scattering center and its actual position as a function of its distance from a scattering center of equal magnitude.

The behavior exhibited in Figure 26 dictates the validity of an individual peak. As two scattering centers approach each other the maximums for their corresponding peaks shift with respect to the actual down range position of the scattering centers. This distortion results in an error in the estimated position of the scattering center. The accuracy of the estimated position degrades as the two scattering centers approach each other in down range. This error is a result of the interference between the envelope terms of Equation (5.7) and specifically the interaction term. The probability that the location of the maximum of a peak corresponds to the actual down range position of the associated scattering center is dependent on the proximity of the nearest neighboring peak. Also, the larger the

amplitude of the neighboring peak, the greater its side lobe levels will be and the greater the impact it will have on the estimated position of the scattering center. Therefore, the validity of a peak is proportional to the distance of separation between it and its nearest neighbor, and inversely proportional to its nearest neighbor's relative magnitude.

As a practical example of the effects of interference on position estimation, consider again the target composed of corner reflectors for the look angle of -15 degrees. The envelopes of the target for this look angle are shown in Figure 27. The locations of the possible matches resulting from the envelopes of the target are shown in Figures 28 and 29. For this look angle the leading pair of corner reflectors are interfering to produce a single peak in A and pairs of peaks in B and C. The scattering centers resulting from these peaks lie outside the space defined by the maximum dimension limit, and therefore no scattering centers are associated with the leading corner reflectors. The second pair of corner reflectors are interfering to form one peak in each envelope. The resulting scattering center lies midway between the locations of the actual scattering centers. The scattering center corresponding to the largest corner reflector is estimated correctly, but some of its higher order effects are interfering with the return from the smaller corner reflector to cause its estimated position to deviate from its actual position as shown in Figures 28 and 29.

The behavior displayed in Figure 26 and in the example just presented leads one to redefine resolution between two scattering centers. Resolution is defined as the down range separation required between scattering centers to insure that the deviation in estimated position is within acceptable limits. The acceptable limits are determined by the error that can be tolerated in the estimated cross range position. From Equation (2.1) it is clear that small deviations in estimated down range position can result in

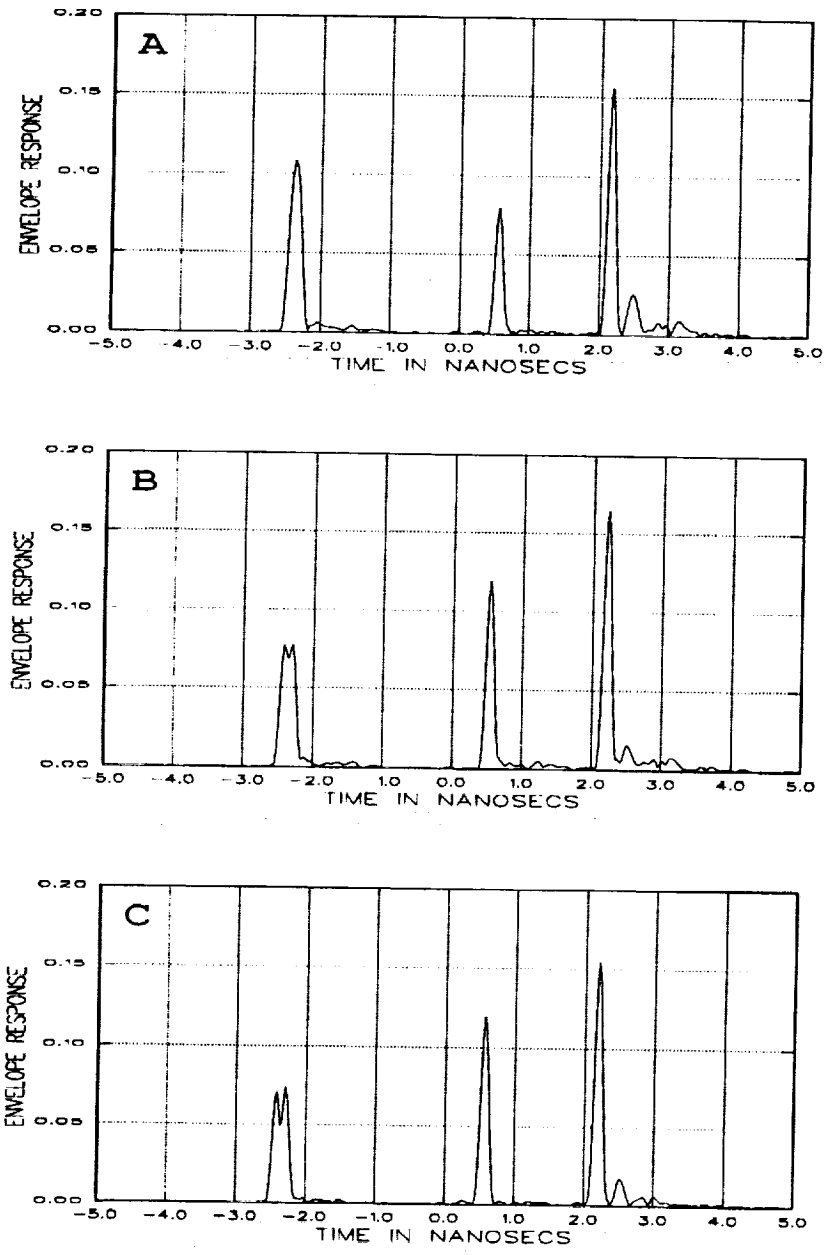

Figure 27: Envelope of each plane wave for corner reflectors at $\phi = -15°$.

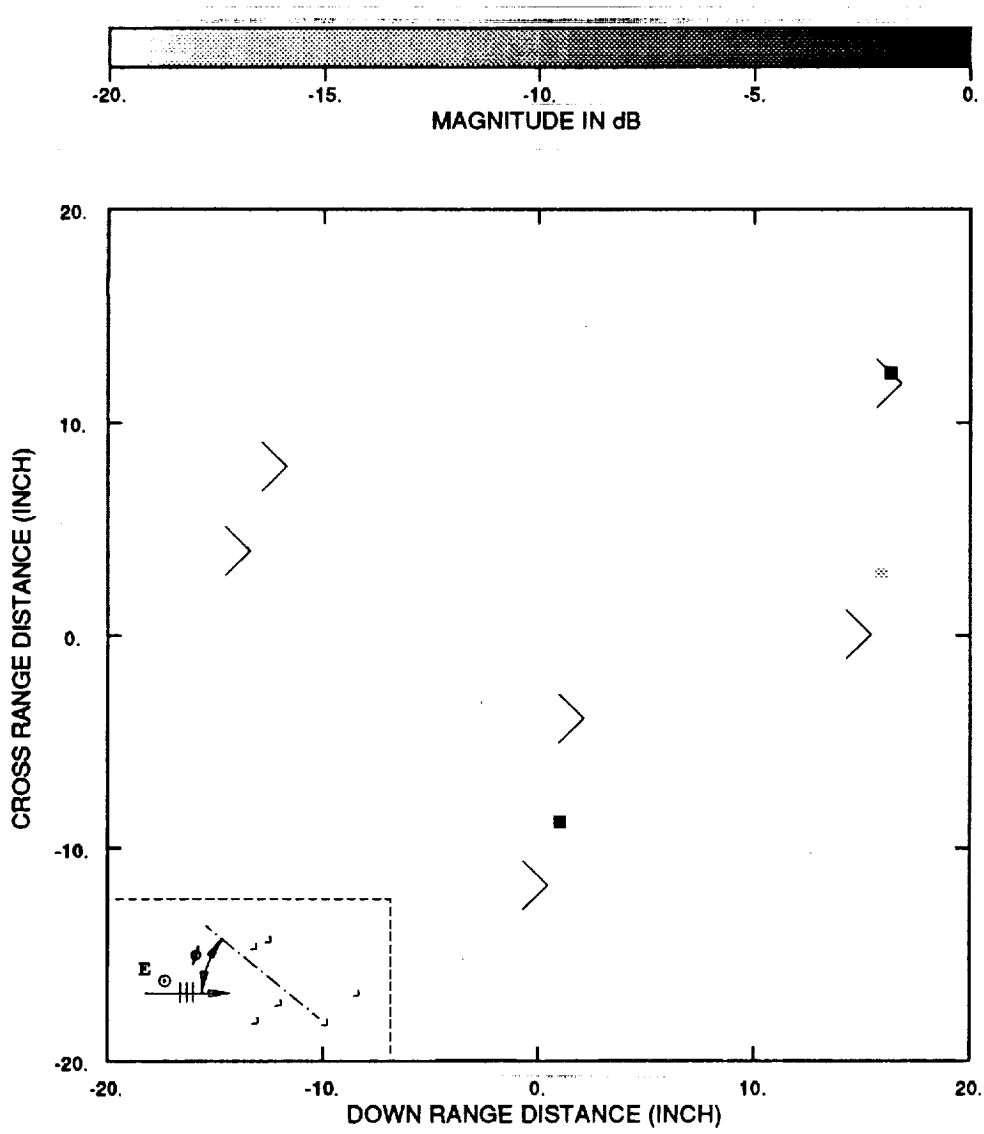

Figure 28: Top view of scattering centers resulting from measurements at $\phi = -15°$.

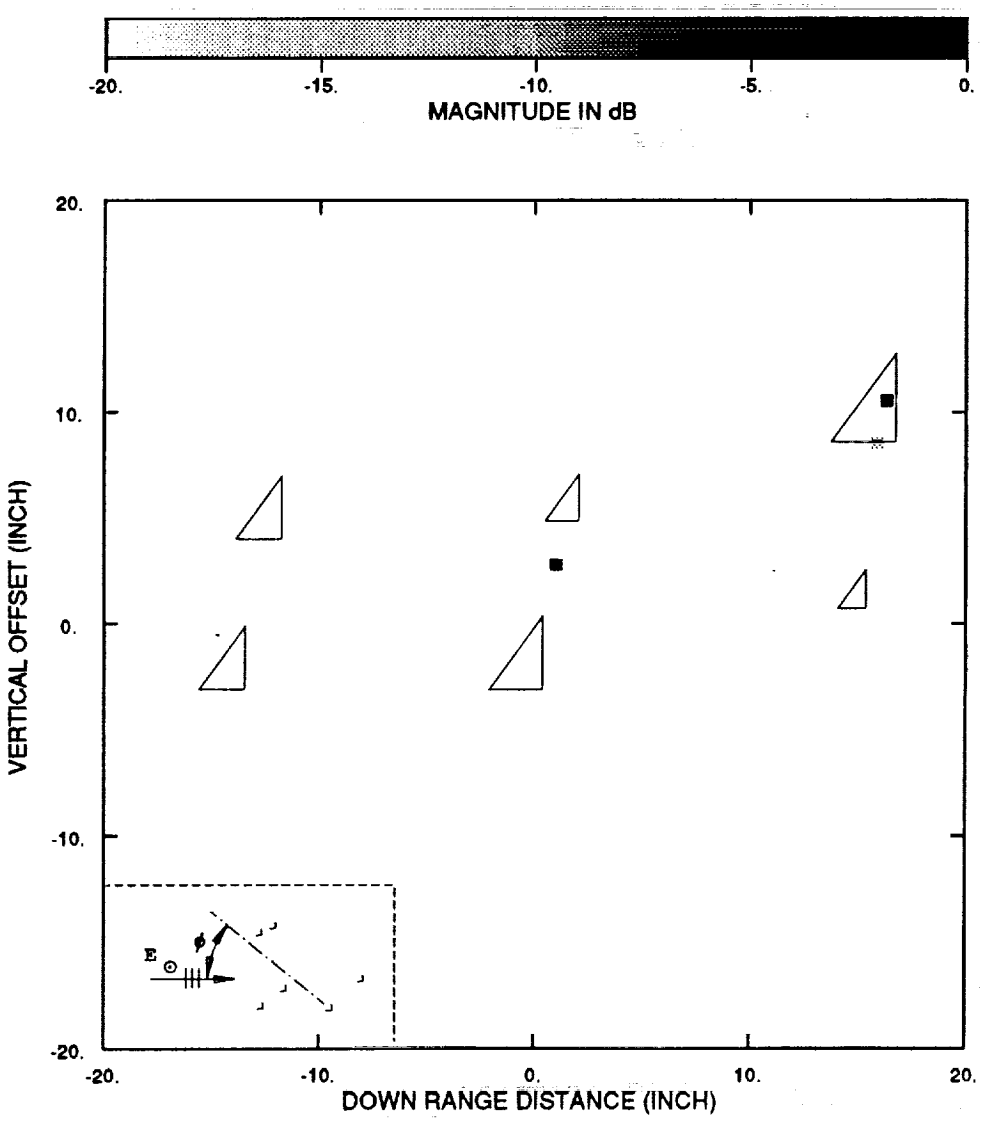

Figure 29: Side view of scattering centers resulting from measurements at $\phi = -15°$.

large deviations in estimated cross range position for small angles of separation between the illuminating plane waves. The limit used in this paper is determined by a requirement for a maximum cross range deviation of less than 0.5 inches for plane waves separated by one degree. With these requirements, the maximum resolution between point scatterers of equal magnitude is 0.8 inches.

5.3 Validity of Possible Matches

The validity of a possible match is a measure of the probability that two peaks correspond to the same scattering center and that the resulting position of the match is accurate, given the characteristics of each peak composing the match. The characteristics most important to the validity of a match are the relative amplitudes of the peaks, the validity of the individual peaks, and the number of possible matches for each peak making up the match. The envelopes of realistic targets often have peaks associated with the same scattering center whose magnitudes differ in the envelopes of the three plane waves. The variation in magnitude can be due to the dependence of the scattering center's magnitude on azimuth and aspect angle. The angular separation between the plane waves in this work though, is only one degree. Given this small offset, variation in amplitude between the envelopes is most likely due to interference from other scattering mechanisms. An illustration of this problem is shown in Figure 27. For the look angle at which these envelopes were generated, the middle pair of corner reflectors have down range positions close enough that they interfere to form one peak in each envelope. There exists only one possible match to correspond to each of the three peaks and that is pictured in Figures 28 and 29. Note that the individual peaks have high validity because they have no significant neighbors, even though they generate an incorrect estimated

position for the scattering center. The difference in amplitude between the peaks is the key indicator that the position of the possible scattering center, estimated from these peaks, may not reflect the actual scattering center's position. In this case, the possible scattering center lies midway between the two actual scattering centers. The measure of validity associated with this phenomenon is inversely proportional to the difference in amplitude of the peaks.

Another characteristic of an individual peak which affects the validity of a possible match is the number of possible matches with which a peak is associated. This is generally not a problem for smaller targets. For large targets though, a peak may have several possible matches. An example of such a case can be obtained by positioning two corner reflectors as shown in Figure 31 and increasing the maximum dimension specification. Consider the envelopes of Figure 30. In this case, the peaks would each have two possible matches. The resulting possible scattering centers are located in down range and cross range as pictured in Figure 31. Note that two possible matches exist for each peak, and both are equally likely. This ambiguity decreases the probability that either match is correct which reduces the validity of both.

5.4 Quantifying Validity

In the previous two sections, the impact of various phenomenon on the validity of possible scattering centers was discussed. Validity is defined by two criteria:

1. the peaks grouped together correspond to the same scattering center, and
2. the estimated position of a scattering center corresponds to its actual position.

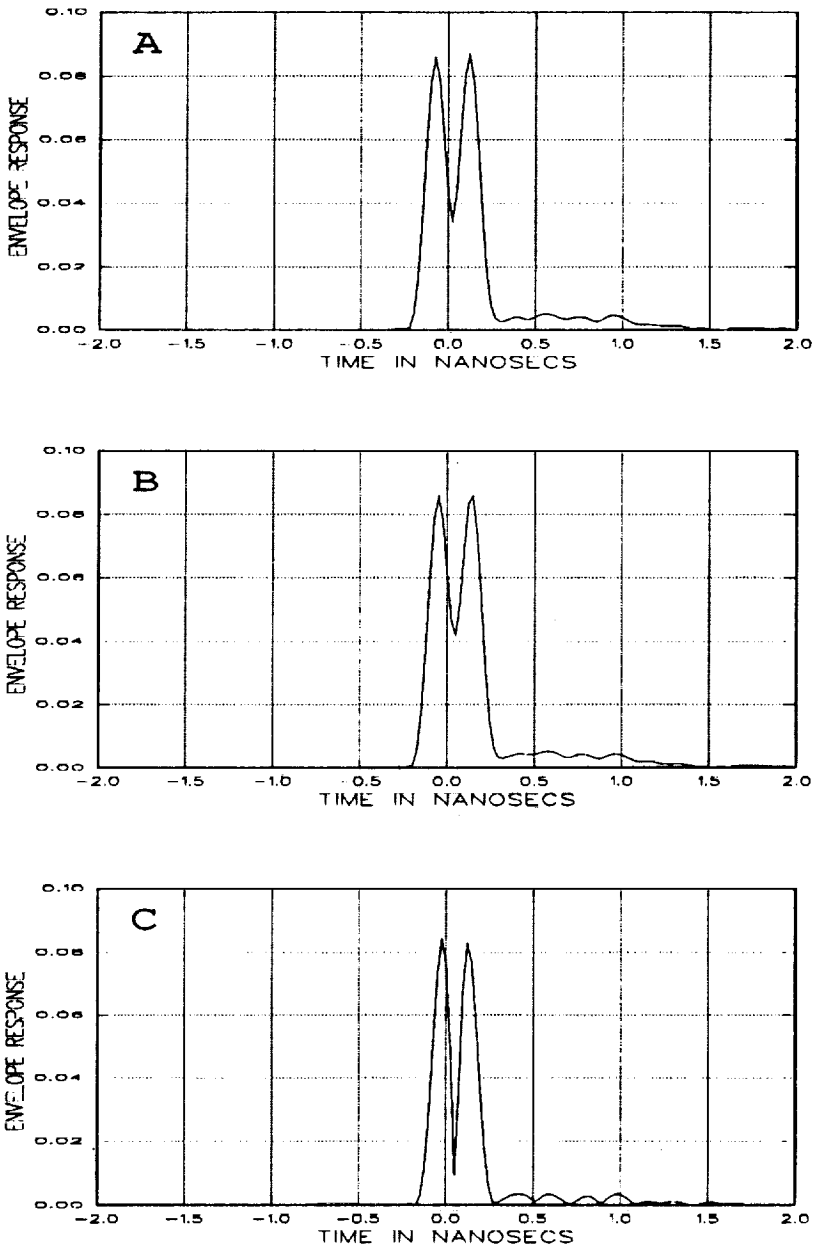

Figure 30: Envelope of each plane wave for corner reflectors at $\phi = 0°$.

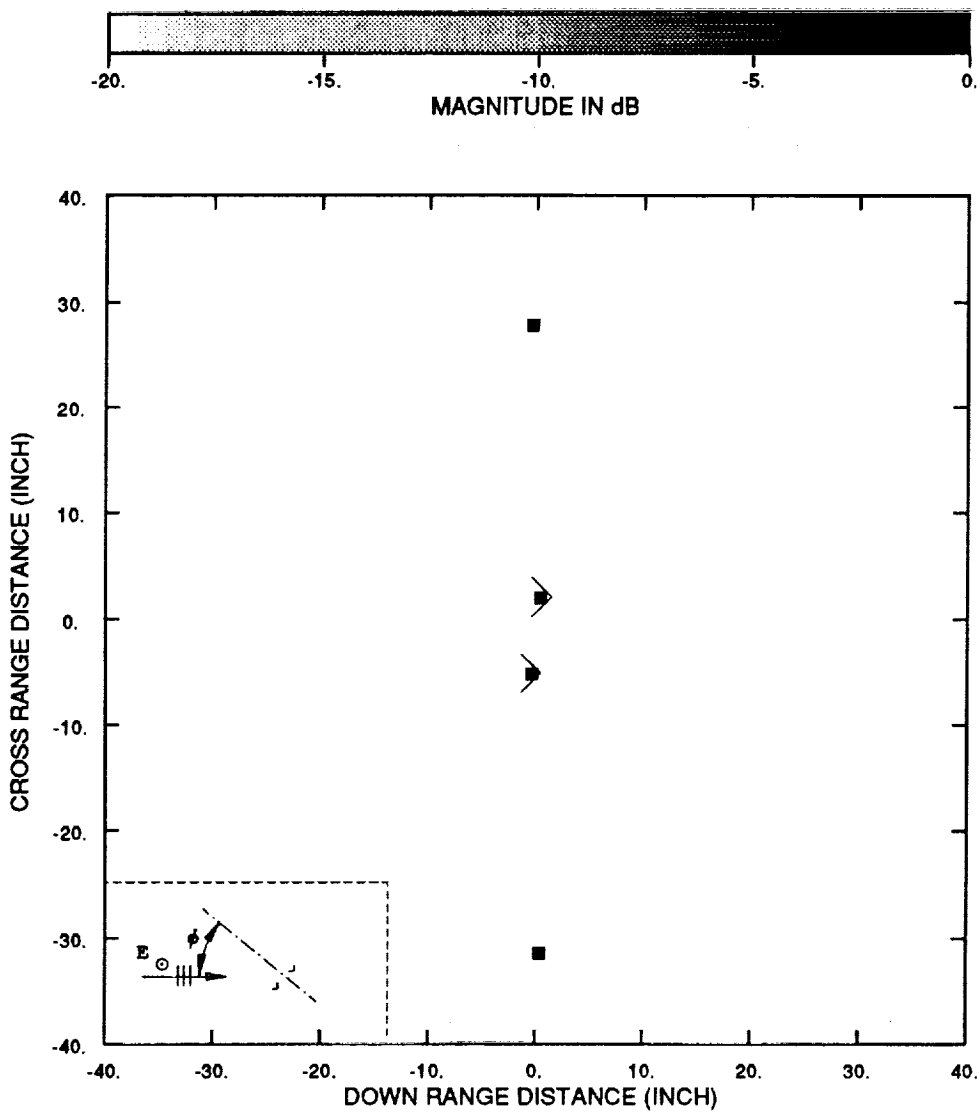

Figure 31: Top view of scattering centers resulting from measurements at $\phi = 0°$.

In order to determine which matches are most likely to correspond to actual scattering centers, as well as to determine the confidence in accuracy of a given match, it is necessary to quantify the validity of a match. The method presented here to quantify the validity of a match is similar to that presented by Boyer in [2], which deals with the corresponding problem in stereo vision.

In the previous two sections, it was demonstrated that the way of evaluating the validity of a match from the information available in the envelope, was by evaluating the characteristics of individual peaks. For this reason, it will be advantageous to express an antenna's envelope symbolically, in terms of the peaks composing it. Each peak extracted from an envelope has certain attributes. The previous sections identified the attributes of a peak: its position, its amplitude, the proximity and magnitude of its nearest neighbor, and the number of possible matches. Each of these attributes has an associated value. A natural way to represent a peak is as a member of the product set $\mathcal{A} \times \mathcal{V}$ such that

$$\mathbf{a}_i \subseteq \mathcal{A} \times \mathcal{V} \tag{5.8}$$

where $\mathcal{A}$ is a set of attributes, and $\mathcal{V}$ is a set of values for those attributes. An envelope can then be represented as a set of these peaks where

$$\mathbf{A} = \{\mathbf{a}_1, ..., \mathbf{a}_m\}. \tag{5.9}$$

Note that m is the number of peaks in the envelope of plane wave $\mathbf{A}$. The envelope of a second plane wave, plane wave $\mathbf{B}$, with which the peaks of plane wave $\mathbf{A}$ are to match, can be similarly defined as

$$\mathbf{B} = \{\mathbf{b}_1, ..., \mathbf{b}_n\}. \tag{5.10}$$

Now that a symbolic representation of the set of peaks from the two plane waves has been established, a quantity corresponding to the validity of the matches between these two sets of peaks must be defined. Such a quantitative measure can be arrived at by modeling the matching process as an information channel. An information channel is described by giving an input alphabet such that

$$\mathbf{R} = \{r_j\}, \qquad j = 1, 2, ..., m \tag{5.11}$$

an output alphabet,

$$\mathbf{S} = \{s_k\}, \qquad k = 1, 2, ..., m, \tag{5.12}$$

and a set of conditional probabilities $P(r_j|s_k)$ for all j and k. $P(r_j|s_k)$ is the probability that the output symbol s_k will be received if the input symbol r_j is sent [1].

For matching purposes, an information channel connects a single attribute from a peak of plane wave **A** with the corresponding attribute of a peak of plane wave **B**. The input alphabet is the set of values the attributes take on for the peak of plane wave **A**. The output alphabet is the set of values the attributes take on for the peak of plane wave **B**. If one expresses an attribute value as a function $v_j(a_i)$, where the i^{th} attribute takes on the value v_j, then a peak from plane wave **A** can be expressed as a set of these values given by

$$\mathbf{a}_j = \{v_j(a_i)\} \qquad i = 1, ..., m. \tag{5.13}$$

Similarly, a peak from plane wave **B** can be expressed as

$$\mathbf{b}_k = \{v_k(a_i)\} \qquad i = 1, ..., m. \tag{5.14}$$

In Sections 5.2 and 5.3, it was shown that the validity of a given match was dependent on the attributes of the peaks making up the match. This fact is expressed in terms of the conditional probabilities of the information channel. The conditional probabilities which characterize the information channel correspond to the probability that the peak of plane wave **A** matches the peak of plane wave **B**, based on the value of the i^{th} attribute for each peak. The conditional probability for the i^{th} attribute would be $P(v_j(a_i)|v_k(a_i))$. It should be noted that this probability includes not only the probability that the two peaks correspond to the same scattering center, but that its estimated position is also accurate.

The conditional probabilities presented above enable one to quantify validity based on the concept of information. If an event u_i occurs, one obtains an amount of information equal to

$$I(u_i) = log(\frac{1}{P(u_i)}) \text{ bits.} \tag{5.15}$$

In [1], $I(u_i)$ is interpreted as the information needed to make the occurence of u_i certain. Substitute $v_j(a_i)|v_k(a_i)$ as the event in Equation (5.15). The information measure of Equation (5.15) can now be interpreted as a quantity to measure the validity of a match. A liberty is now taken by renaming this information measure as a cost. Since each attribute has a cost associated with it, the total cost of a match is a sum of the costs of each attribute. The total cost of a match between the j^{th} peak of plane wave **A** and the k^{th} peak of plane wave **B** is a sum of the costs associated with the four possible attributes such that

$$COST_{j,k} = \sum_{i=1}^{4} log(\frac{1}{P(v_j(a_i)|v_k(a_i))}). \tag{5.16}$$

Obviously those matches of least cost are most likely to accurately estimate a scattering center's position. The details of determining the probability

density functions for each of the attributes is discussed in more depth in Appendix A.

5.5 Scattering Center Confirmation Through Rotation

Upon completing the evaluation for one look angle, one will have a set of data composed of possible scattering centers, their amplitudes, positions, and costs. The information acquired for one look angle gives an idea of the number of scattering centers on a target at a particular look angle. This information though, is insufficient to decide whether a scattering center is actually present or that its estimated position is correct. Even if the three peaks of a possible scattering center are correctly grouped, if there estimated positions are distorted, there is no way to determine the position of the actual scattering center. Both of these problems result from scattering centers which are located too closely to each other along the down range direction. A solution to these problems is to move the target so that the interfering scattering centers separate from each other in down range. In this work, the required separation is obtained by rotating the target with respect to the incident plane waves.

Given that the target is rotated to different look angles, the two problems presented in the last paragraph share a common characteristic. The scattering center, either erroneously identified or incorrectly located due to interference, appears over only a limited number of look angles. The error in estimated position as a function of the distance of separation is shown in Figure 26. As the target is rotated, the separation between interfering scattering centers in the down range direction changes. The distortion in the estimated down range position will therefore change and cause the estimated cross range and vertical offset of the scattering center to change

with changing look angle. When the target is rotated to a look angle where the two scattering centers separate sufficiently, the estimated positions of the scattering centers will be accurate. They will subsequently fall on the same place on the target over successive look angles until the scattering centers again experience interference.

Finding a scattering center at the same position on a target over consecutive look angles will be referred to as tracking. In this work, tracking is used to validate a scattering center. The need for tracking was demonstrated in Figures 27 - 29. Most of the possible scattering centers resulting from these envelopes were either located incorrectly or fell outside the target zone. In order to resolve the scattering centers the target is rotated. Figures 32 - 34 show the results for measurements taken at -10 degrees. Note the leading corner reflectors are separating in the down range direction and are located fairly accurately on the target body. The middle pair of corner reflectors is still suffering interference resulting in distorted estimated positions. The large corner reflector's position is estimated accurately but it is now swamping the return from the smaller reflector. If the possible scattering centers are analyzed over a sufficient angle width, all of the primary scattering centers will emerge from interference and can be tracked. Figures 35 and 36 show the result of applying the tracking routine to measurements taken from -15 degrees to +10 degrees at 1 degree intervals. In this case, all the scattering centers are correctly located and the amplitude responses indicate the difference in corner reflector sizes. For more detailed information concerning the tracking algorithm, one should refer to Appendix B.

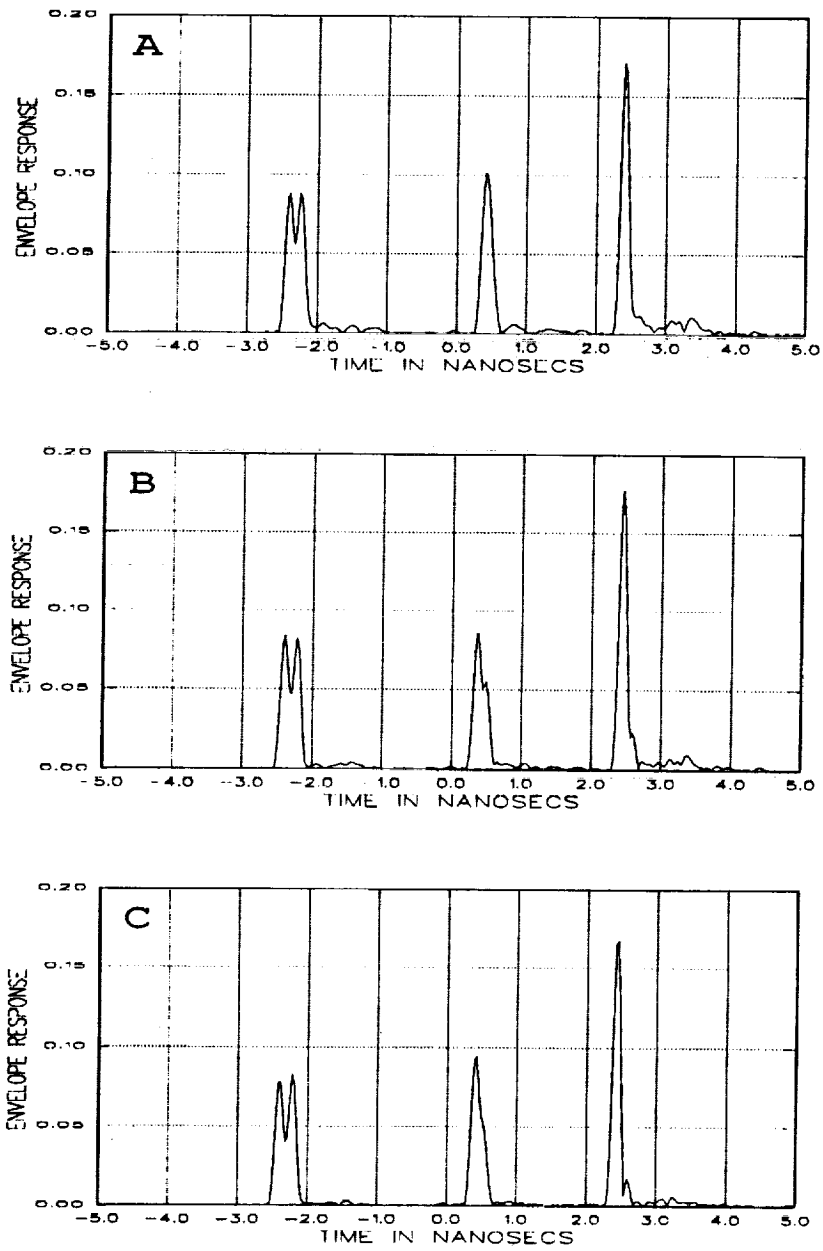

Figure 32: Envelope of each plane wave for corner reflectors at $\phi = -10°$.

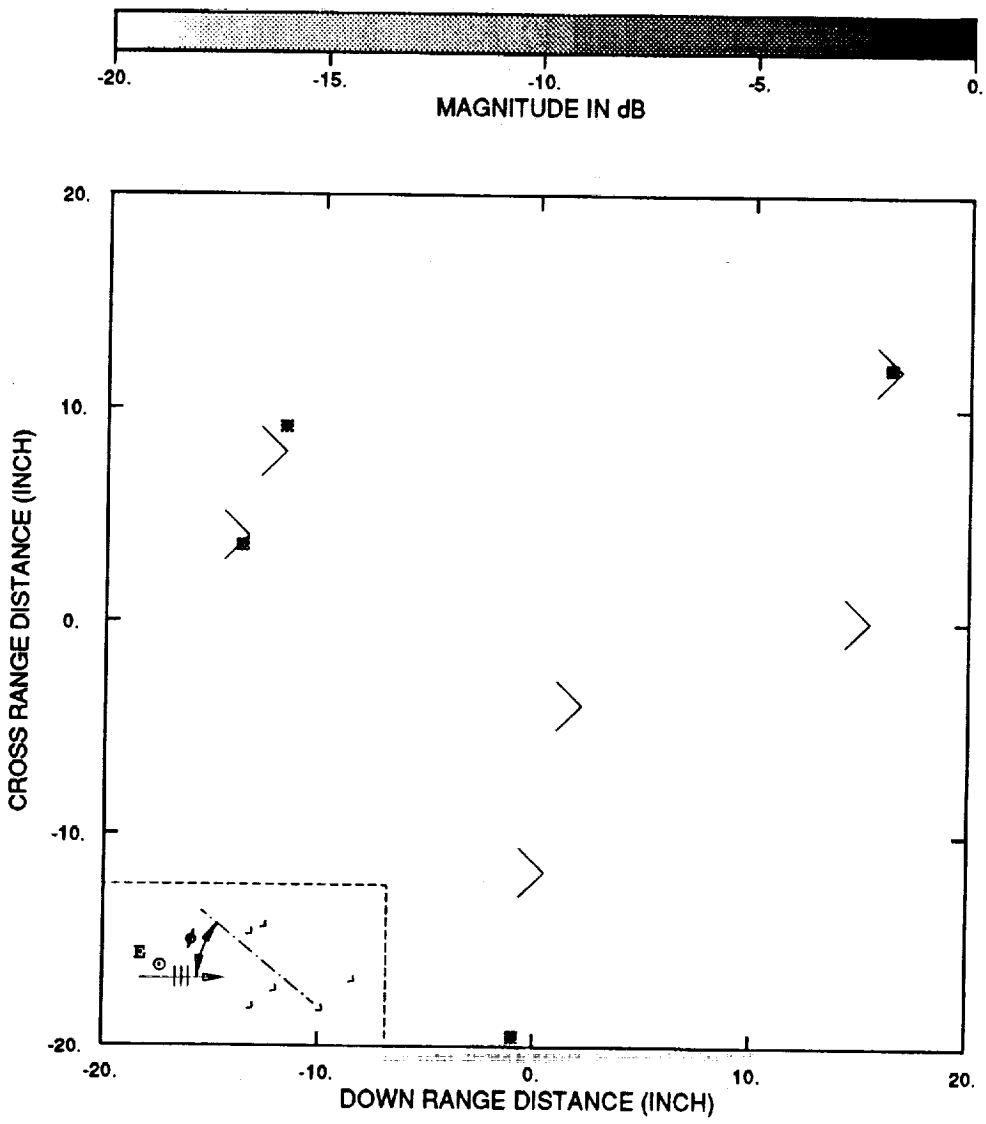

Figure 33: Top view of scattering centers resulting from measurements at $\phi = -10°$.

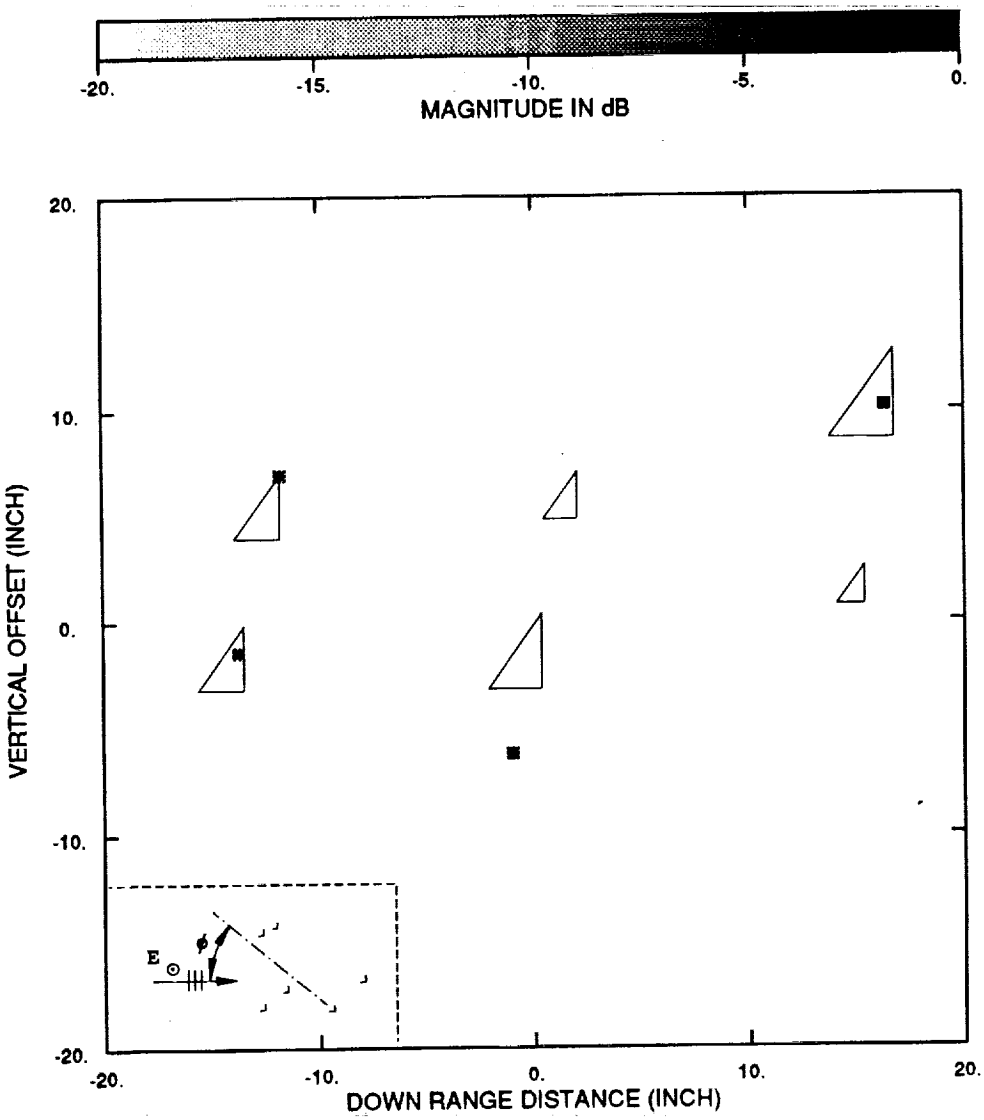

Figure 34: Side view of scattering centers resulting from measurements at $\phi = -10°$.

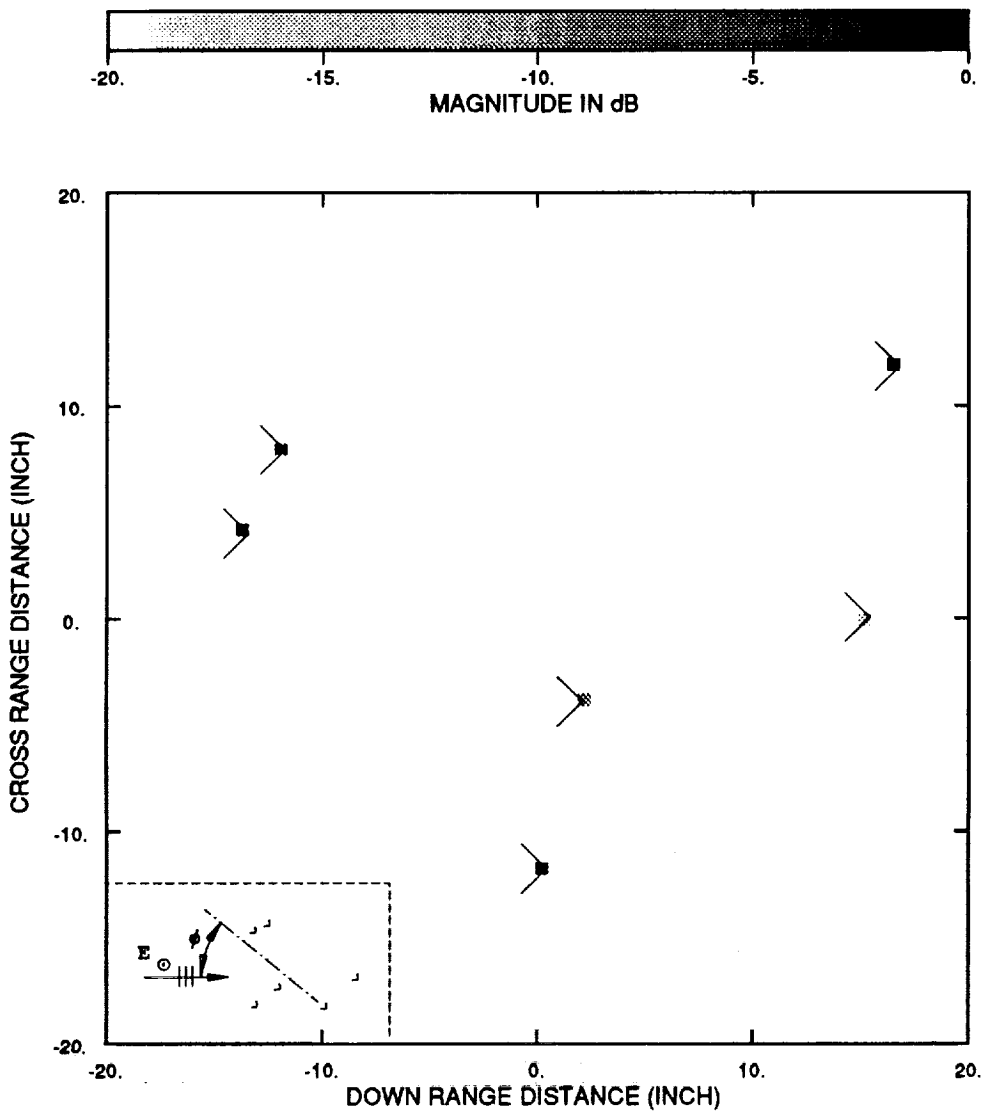

Figure 35: Top view of scattering centers obtained by tracking from $\phi = -15°$ to $\phi = 10°$.

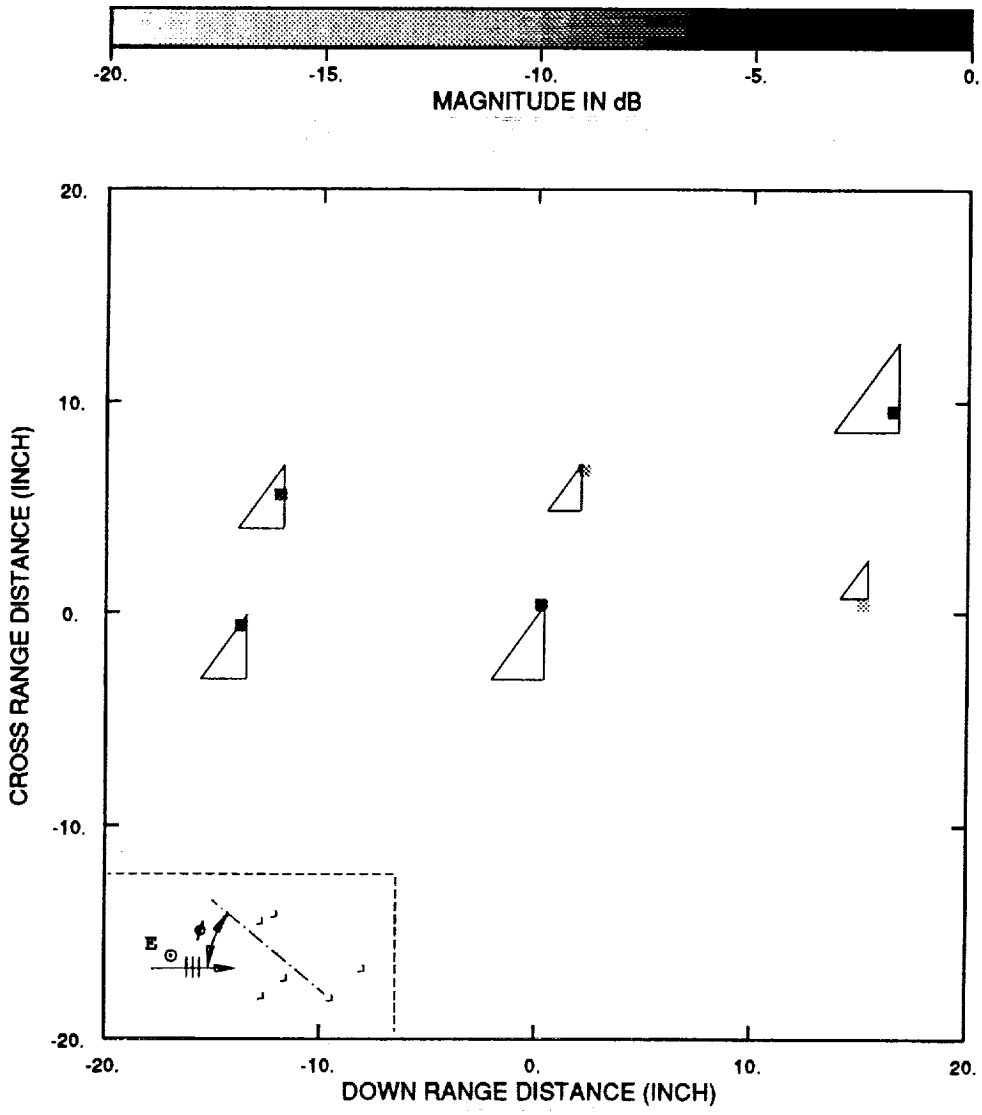

Figure 36: Side view of scattering centers obtained by tracking from $\phi = -15°$ to $\phi = 10°$.

Chapter 6

Three Dimensional ISAR Generated Images

As discussed earlier an RCS image generated from ISAR processing is used to determine the relative amplitudes, down range, and cross range positions of the scattering centers of a target. In this chapter, a method is presented to use images generated from measurements taken by vertically offset antennas to determine the location of scattering centers in three dimensions.

Consider the two coordinate systems shown in Figure 37. Coordinates t_x, t_y, and t_z correspond to the down range, cross range, and vertical offset axes, respectively, referenced to plane wave A. Coordinates $\bar{t}_x$, $\bar{t}_y$, and $\bar{t}_z$ correspond to the down range, cross range, and vertical offset with respect to plane wave C. The relationship between the two coordinate systems is a rotation of γ about the t_y axis, such that

$$\bar{t}_x = t_x \cos\gamma + t_z \sin\gamma \tag{6.1}$$

$$\bar{t}_z = -t_x \sin\gamma + t_z \cos\gamma, \text{ and} \tag{6.2}$$

$$\bar{t}_y = t_y. \tag{6.3}$$

In Chapter 3, the scattering behavior of the target was characterized as a reflectivity density function in three dimensions $\mu(t_x, t_y, t_z)$. The image

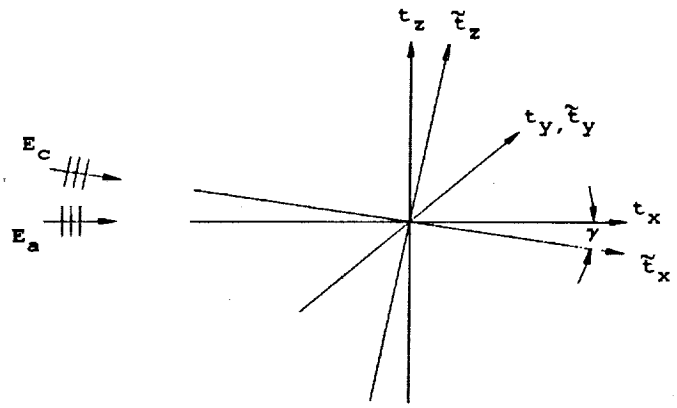

Figure 37: Offset coordinate systems.

generated from measurements taken in the t_x, t_y plane was shown to be the projection of the three dimensional reflectivity function onto the t_x, t_y plane, $\mu_a(t_x, t_y)$. Similarly, the image generated by the backscatter measurements from plane wave C is the projection of $\mu(t_x, t_y, t_z)$ onto the $(\tilde{t}_x, \tilde{t}_y)$ plane, where

$$\mu_c(\tilde{t}_x, \tilde{t}_y) = \int_{-\infty}^{\infty} \mu(\tilde{t}_x, \tilde{t}_y, \tilde{t}_z) d\tilde{t}_z. \tag{6.4}$$

Assume now that a scattering center is located at (t_{x0}, t_{y0}, t_{z0}). The scattering center's position in the image of A is (t_{x0}, t_{y0}), and its position in the image of C is $(t_{x0} \cos\gamma + t_{z0} \sin\gamma, t_{y0})$. By knowing the position of the scattering center in both images and the angle of separation between the antennas, the vertical offset of the scattering center is determined from the relation:

$$t_z = \frac{\{\tilde{t}_x - t_x \cos\gamma\}}{\sin\gamma} \tag{6.5}$$

which, for small angles of separation, is

$$t_z = \frac{\{\tilde{t}_x - t_x\}}{\gamma}. \tag{6.6}$$

This simple result is used to identify the locations of scattering centers in three dimensions.

The two tasks which must be accomplished in order to apply this result are to identify the scattering center in the images for plane waves A and C, and to determine the offset in the down range direction between the two images. Scattering centers are identified in down range and cross range by locating peaks in the envelope of the image of plane wave A. Once a peak is identified, the image of the scattering center associated with that peak is extracted from the total image. The image of the scattering center is then correlated with the image for plane wave C to determine its offset in the down range direction. From this value the vertical offset is calculated.

In order to demonstrate the validity of this approach please refer back to the target composed of corner reflectors shown in Figure 22. Figure 38 is an image generated from ISAR measurements taken of this target. The measurements were taken from 2-18 GHz at 40 MHz steps over a 20 degree sweep at .25 degree steps. By applying the technique just presented to the images of both plane waves, the scattering centers shown in Figures 39 and 40 were obtained. Note that each of the scattering centers associated with the corner reflectors are correctly located. The following chapter will present the results of this technique applied to a more realistic target.

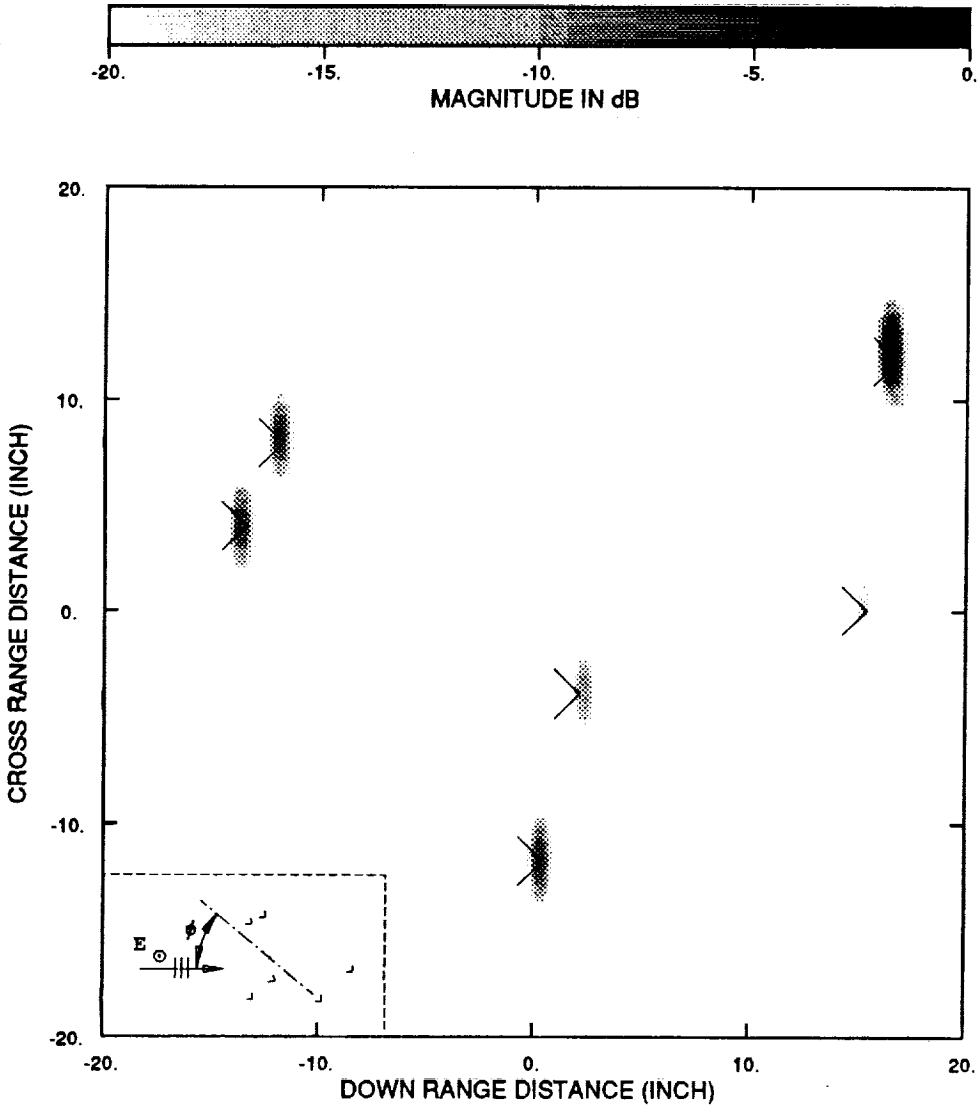

Figure 38: Image of scattering centers resulting from ISAR measurements from $\phi = -10°$ to $10°$.

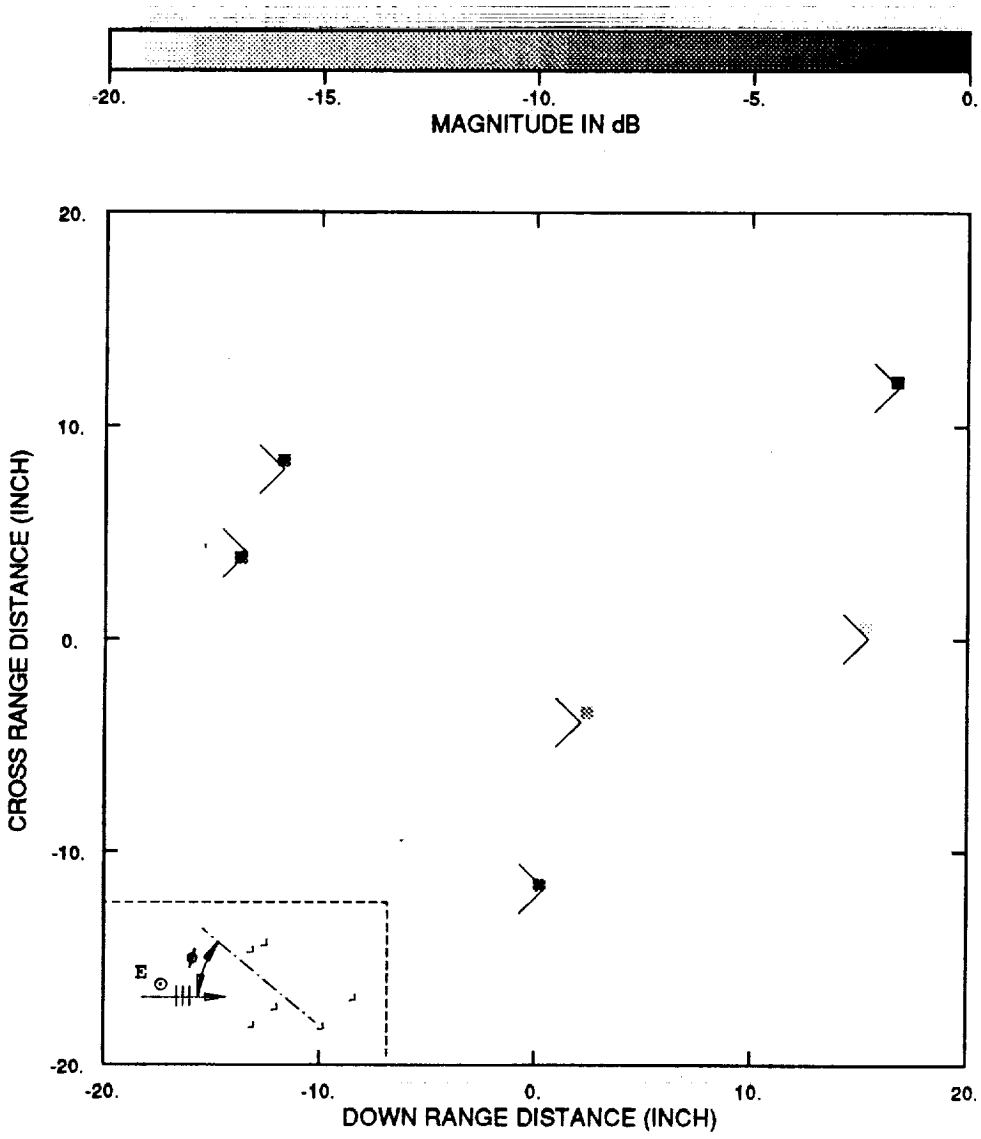

Figure 39: Top view of scattering centers resulting from measurements at $\phi = 0°$.

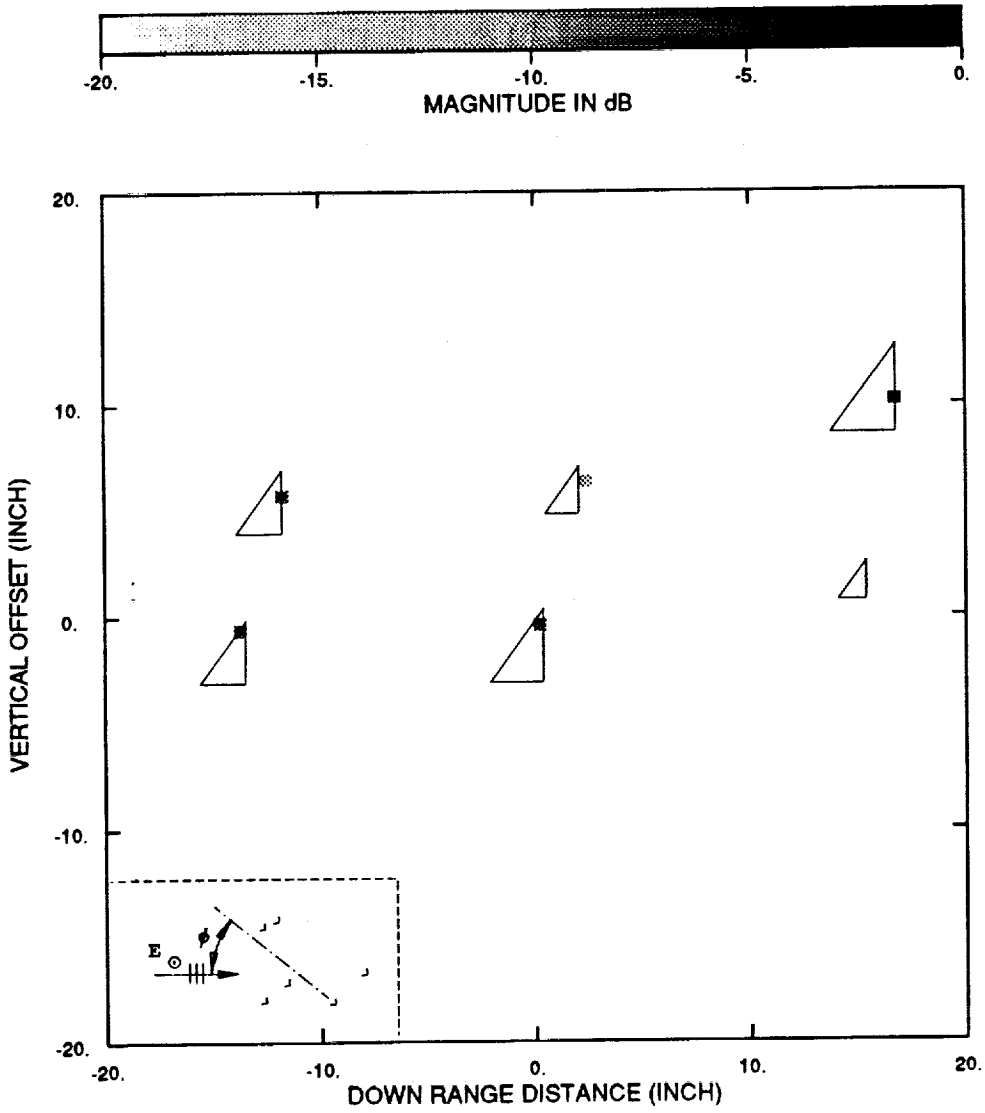

Figure 40: Side view of scattering centers resulting from measurements at $\phi = 0°$.

Chapter 7

Results Using a Complex Real-World Target

7.1 Locating Scattering Centers in Three Dimensions Using Two Dimensional Images

In Chapter 6, a technique was introduced to identify the three dimensional positions of scattering centers using two dimensional images generated from ISAR measurements taken by vertically offset antennas. This technique was shown to work well in identifying and locating the scattering centers of the target composed of corner reflectors. Having shown that the basic concept is sound, it is now appropriate to apply the technique to a real world target. The target chosen for this demonstration is the fighter aircraft shown in Figure 41. This target has a relatively low radar cross section and much of the significant scattering comes from tips and corners of the aircraft's structure as well as discontinuities along its surface. Due to the aircraft's relatively small size and the complexity of the target, there is a high density of scattering centers on the target. For these reasons, the target is a challenging test case for determining the three dimensional positions of the scattering centers, and it demonstrates the effectiveness of the technique.

Figure 41: Generic fighter aircraft.

The images used in this section are generated from ISAR measurements sampled from 2-18 GHz at 40 MHz steps over a 20 degree sweep at .25 degree intervals.

The first step in locating the positions of scattering centers in three dimensions is to locate the scattering centers in down range and cross range. The two dimensional image generated from the ISAR measurements for the aircraft at an angle of 10 degrees is shown in Figure 42. Since the aircraft at this angle has a very small radar cross section, the prominent mechanisms present in the image correspond to the tips or corners of the aircraft as well as the discontinuities along the surface of the body of the aircraft. The

result of identifying and extracting the mechanisms is shown in Figure 43. Note that the scattering centers are identified by the technique presented in Chapter 6 and correspond to the expected scattering features on the aircraft.

After finding the significant scattering centers of the target in one image, it is then necessary to correlate the image of the individual scattering centers with the image generated from measurements taken by the vertically offset horn. Figure 44 shows the results of performing this operation on the offset images of the aircraft at 10 degrees. Note the accuracy of the positions determined by this technique. The wing features fall right along the wing, the top of the engine inlet is located appropriately, and the back tip of the vertical stabilizer is located accurately. Also note the return located below the body of the aircraft which corresponds to the styrofoam mount used to hold the aircraft during the measurement. This plot shows that even on complex real-world targets, this technique is effective in determining the positions of scattering centers in three dimensions.

Figures 45 - 52 show the results for several other look angles. In these images, one can see the changing scattering behavior of the aircraft with changing look angle. The dominance of the specular term from the leading edge of the wing at 20 degrees and the canard at 40 degrees are very apparent. After passing through these look angles, the significant scattering again results from the tips and corners of the aircraft. These plots clearly demonstrate the ability of this technique to accurately locate the positions of the scattering mechanisms.

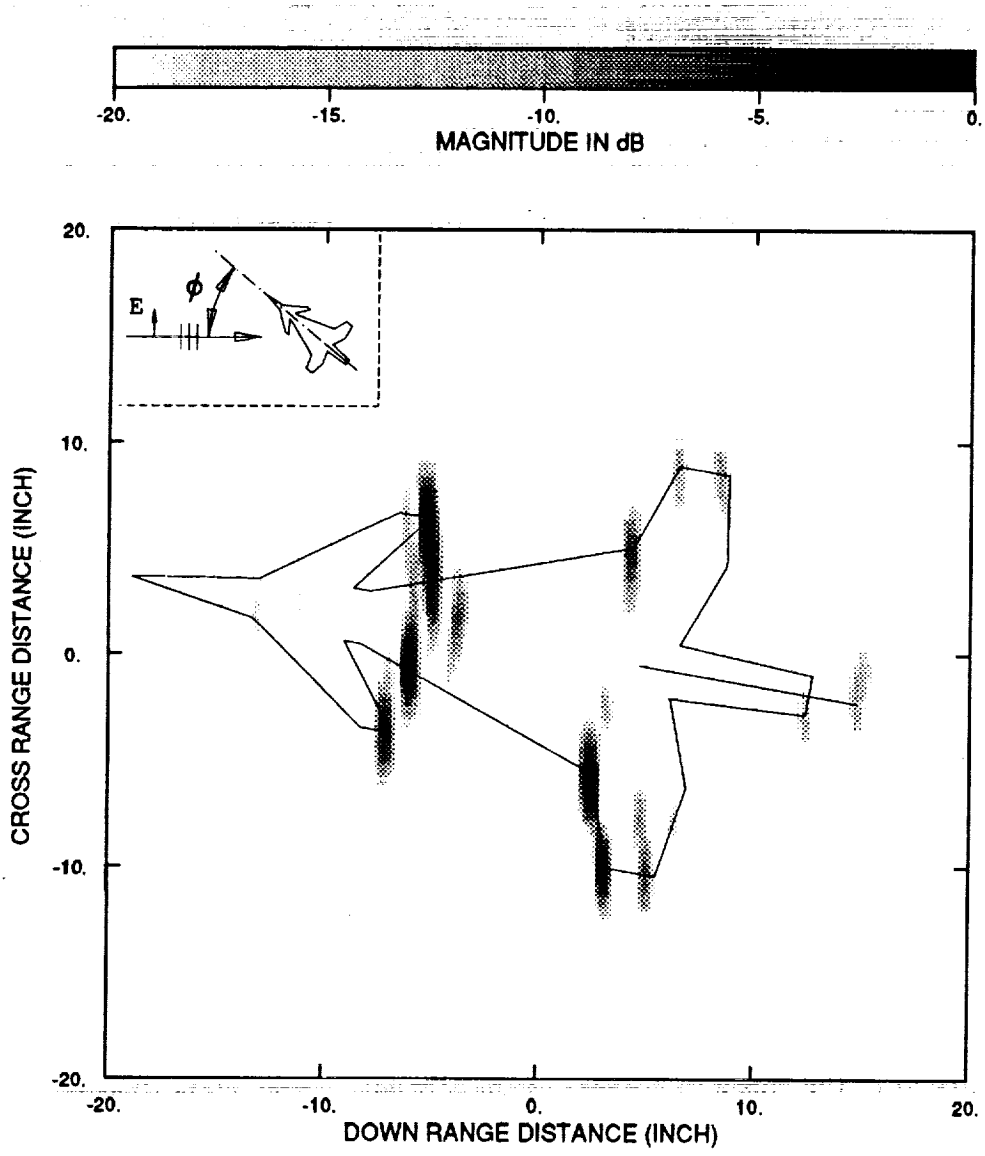

Figure 42: Two dimensional ISAR image of aircraft centered at $\phi = 10°$.

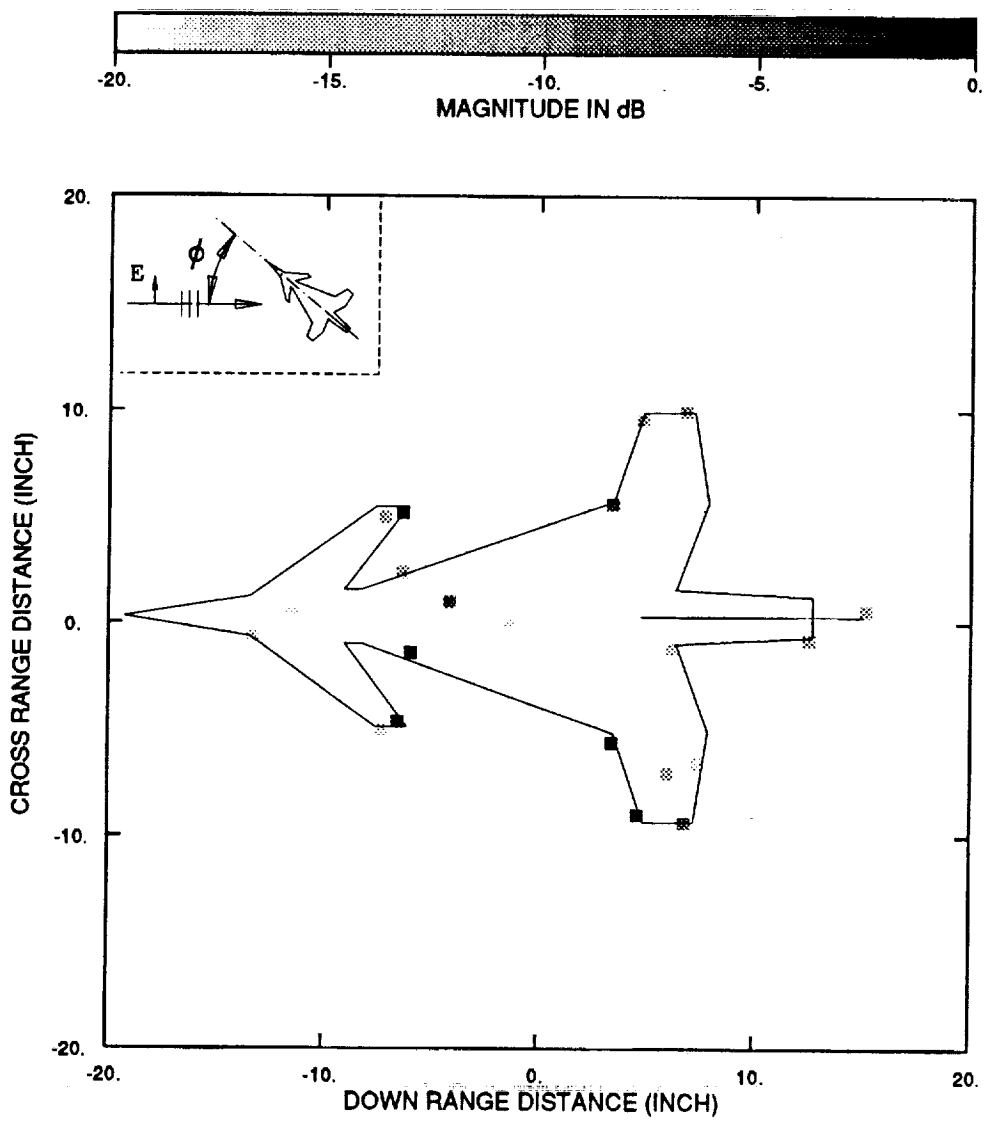

Figure 43: Top view of scattering centers resulting from ISAR measurements centered at $\phi = 10°$.

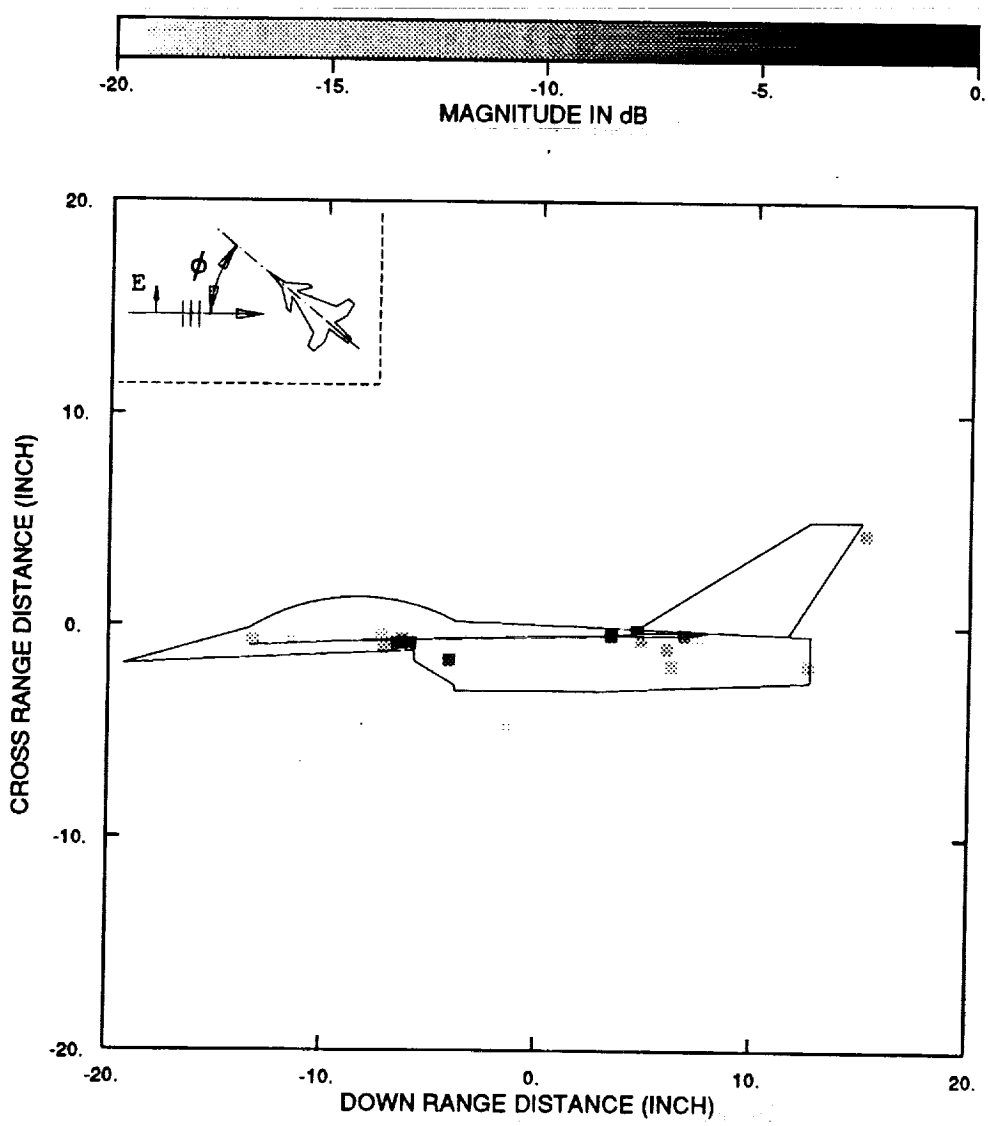

Figure 44: Side view of scattering centers resulting from ISAR measurements centered at $\phi = 10°$.

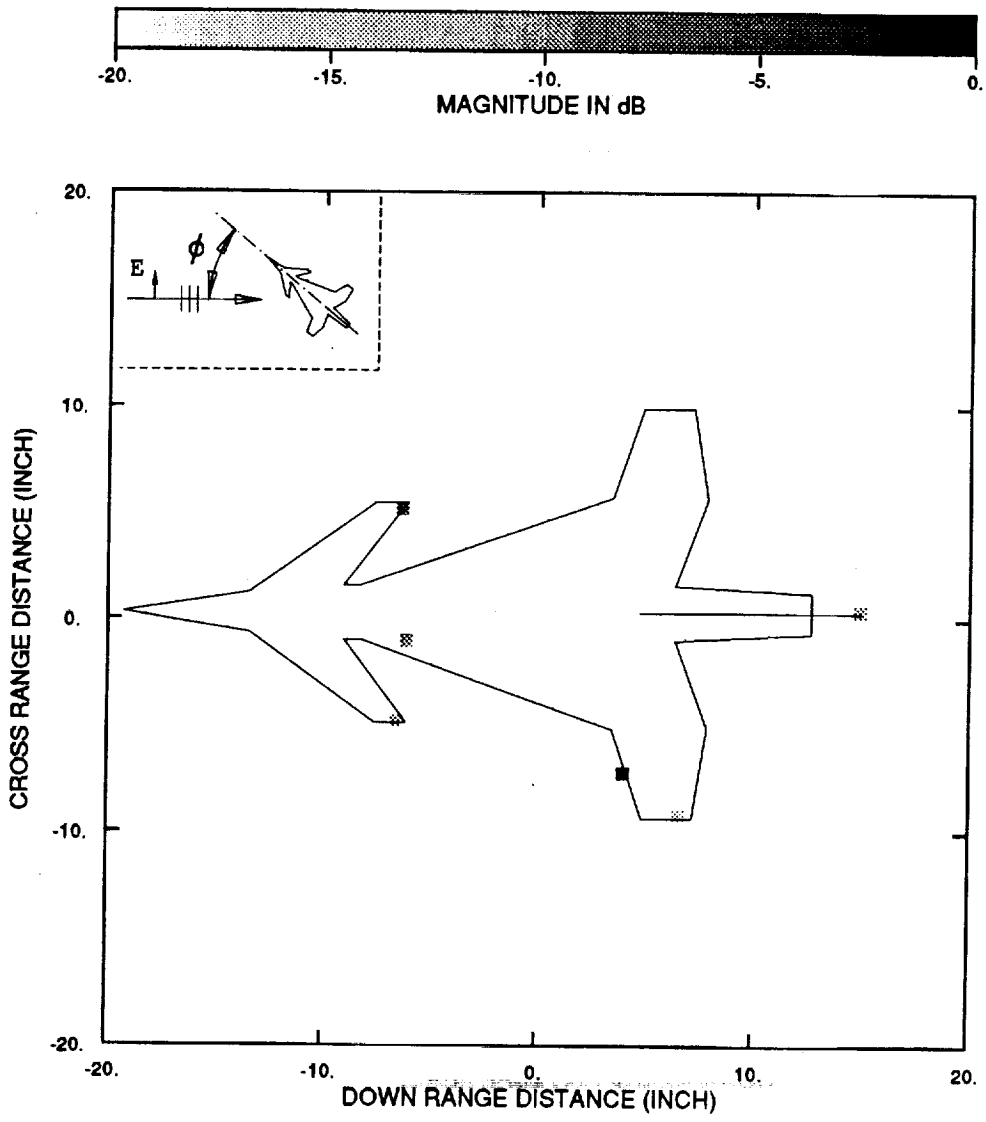

Figure 45: Top view of scattering centers resulting from ISAR measurements centered at $\phi = 20°$.

C-2

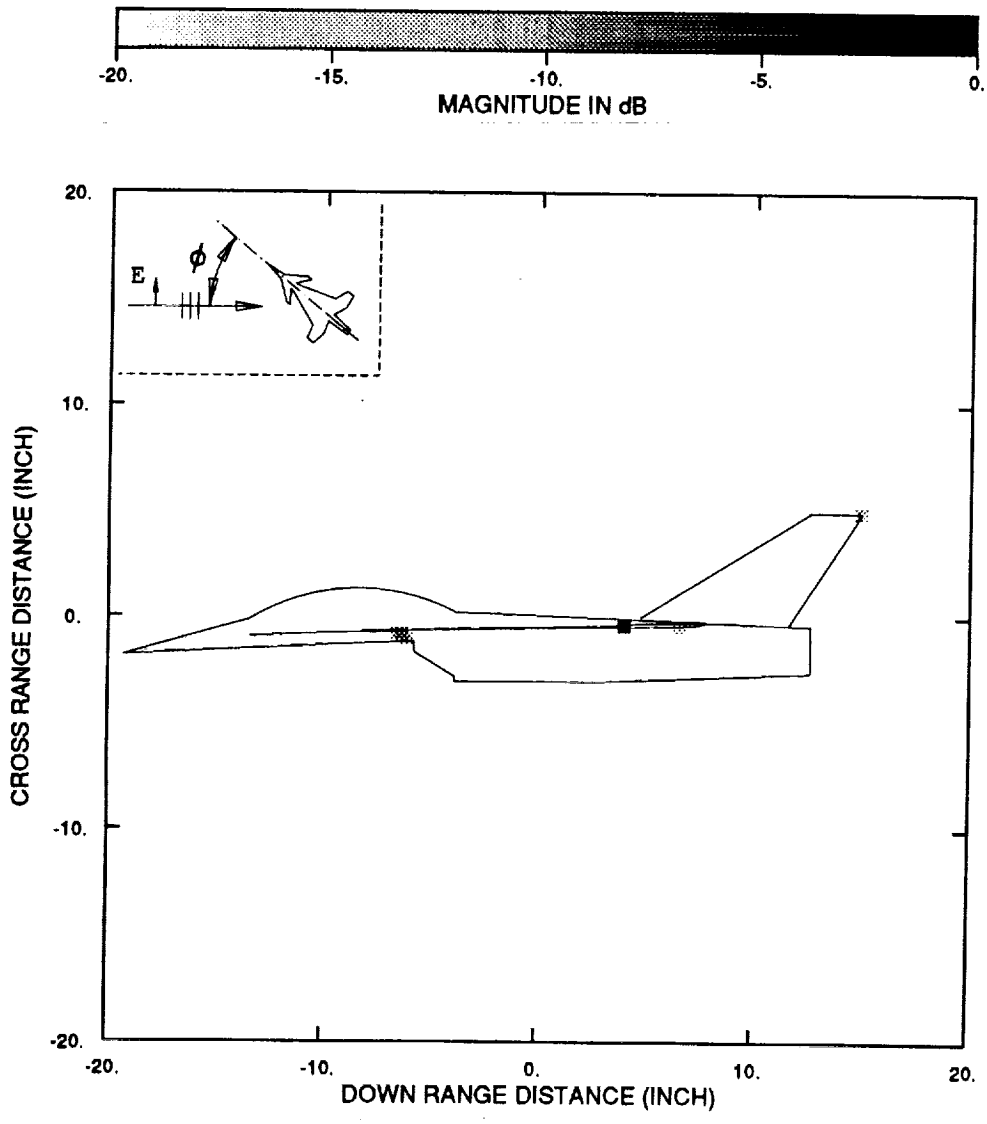

Figure 46: Side view of scattering centers resulting from ISAR measurements centered at $\phi = 20°$.

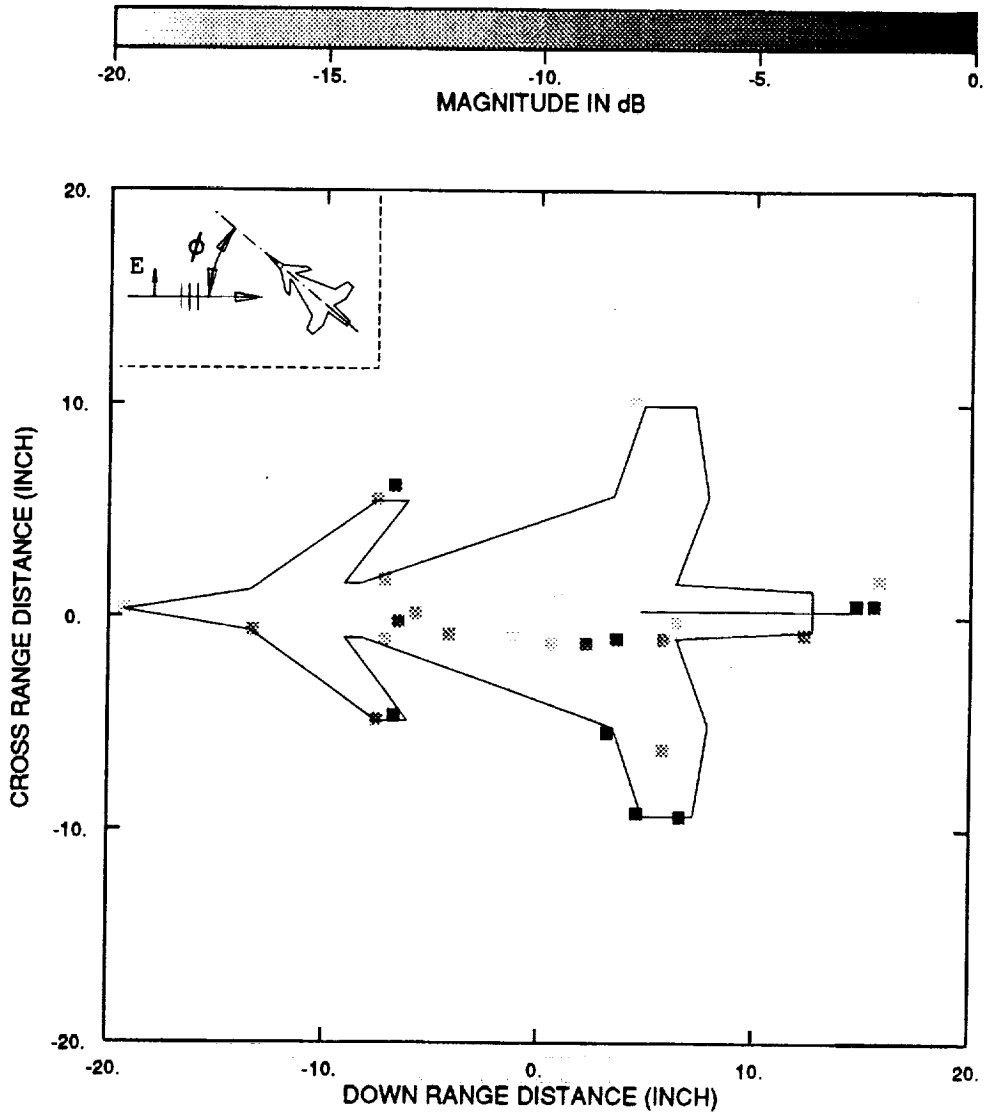

Figure 47: Top view of scattering centers resulting from ISAR measurements centered at $\phi = 30°$.

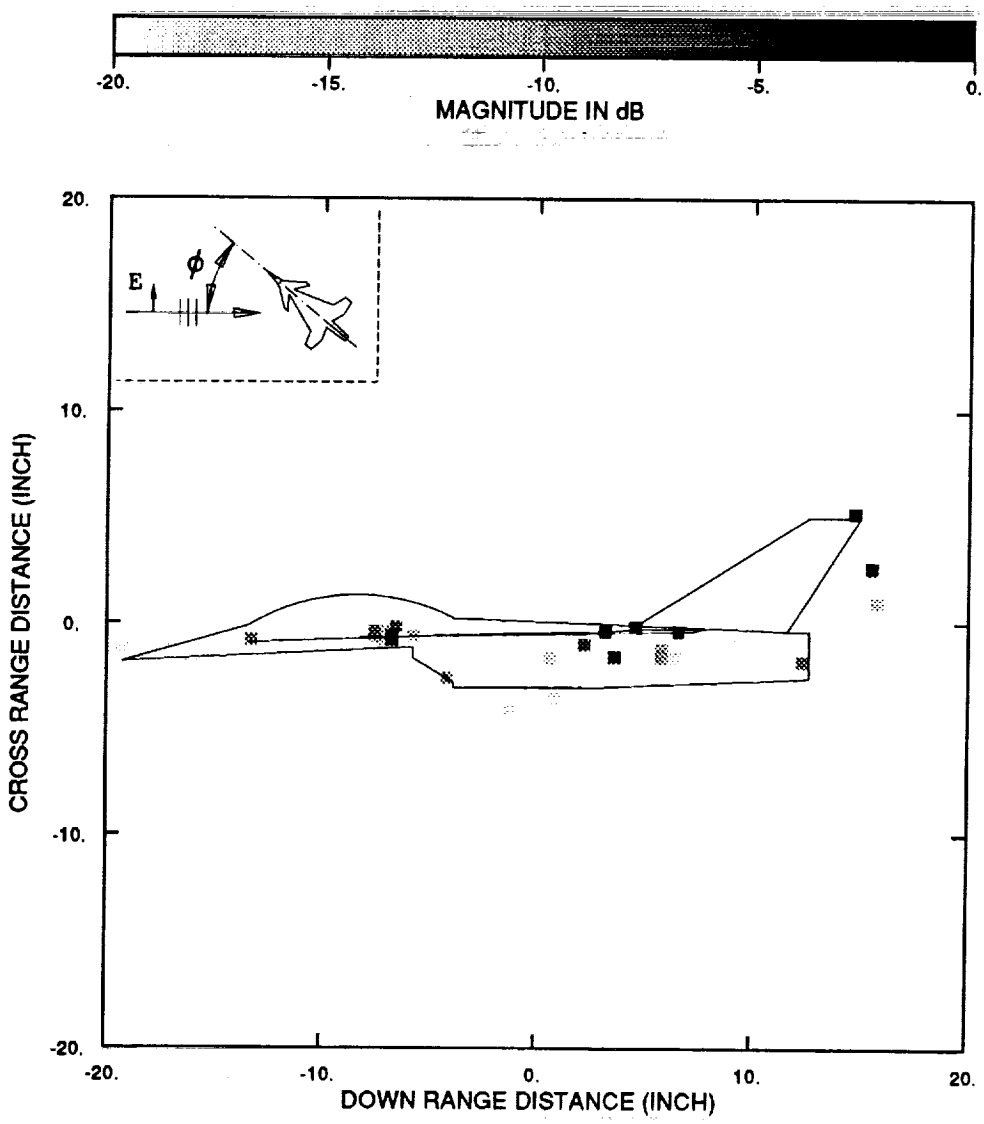

Figure 48: Side view of scattering centers resulting from ISAR measurements centered at $\phi = 30°$.

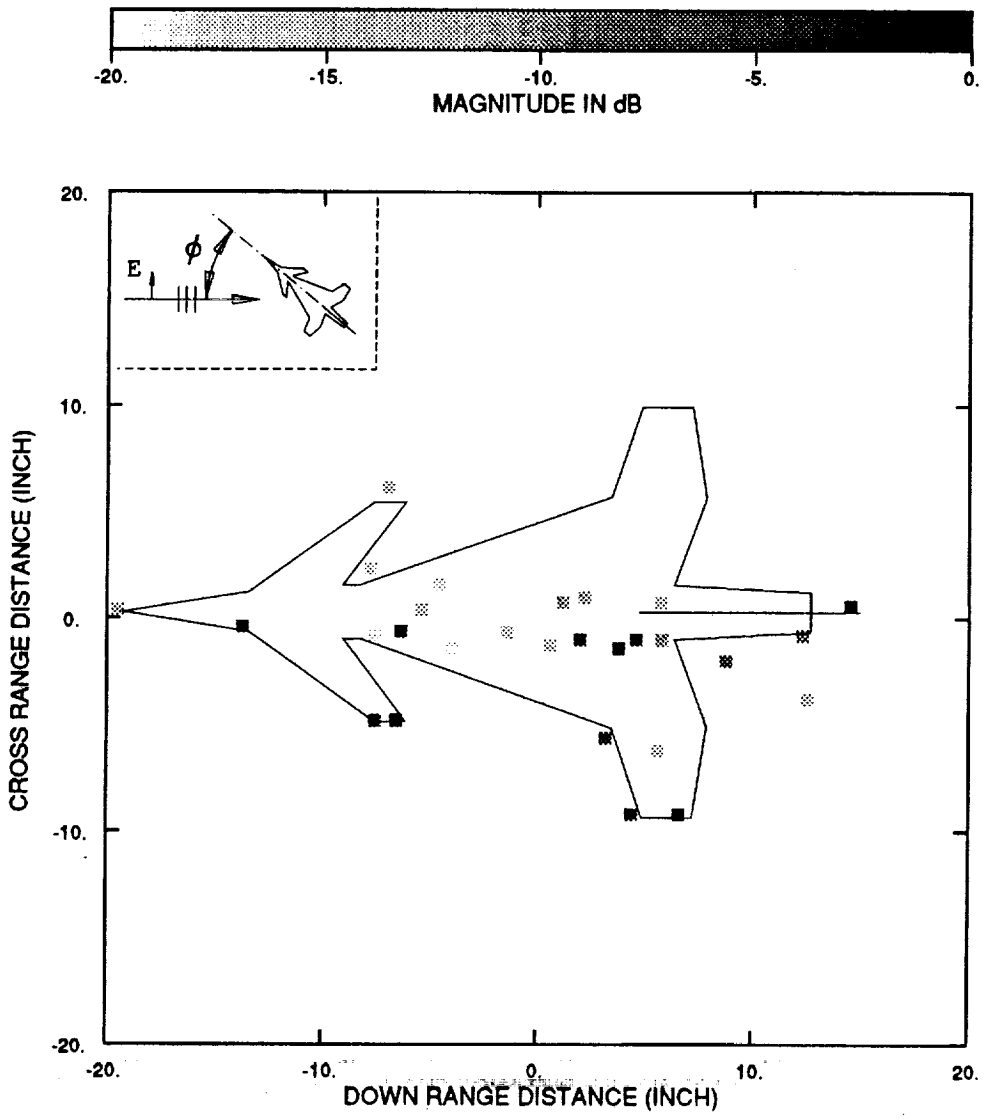

Figure 49: Top view of scattering centers resulting from ISAR measurements centered at $\phi = 40°$.

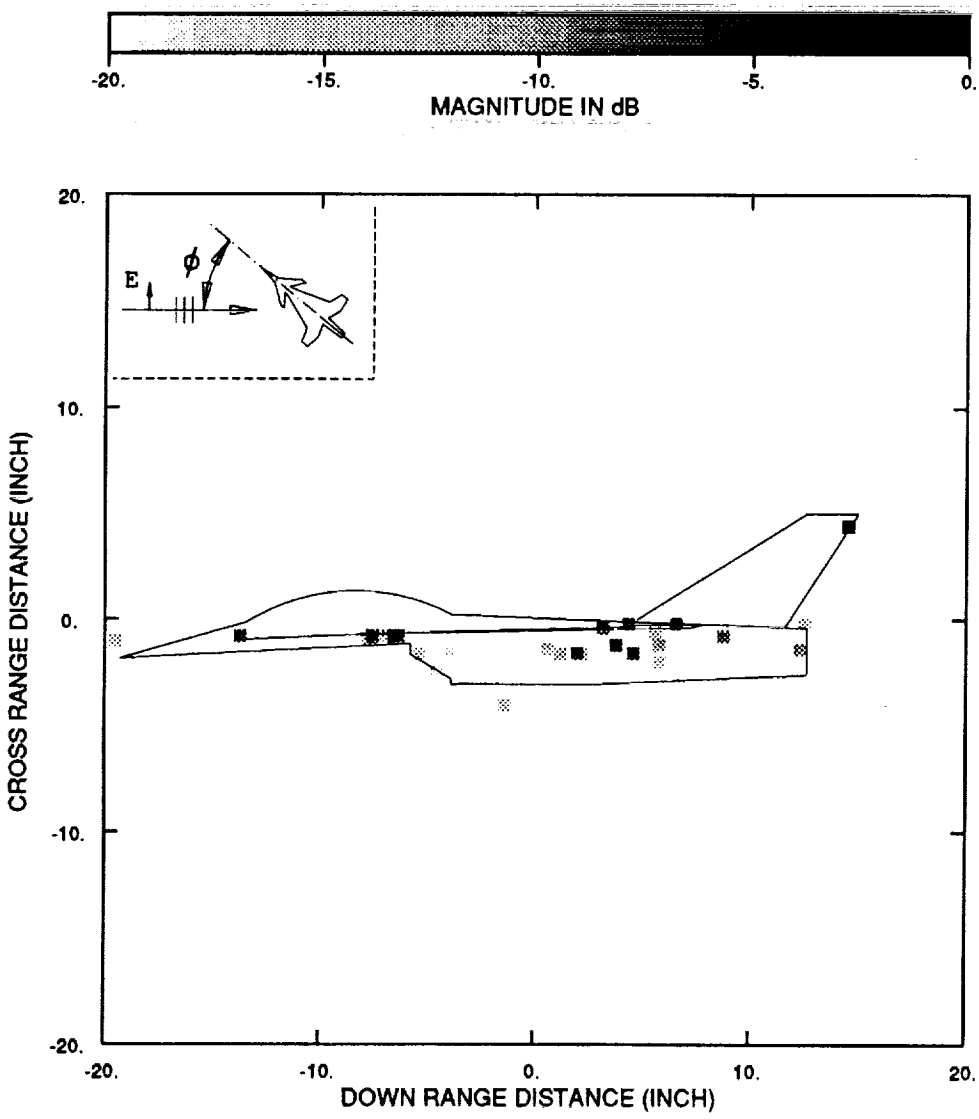

Figure 50: Side view of scattering centers resulting from ISAR measurements centered at $\phi = 40°$.

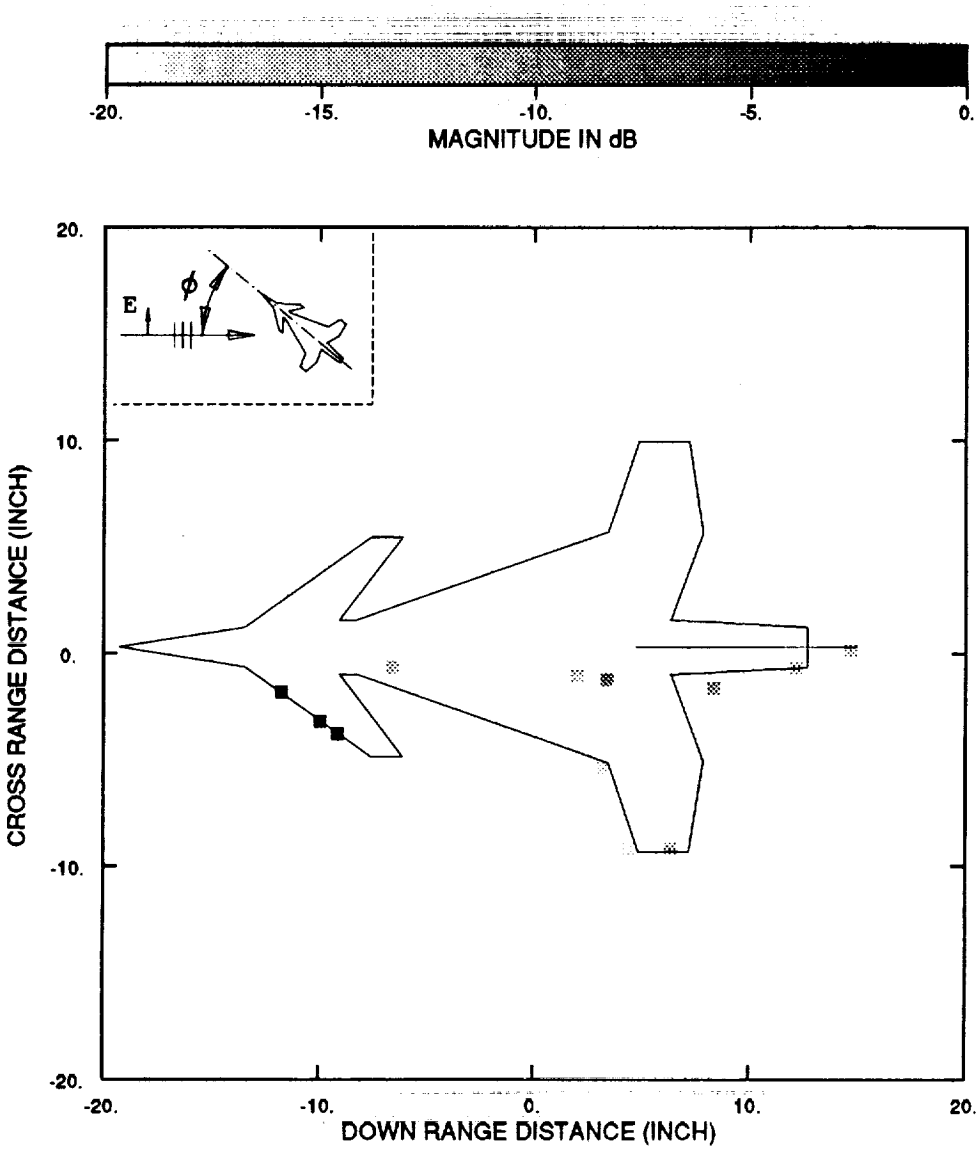

Figure 51: Top view of scattering centers resulting from ISAR measurements centered at $\phi = 50°$.

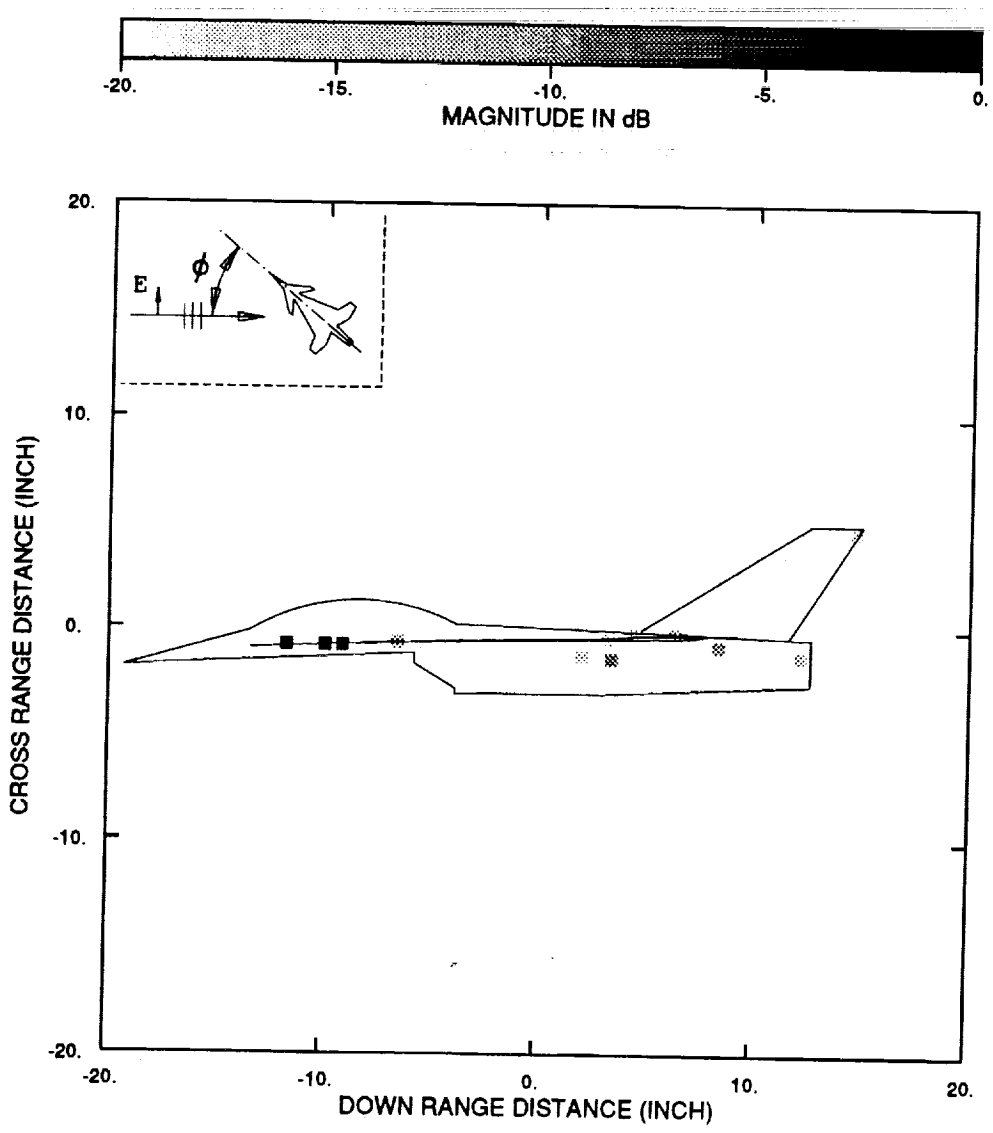

Figure 52: Side view of scattering centers resulting from ISAR measurements centered at $\phi = 50°$.

7.2 Scattering Center Location in Three Dimensions Using Target Impulse Responses

In this section, the results of applying the tracking algorithm to the aircraft of Figure 41 are presented. This aircraft presents a formidable task in terms of the tracking algorithm in that the aircraft has a relatively low radar cross section and a high density of scattering mechanisms. The high density of scattering mechanisms is a critical problem. The basic technique of locating a target's scattering centers in three dimensions was shown to work well when the scattering centers of the target do not suffer from interference. This was demonstrated in terms of the simulated target composed of corner reflectors. In Chapter 5, it was also shown that when a scattering center experiences interference, its estimated position can be highly inaccurate. This fact was demonstrated in Figures 28 and 29. The same behavior giving rise to the distortions in those figures is also present in the scattering characteristics of the aircraft. Consider Figure 53, where the down range envelope response for the aircraft from each of the three antennas with the target at 0 degrees is shown. The scattering centers resulting from these envelopes are pictured in Figures 54 and 55. Note that at this angle, several of the airplane's scattering mechanisms are located at the same down range position: the back tips of the canards, the corners of the engine inlet, and the front and side corners of the wing. The interference of these mechanisms causes their estimated positions to be distorted. Because of this distortion, it is necessary to obtain information from other look angles and to apply the tracking routine in order to obtain accurate estimated positions for the scattering centers.

Figures 56 and 57 display the scattering centers found by applying the tracking technique to measurements taken from 0 to 20 degrees every 1

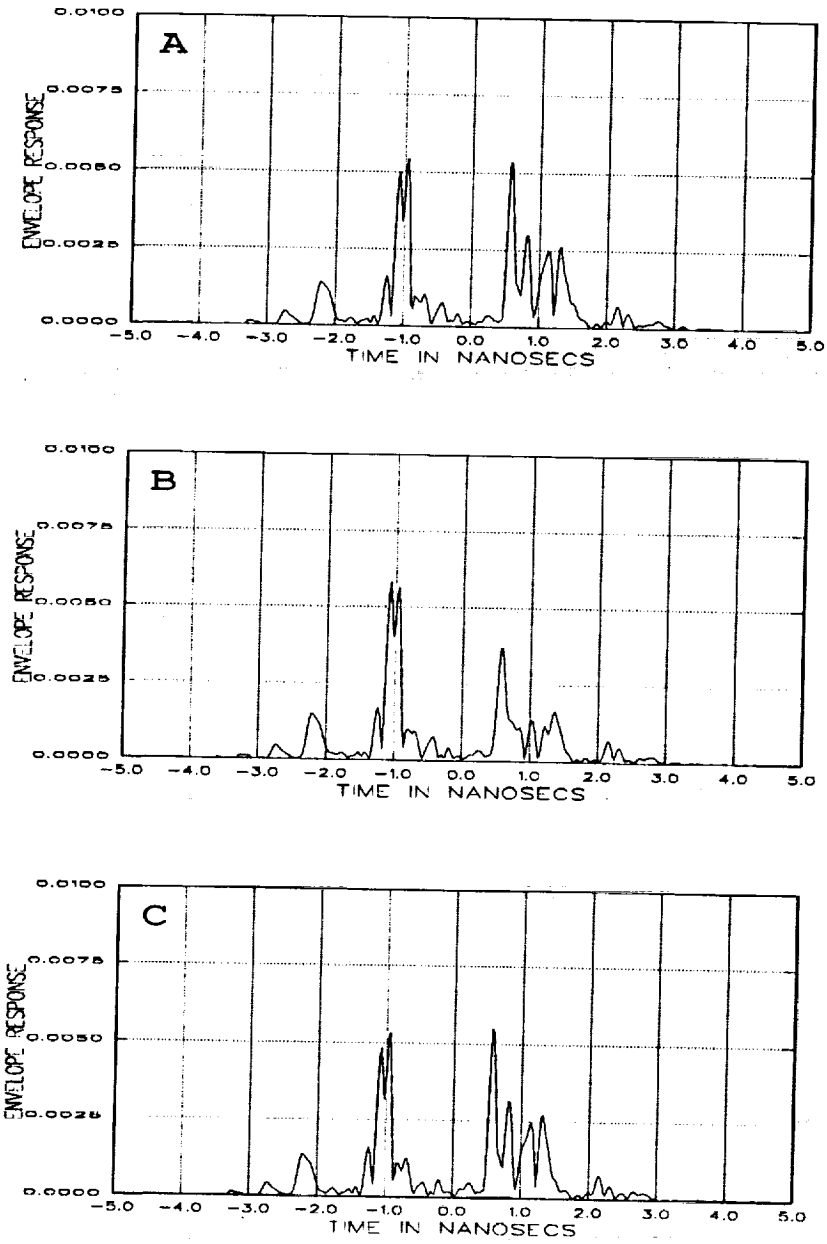

Figure 53: Envelope of each plane wave for aircraft at $\phi = 0°$.

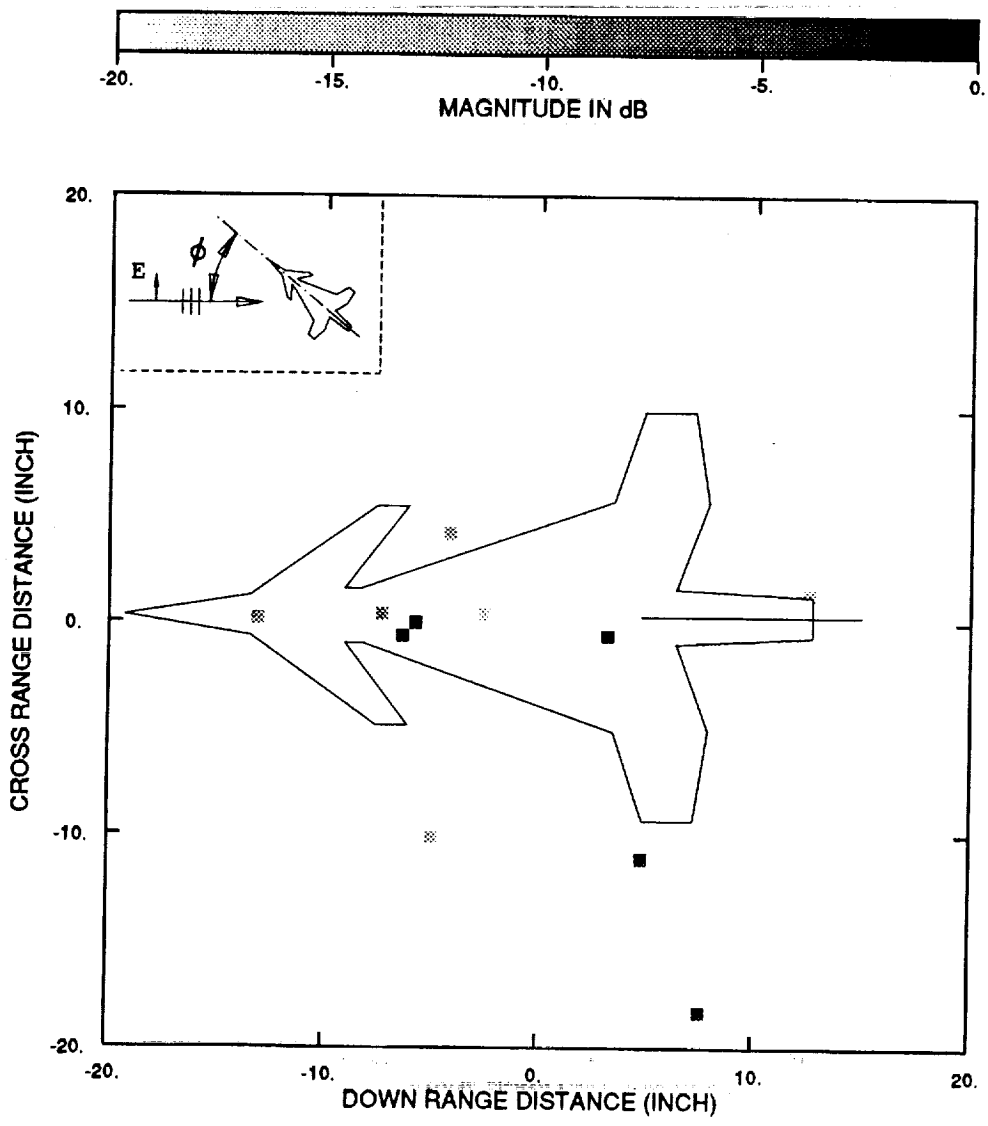

Figure 54: Top view of scattering centers resulting from measurements at $\phi = 0°$.

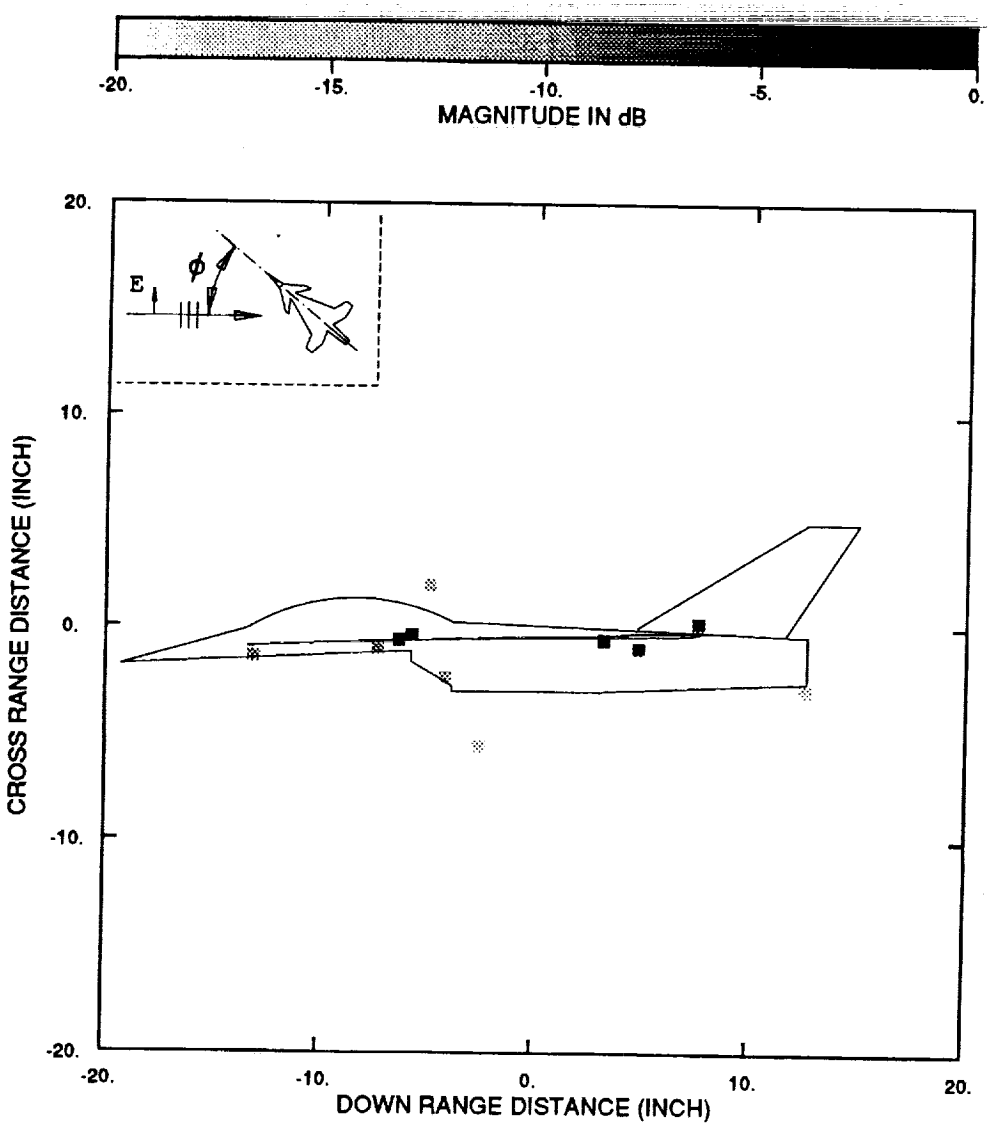

Figure 55: Side view of scattering centers resulting from measurements at $\phi = 0°$.

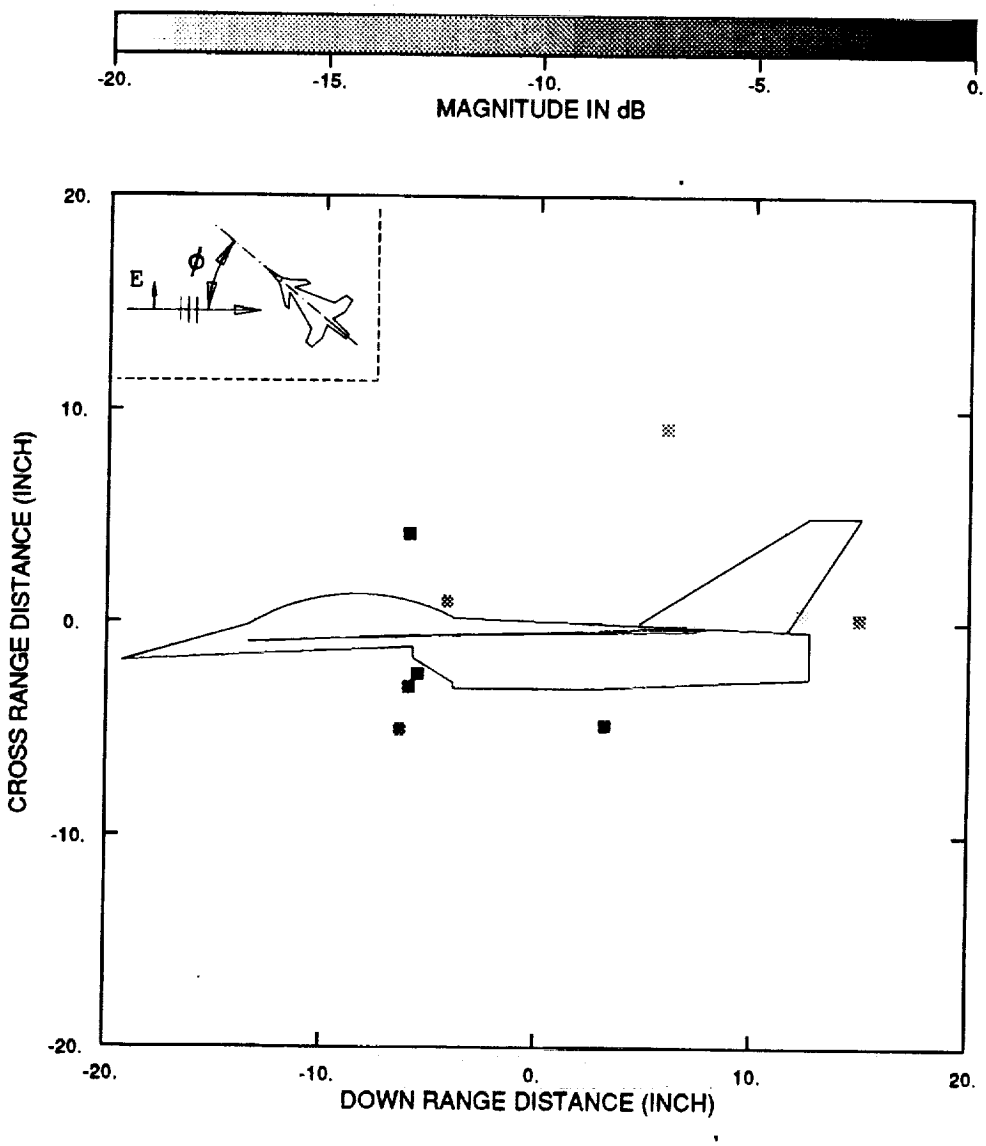

Figure 56: Top view of scattering centers resulting from tracking centered at $\phi = 10°$.

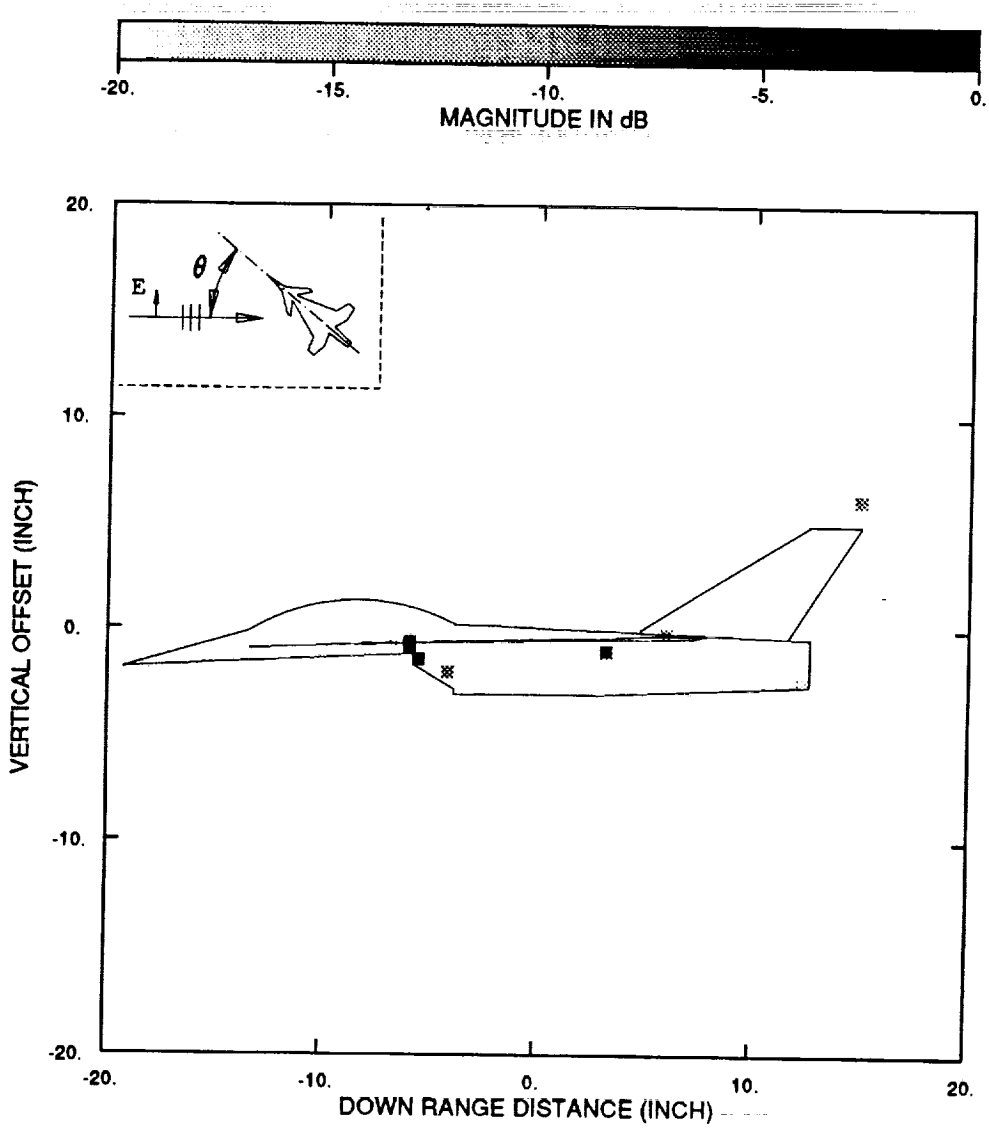

Figure 57: Side view of scattering centers resulting from tracking centered at $\phi = 10°$.

degree and evaluated at 10 degrees. The main scattering centers corresponding to the back tips of the canard, the engine inlet, the front corner of the wing, and the tail section are all identified and located accurately. The routine was able to identify these mechanisms because, after rotating the target, they separated sufficiently in the down range direction and could then be tracked. Noticeably absent from this image are the scattering centers corresponding to the back corners of the wings. The reason for this is that as the target rotates, the left wing travels in the negative down range direction, while the right wing travels in the positive down range direction. The result is that the only scattering center which emerges from interference over a significant number of look angles is the left front corner. Despite this drawback, the performance of the routine is very good considering that the target is only sampled every 1 degree as opposed to every 0.25 degrees for the ISAR measurements.

Figures 58 - 65 show the results of applying the tracking technique to measurements of the aircraft over several different angle spans. The images resulting from the tracking algorithm are presented for a look angle which is at the center of the angular sweep of the sampled data. The images are a result of applying the tracking routine to measurements taken every 1 degree over a 20 degree sweep. The frequency measurements were taken from 2-18 Ghz at 10 MHz steps. These figures demonstrate the viability of the tracking routine in identifying scattering centers in three dimensions for a complex real-world target. They also demonstrate some of the phenomena associated with the tracking routine. For example, scattering centers which have strong returns and are separated sufficiently from other mechanisms can be identified over a wide range of angles. These include the back tip of the left canard, the top corners of the engine inlet, the junction of the canard and the airplane body, the front tip of the aircraft, and the scattering off

of the rear end of the fuselage. Another characteristic evidenced in this set of plots is that some scattering centers appear and disappear due either to their angular dependence or interference from other scattering centers. An example of this is the front tip of the canard. It is a lower level scatterer and experiences interference from the back tip of the canard, the front tip of the opposite canard, and the front junction between the left canard and the aircraft. At 30 degrees though, it is free from interference long enough to be identified and located accurately.

Another aspect of the tracking procedure which makes it different from traditional imaging techniques is that it is not dominated by speculars. For example, the specular from the canard which dominates the traditional image in Figure 51 is not present at the same look angle when applying the tracking technique. This is due to the fact that for long edges the specular term appears and disappears with a relatively small change of look angle. The tracking algorithm cannot track the scattering center over a sufficient number of angles and therefore cannot confirm it as being accurately located. A slightly different case is presented when looking at the specular of the front of the wing. In this case the edge is short enough that the routine tracks the specular and the interference of the two corners at the end of the edges as one scattering mechanism.

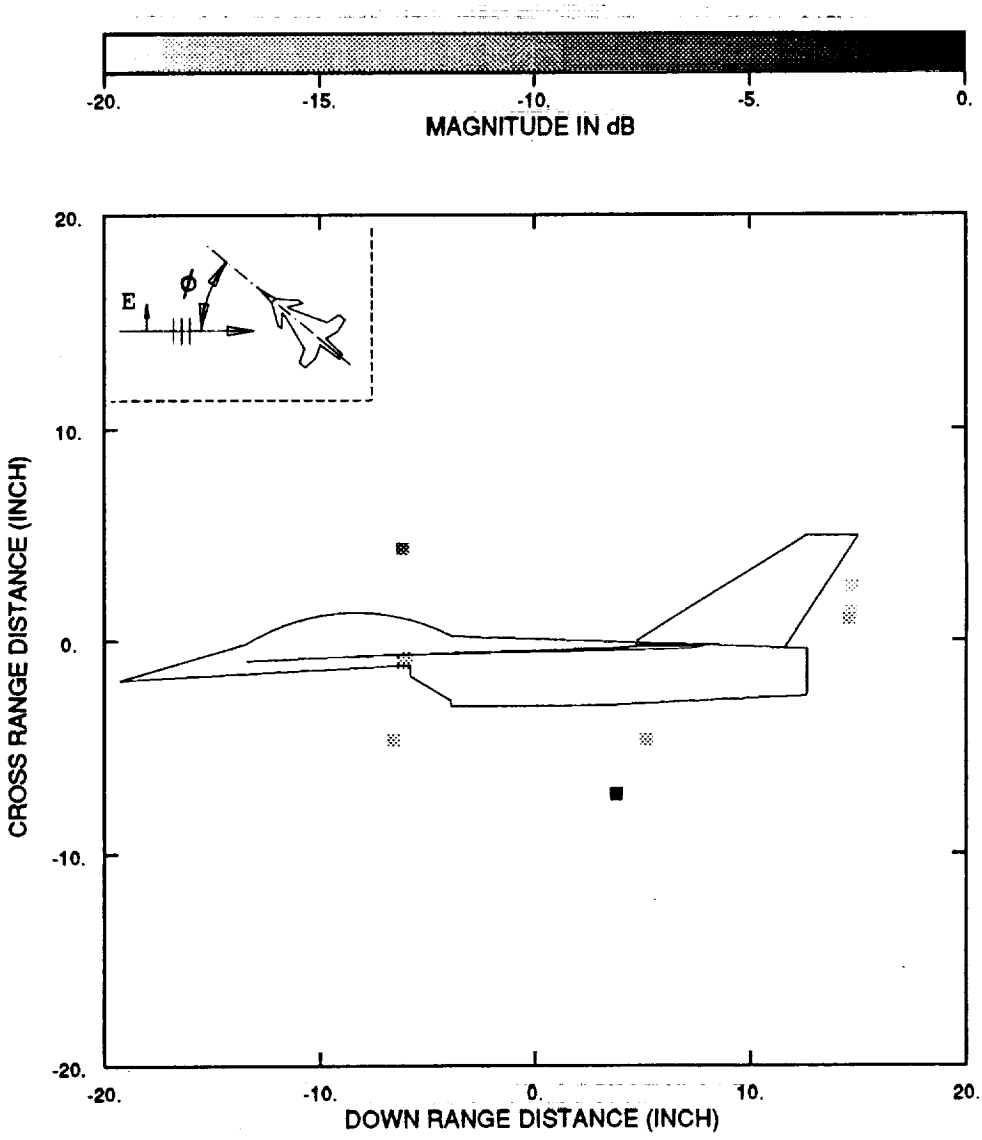

Figure 58: Top view of scattering centers resulting from tracking centered at $\phi = 20°$.

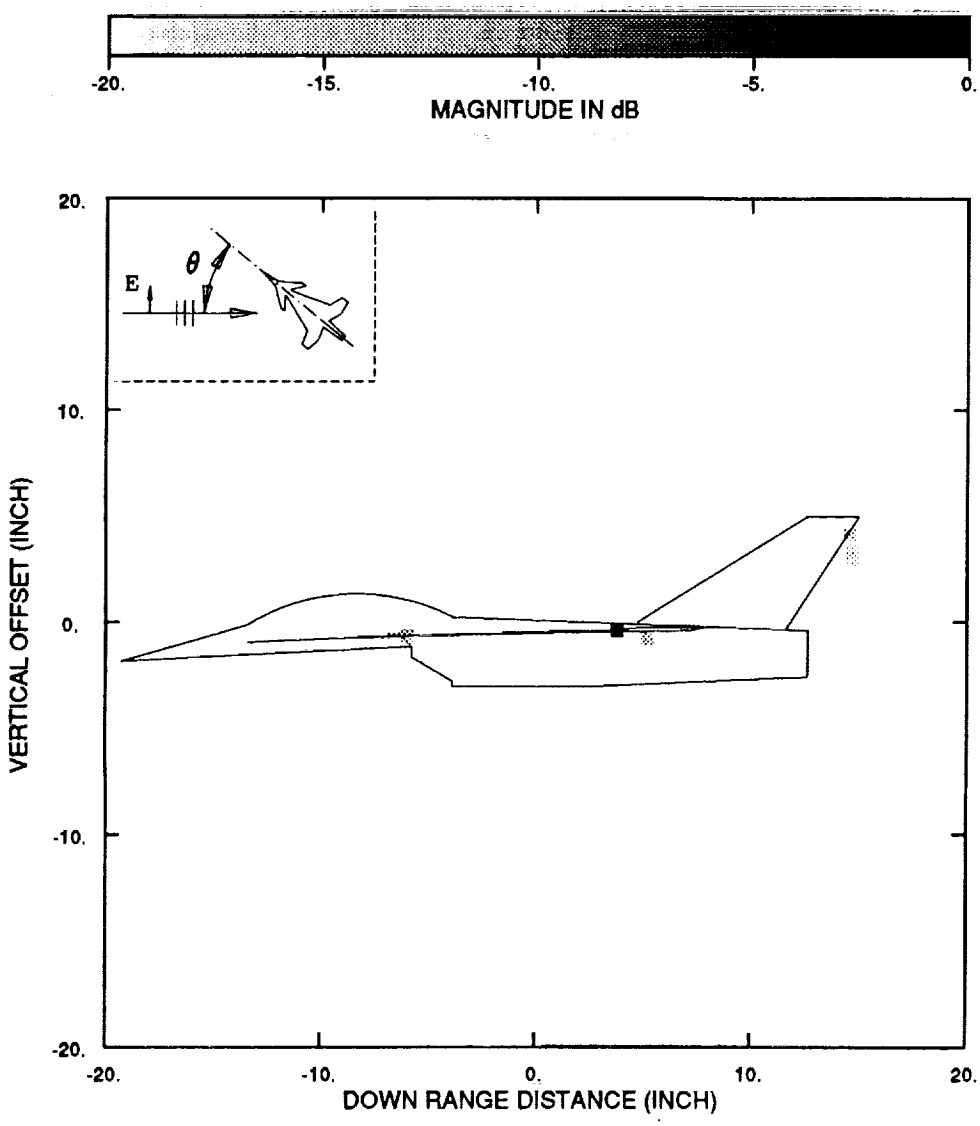

Figure 59: Side view of scattering centers resulting from tracking centered at $\phi = 20°$.

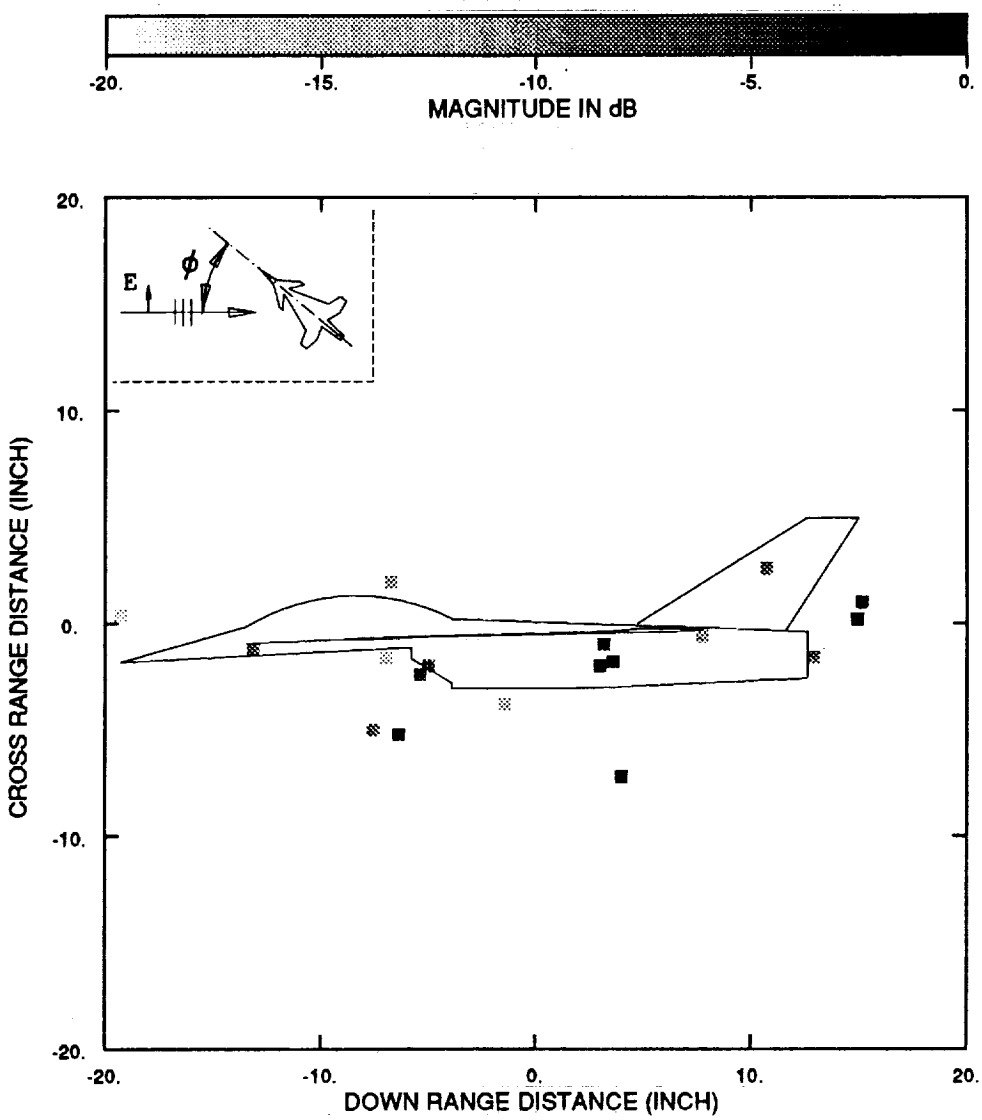

Figure 60: Top view of scattering centers resulting from tracking centered at $\phi = 30°$.

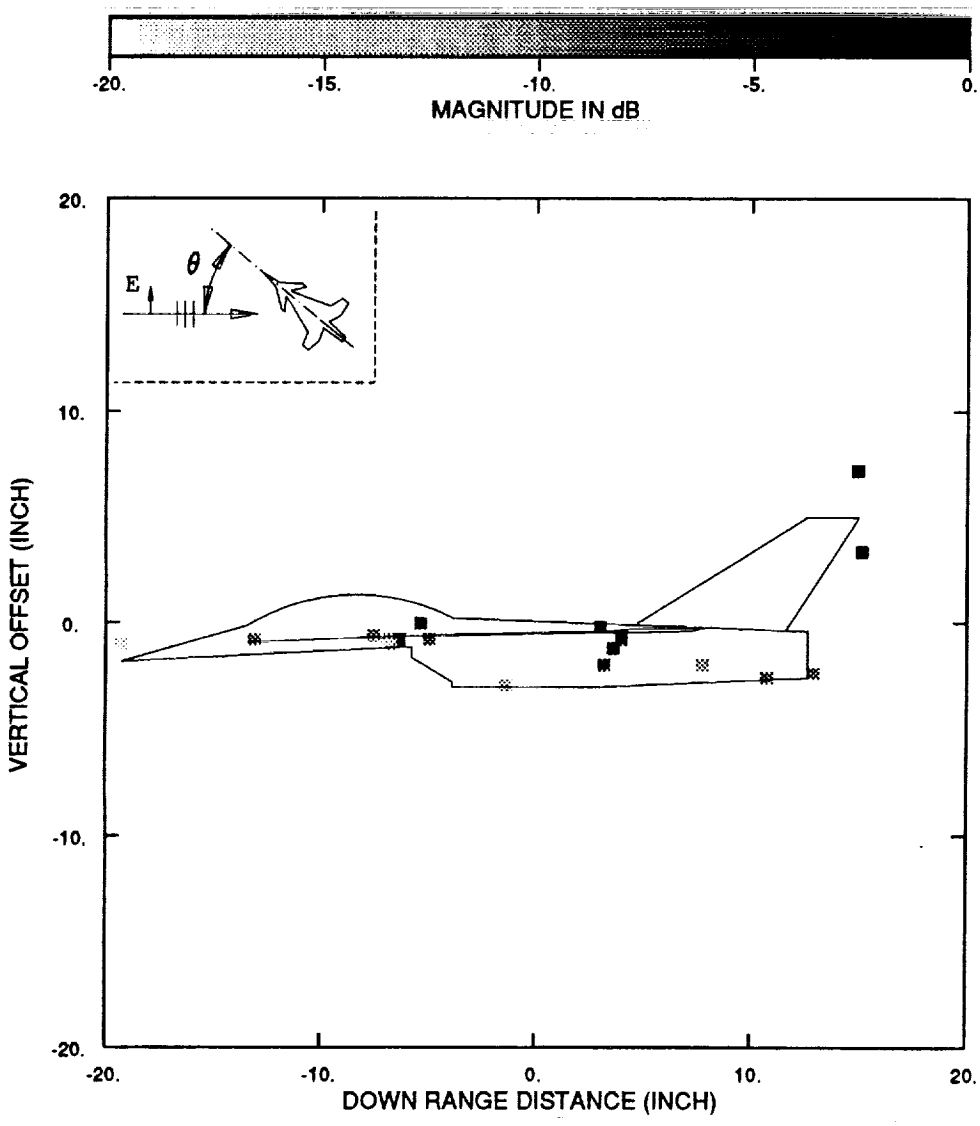

Figure 61: Side view of scattering centers resulting from tracking centered at $\phi = 30°$.

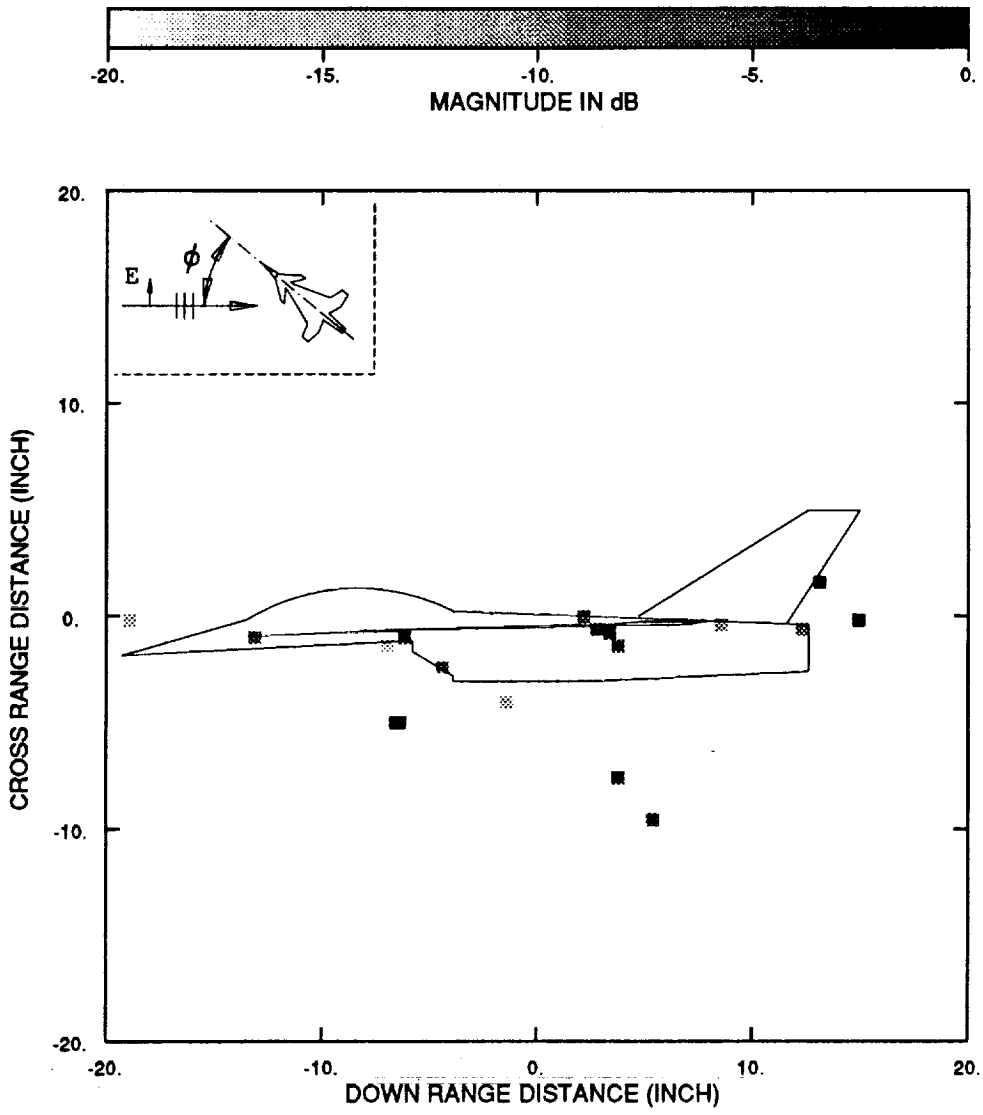

Figure 62: Top view of scattering centers resulting from tracking centered at $\phi = 40°$.

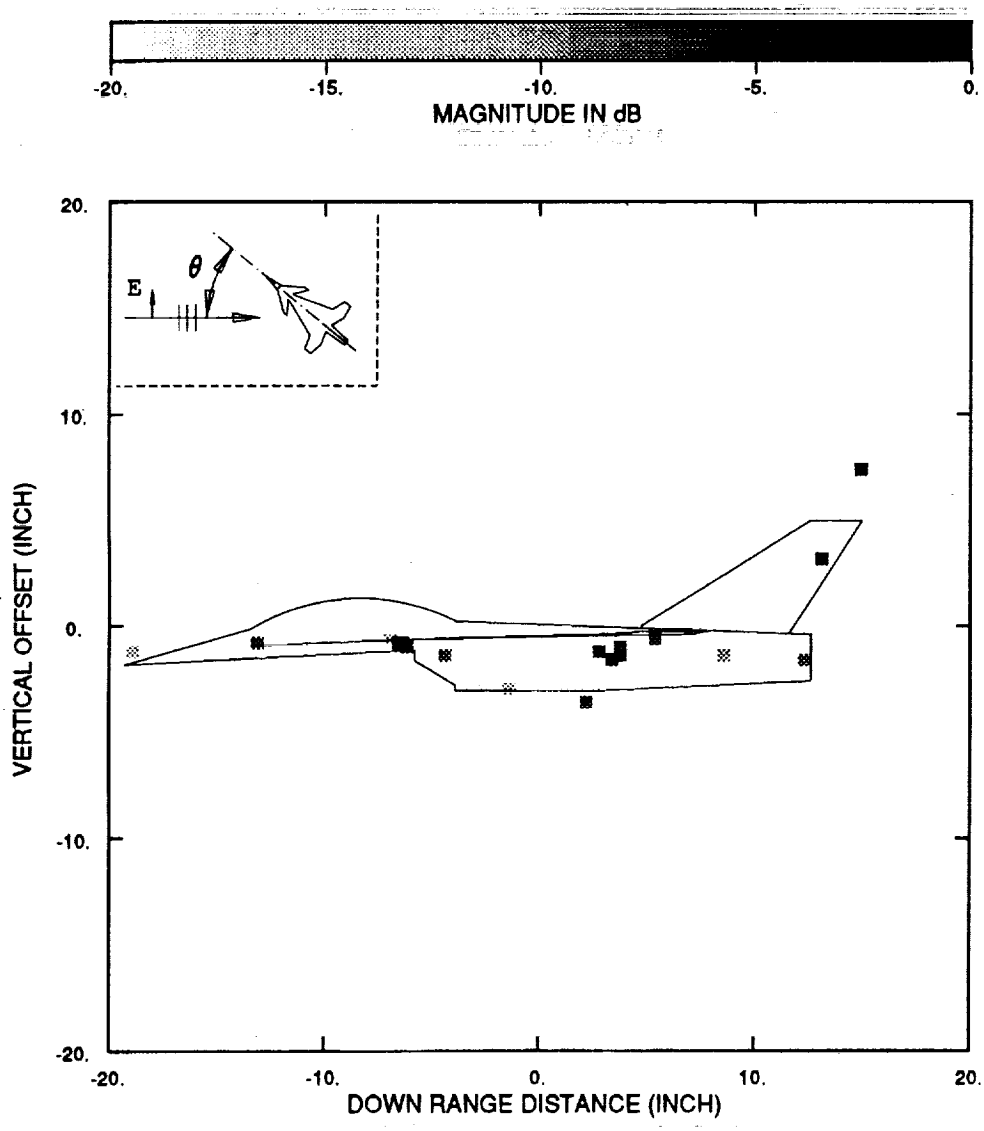

Figure 63: Side view of scattering centers resulting from tracking centered at $\phi = 40°$.

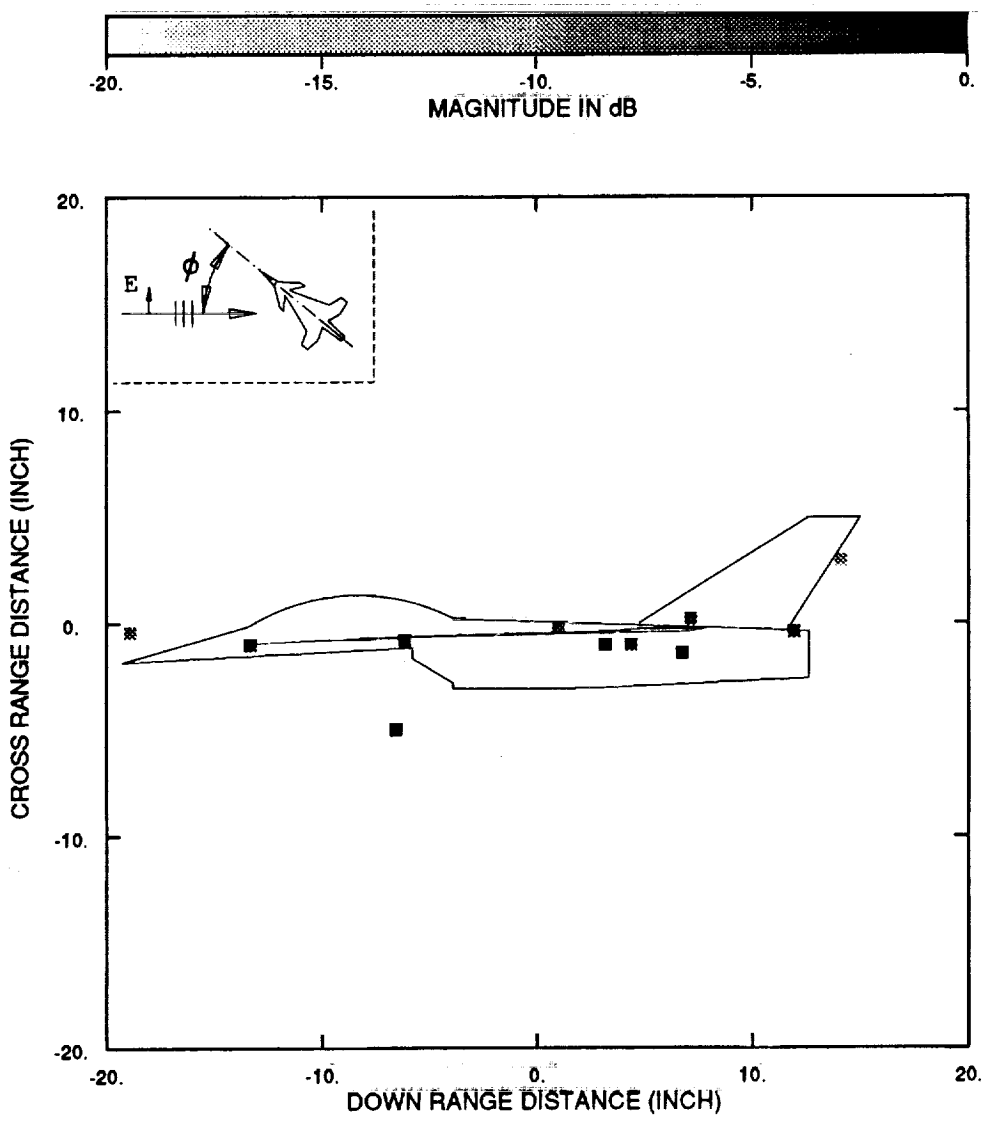

Figure 64: Top view of scattering centers resulting from tracking centered at $\phi = 50°$.

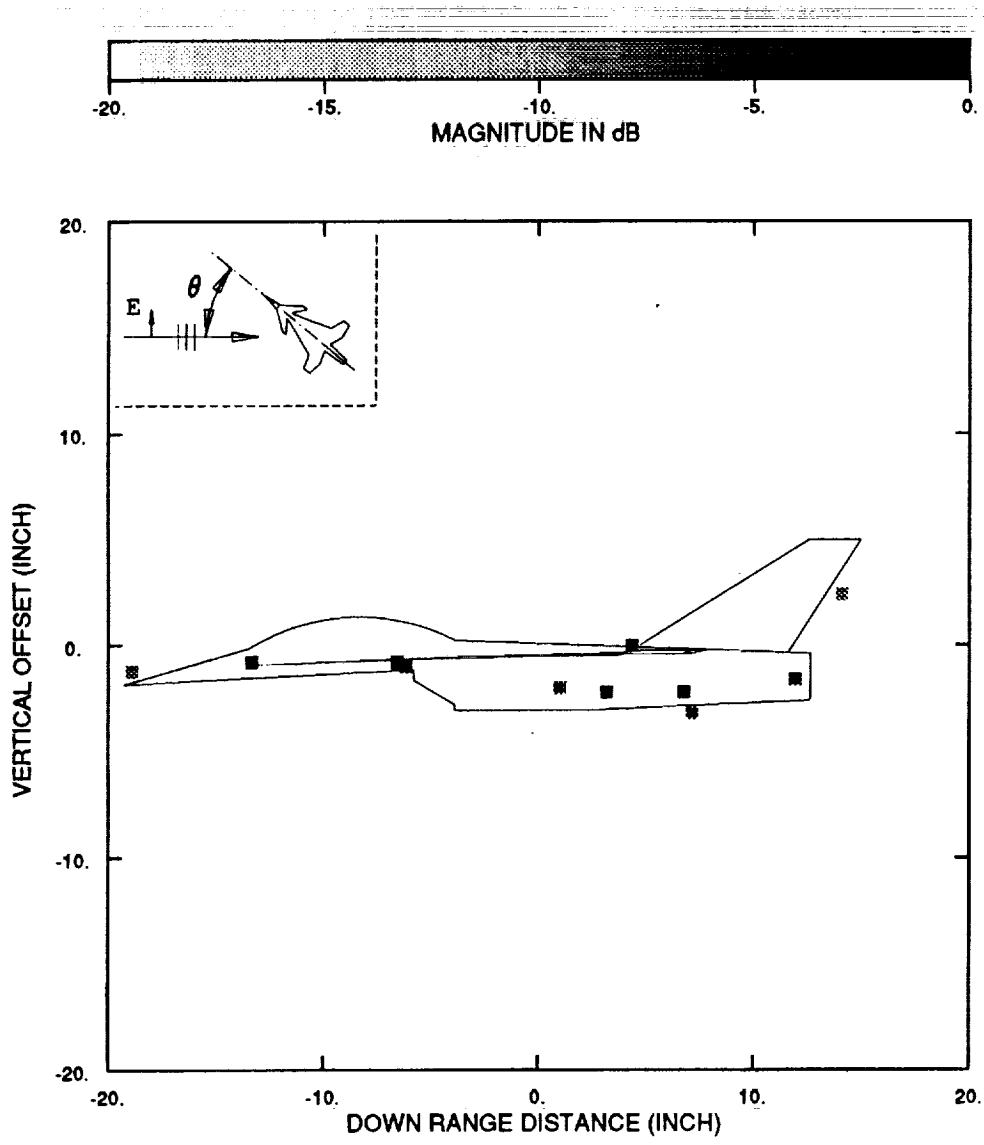

Figure 65: Side view of scattering centers resulting from tracking centered at $\phi = 50°$.

7.3 Summary and Comparison

The two techniques demonstrated in this chapter work well when appropriately applied. The technique using images generated from ISAR measurements is very accurate in estimating the down range and cross range positions of scattering centers as well as their vertical offsets. The results presented in Section 7.1 show that this technique locates the major scattering centers on the expected scattering features of the aircraft. This technique does suffer the same problems that arise in traditional imaging. These include higher order scattering terms which are located away from the source of their scattering and limited resolution between scattering mechanisms. Despite these shortcomings, two dimensional images are still a powerful RCS analysis tool and are widely used. Since two dimensional imaging is so widely used, the three dimensional imaging technique is an attractive extension of its capabilities. In addition to identifying scattering centers in three dimensions, this technique is relatively easy to implement for measurement systems which already collect ISAR measurements. The measurements from the antenna at the focus of the parabolic reflector still yield all of the information necessary for two dimensional imaging. By simply adding a second vertically offset antenna, a measurement system can produce the information necessary to identify scattering centers in three dimensions. Since this modification can be performed relatively easily, this technique offers an inexpensive way to expand the capabilities of an existing measurement system.

The results of Section 7.2 show the effectiveness of the tracking technique in identifying scattering centers in three dimensions using a limited measurement set. When compared with the results from Section 7.1, the tracking technique is shown to identify most of the dominant scattering centers on the target. The tracking technique generally does not estimate

the positions of the scattering centers as accurately as the technique incorporating the two dimensional images. But it is using a much more limited data set. The images of Section 7.2 were generated from only 21 look angles, whereas, the images of Section 7.1 required 81 look angles.

This three antenna technique is most appropriate for applications where the dominant scattering centers of a target need to be identified very quickly. This technique is used in the compact range at the OSU ElectroScience Laboratory to obtain the dominant scattering mechanisms of targets. The results are then overlaid on a pictorial image of the target. This gives a person taking measurements a physical understanding of the target's scattering characteristics and suggests areas on the target which would be of most interest for taking more extensive ISAR measurements. Another application where this technique would be appropriate is one in which the target's scattering characteristics are to be approximated by its dominant scattering mechanisms. Once a scattering mechanism on a target is identified, the response of the mechanism could be extracted from the target's impulse response at the desired look angle. The extracted mechanism is then transformed to the frequency domain and a curve is fit to the frequency response of the scattering center. The scattering center would then be described by its position in space and the coefficients of the curve fit to its frequency response. By performing this process on each of the dominant scattering centers on the target, the target can be described with a greatly reduced data set.

The targets on which this three antenna technique works best are ones in which the scattering centers on the target are separated in down range by sufficient distances. The figures of Section 7.2 demonstrate that the tracking technique works well for scattering centers which are relatively strong and separated in down range from other scattering mechanisms. These fig-

ures also show that when scattering centers suffer from interference, their positions cannot be accurately estimated. In this respect, the technique using two dimensional images is superior to the tracking technique. The two dimensional technique is capable of identifying scattering centers located at the same down range position but which are sufficiently separated in the cross range direction. This weakness of the tracking technique is diminished if the target is large relative to the resolution resulting from the measurement data. The scattering mechanisms on a larger target are generally separated by greater distances and therefore separate out more quickly with changing look angle. This fact makes the tracking technique attractive for imaging large targets. Using traditional imaging techniques, the angular step required to satisfy the Nyquist criterion for a target is inversely proportional to its size. The tracking technique though, has no such restriction on step angle. Its step angle remains constant regardless of target size. The tracking technique can therefore identify a large target's scattering centers with a greatly reduced data set, in a very short period of time.

Another difference between the two techniques is that the two dimensional images are dominated by strong speculars such as those coming from the edge of a wing or canard. The tracking technique generally cannot locate these mechanisms over a wide enough angle to confirm the accuracy of their position. It therefore identifies only those scattering centers which satisfy the definition of a point scatterer. This becomes a particular problem when coming broadside to the side of the aircraft. At these look angles, the scattering from the aircraft does not satisfy the point scatterer definition. In such situations the algorithm tracking the scattering centers would alert the calling program that a dominant scattering mechanism is present but that it cannot be located accurately. On the other hand, the tracking

technique can identify the positions of point scatterers immediately before and after the appearance of the specular. Because of the averaging characteristics of the two dimensional imaging procedure, the point scatterers which appear before and after the specular are swamped by the specular's return and cannot be identified as isolated scattering centers.

Chapter 8

Conclusion

The objective of this research has been to identify the positions of scattering centers on a target in three dimensions using swept frequency backscatter measurements resulting from plane wave illumination. This has been accomplished using two techniques: one utilized the impulse response of the target from three slightly different look angles, and the second used two dimensional target images generated from ISAR measurements taken by vertically offset antennas.

It has been shown that the method using two dimensional images generated from vertically offset antennas correctly identified the three dimensional positions of the corner reflectors. It was also shown to be effective in finding scattering centers on the generic fighter aircraft, despite the complexity of its scattering behavior. Since two dimensional imaging is widely used as a RCS analysis tool, this technique offers an easy way to expand the scattering center identification into three dimensions. The measurements from the antenna at the focus of the parabolic reflector still yield all of the information necessary for two dimensional imaging; but by simply adding a second vertically offset antenna, a measurement system can produce the information to identify scattering centers in three dimensions. This three dimensional imaging technique is therefore appropriate for any

measurement system currently used to take ISAR measurements.

The technique using three target impulse responses has been shown to work very well when imaging the simulated target composed of corner reflectors. The positions of the corner reflectors could be found from a single look angle if the scattering centers were separated sufficiently in the down range direction. If there was not sufficient separation, the estimated positions of the scattering centers became distorted. To solve this problem a technique was developed which used target measurements from several different look angles. This technique incorporated a tracking routine which follows a scattering center through several different look angles in order to confirm its existence. In addition to identifying the point scatterers represented by the corner reflectors, the tracking routine was also able to identify the dominant scattering centers on a much more complicated target, the generic fighter aircraft. Although the tracking technique generally does not estimate the positions of the scattering centers as accurately as the technique incorporating the two dimensional images, it uses a much smaller data set. In the case of the fighter aircraft, four times as many measurements are required to generate the two dimensional images.

The tracking technique is most appropriate for applications where the dominant scattering centers of a target need to be identified very quickly. This technique is used in the compact range at the OSU ElectroScience Laboratory to obtain the dominant scattering mechanisms of targets. The results are then overlaid on a pictorial image of the target. This gives a person taking measurements a physical understanding of the target's scattering characteristics and suggests areas on the target which would be of most interest for taking more extensive ISAR measurements. Another application where this technique is useful is when the scattering characteristics of a target are needed for a particular look angle. Due to the averaging

behavior of the two dimensional images, large scattering centers, such as specular terms, can swamp out lower level scattering mechanisms, even if the specular term is present only over a small number of look angles. Although the tracking technique uses information from other look angles to confirm the presence of scattering centers, the amplitudes of the scattering centers at a particular look angle are determined from the measurements at that look angle. The tracking technique may therefore present a truer picture of the target's scattering characteristics for a particular look angle than traditional imaging techniques provide.

The targets on which this technique works best are ones in which the scattering centers on the target are separated in down range by sufficient distances. In Section 7.2, the figures demonstrate that the tracking technique works well for scattering centers which are relatively strong and separated in down range from other scattering mechanisms. These figures also show that when scattering centers suffer from interference their positions cannot be accurately estimated. In this respect, the technique using two dimensional images is superior to the tracking technique. The former technique is capable of identifying scattering centers located at the same down range position but which are sufficiently separated in the cross range direction. This weakness of the tracking technique is diminished if the target is large relative to the resolution resulting from the measured data set. The scattering mechanisms on a larger target are generally separated by greater distances and therefore separate out more quickly with changing look angle. This fact makes the tracking technique attractive for imaging large targets. Using traditional imaging techniques, the angular step required to satisfy the Nyquist criterion for a target is inversely proportional to its size. The tracking technique though, has no such restriction on step angle. Its step angle remains constant regardless of target size. The tracking technique can

therefore identify a large target's scattering centers with a much reduced data set, in a very short period of time.

The area of greatest potential for future work in this general area is in the decision making process used to identify scattering centers by the tracking technique. By incorporating more "intelligence" into the tracking routine it may be possible to pick out scattering centers more reliably and extend the dynamic range of the process. A more intelligent tracking technique might be able to identify and locate scattering mechanisms which do not satisfy the definition of a point scatterer. These include specular terms from edges, edge waves, and scattering resulting from more than one reflection. In addition, it might be able to pick out features of the target such as edges, tips, flat surfaces, etc. Other areas of future work include using the tracking technique to reduce the amount of data necessary to describe a target's scattering characteristics. By identifying the positions of the major scattering centers and their frequency behavior, the amount of data necessary to describe a target's frequency response is greatly reduced. Work could also be done in using high resolution techniques to identify the down range positions of scattering centers. This would allow narrower band measurement systems to use the same tracking technique.

Appendix A

Cost Function for Inter-Peak Matching

In Chapter 5 a technique was presented which evaluated the validity of possible scattering center based on the attributes of the matches making up the scattering center. The validity of the possible scattering center was expressed quantitatively as a cost. This appendix goes into the details of determining the probability density functions required to calculate the cost of a match.

In order to compute the cost of a match one must define the conditional probability density function for each of its attributes. The probability density function for the position attribute is the simplest. In Section 5.1, it was shown that given a peak in the envelope of plane wave **A**, there existed only a limited number of possible matches to peaks in the envelope of plane wave **B**. The number of possible matches to the peak in the envelope of plane wave **A** was limited by the target's size, the location of the peak, and the configuration of the plane waves. Equation (5.1) gives the range within the envelope of plane wave **B** where a possible matching peak may be found. The conditional probability density function of Figure 66 expresses the binary behavior described above. If a peak in the envelope of plane wave **B** is within the specified range the probability of an accurate match is a finite

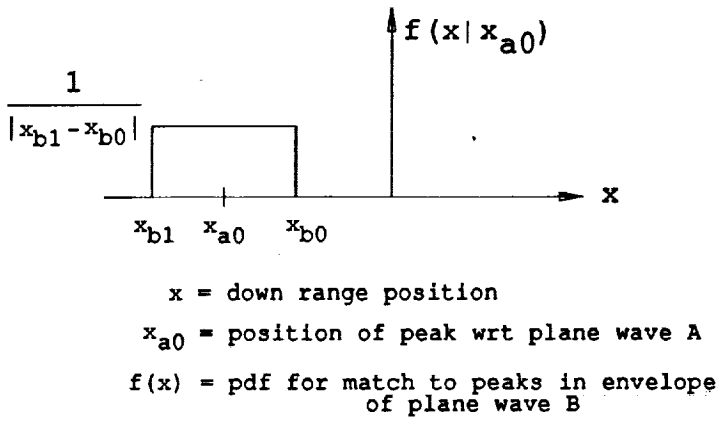

Figure 66: Probability density function for a peak from envelope B to match to a peak at x_{a0} from envelope A.

constant. Those peaks outside of the range have a probability of zero of matching to the peak in the envelope of plane wave **A**. Subsequently, they require an infinite amount of information to confirm their match and can be eliminated by thresholding.

The conditional probability density function based on relative amplitude will be the next function defined. The measurements taken for this paper were from plane waves which were separated by only a small amount in angle. It is assumed therefore that the amplitude of a scattering center should be the same in the envelopes for all three plane waves. If differences in amplitude occur they are most likely due to interference from other scattering mechanisms. Peaks of different amplitude may still correspond to the same scattering center but their estimated positions may be distorted. This results in a lower probability that the match's estimated position is accurate. These observations are incorporated in the conditional probability

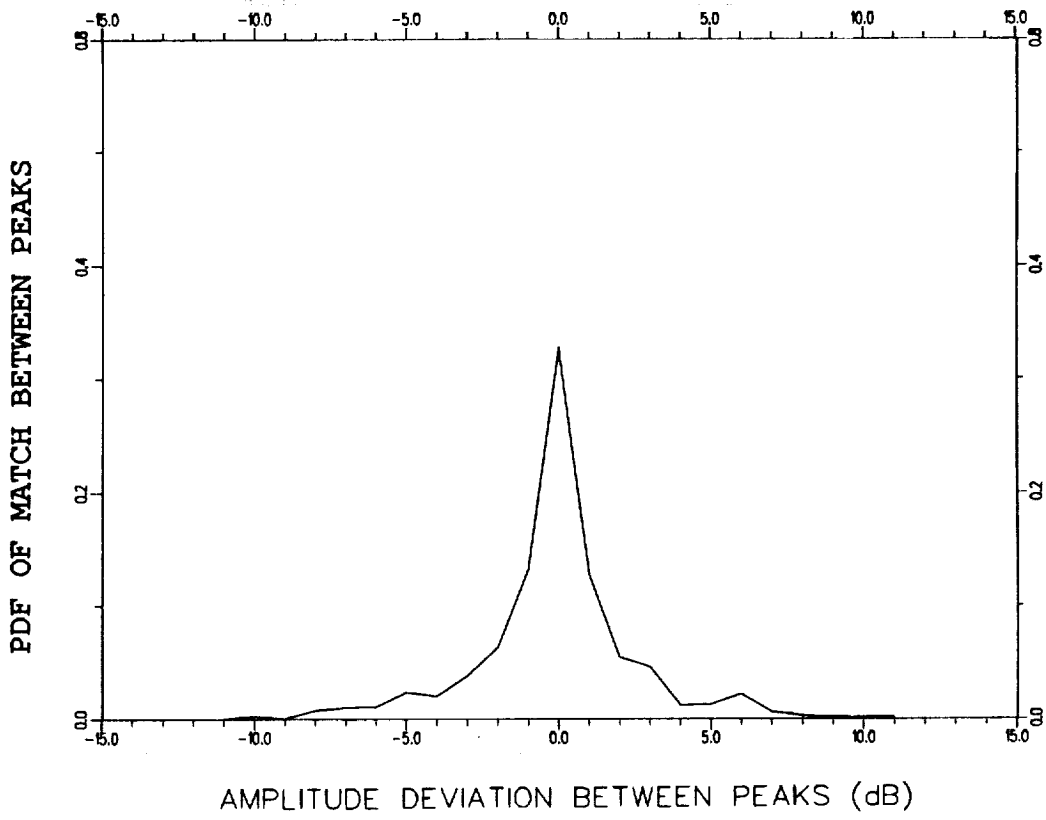

Figure 67: Probability density function of an accurate match as a function of the relative amplitude of the matched peaks.

density function of Figure 67, which was derived empirically.

The conditional probability density function which corresponds to the impact of the peak's nearest neighbors on a match's validity is different than those described above. The proximity and amplitude of a peak's neighboring peak affect the estimated down range position of a peak. The error in the down range position causes error in the estimated cross range position. It is possible that a complimentary error could exist in the matching peak, such that the cross range position defined by the match could be correct. In general though, this is impossible to determine since characteristics of the interfering scattering centers are unknown. It is therefore assumed that the error introduced by the nearest neighbors of the peaks composing the

match are independent. The conditional probability density function is therefore the product of the probabilities that the down range position of the scattering center has been estimated accurately dependent on a peak's nearest neighbor and its amplitude. These probabilities were determined from measurements made on point scatterers as they approached each other in a down range direction. The general trend was that the estimated down range position was accurate up to a certain point and then the accuracy dropped off markedly. Beyond a certain point the accuracy was bad enough that the estimated cross range involving such a peak would be highly suspect. It was also found that as the amplitude of the neighbor increased, the distance of separation required before an accurate position estimation could be made also increased.

The last attribute which has an impact on a match's cost is the number of possible matches to which a peak is a member. When a peak from plane wave **A** can match to several peaks in plane wave **B** an ambiguity is introduced as to which match is correct. The presence of multiple matches decreases the probability that any one match is correct. In the case of Figure 30 the two possible matches for each peak decreased the probability of either match being correct to $\frac{1}{2}$. A function was developed to reflect the dependence of the probability on the difference in amplitudes of the peaks involved in a multi-matching situation.

Appendix B

Tracking Procedure

A tracking procedure was introduced in Chapter 5 to identify scattering centers using measurements taken over several look angles. This appendix reviews the tracking procedure in greater detail.

The information which was collected and processed at each look angle is used to determine which possible scattering centers accurately represent actual scattering centers. The information for each look angle consists of a set of peaks, their associated attribute-value pairs, and a set of possible scattering centers. It will be helpful to symbolically represent the various sets which will be discussed. The set of peaks from the envelope of plane wave A for the n^{th} look angle is

$$\mathbf{A_n} = \{a_{(n,1)}, \cdots, a_{(n,j)}\} \qquad (B.1)$$

where j is the number of peaks in the envelope. The set of peaks for plane waves B and C can be expressed similarly. The set of possible scattering centers for the n^{th} look angle will be represented as

$$\mathbf{P_n} = \{p_{(n,1)}, \cdots, p_{(n,k)}\} \qquad (B.2)$$

where k is the number of possible scattering centers for the n^{th} look angle. A single possible scattering center is associated with a peak from each of

the three plane waves such that

$$p_{(n,l)} = \{a_{(n,l_a)}, b_{(n,l_b)}, c_{(n,l_c)}\}. \qquad (B.3)$$

where l_a, l_b, and l_c are pointers to the peaks associated with the l^{th} scattering center. The ultimate goal of the processing which follows is to associate each peak of an envelope with the actual scattering center to which it corresponds. The method used to decide which possible scattering centers are actual scattering centers is tracking.

Tracking a scattering center through several look angles is used to verify the presence of an actual scattering center. Tracking, in the strictest sense though, is not very effective when dealing with realistic targets. Two characteristics of real targets prevent identifying a scattering center at the same position over several look angles. The first is that the position of a scattering center may move as a function of the look angle. A simple example of this behavior is the specular response of a sphere. The scattering center associated with the specular response of a sphere is always located at the point on the sphere closest to the illuminating plane wave. As the look angle of the plane wave with respect to the sphere changes, the scattering center follows a circular path. The second characteristic of a realistic target which poses a problem to applying tracking, is that many realistic targets have a high density of scattering mechanisms. A target such as the one used in Chapter 7 may have many point scatterers as well as higher order scattering mechanisms in close proximity to one another. The interference caused by the scattering center's closeness in down range shifts the location of the corresponding peaks relative to their actual down range position.

Despite these problems, tracking is still an effective tool for confirming the presence of a scattering center. To accomodate the inherent inaccuracies involved when identifying the scattering centers of a realistic target, a

graduated tracking routine is used. The tracking routine consists of grouping possible scattering centers together from different look angles, verifying whether a particular grouping corresponds to an actual scattering center, and determining the position and amplitude of the scattering center at each look angle. The grouping phase of the tracking routine entails selecting possible scattering centers from different look angles which are thought to correspond to the same actual scattering center. A grouping of possible scattering centers will be called a string. A string consisting of a possible scattering center from the first, second, fifth, and seventh look angle can be expressed as the set

$$\mathbf{S_i} = \{p_{(1,i_1)}, p_{(2,i_2)}, p_{(5,i_5)}, p_{(7,i_7)}\}, \qquad (B.4)$$

where the i_n point to the appropriate scattering centers within each set of possible scattering centers.

As noted before, the positions and amplitudes of the possible scattering centers often deviate from those of the actual scattering center due to interference from other scattering mechanisms. The approach chosen to combat these problems, when grouping possible scattering centers into strings, is the setting of a series of graduated thresholds. The thresholds are applied to two steps of the grouping process. The first step in the grouping process is to select a set of possible scattering centers to be considered for grouping. This set will be a subset of all the possible scattering centers identified at each look angle. The criteria by which possible scattering centers are considered eligible for grouping is the cost of each scattering center. The first threshold is therefore a maximum cost. The set of scattering centers which are considered eligible for the first grouping are

$$\mathbf{T}_1 = \{p(i,j)\} \quad COST_{i,j} \leq \text{ cost threshold} \qquad (B.5)$$

where

$$p(i,j) \subset \mathbf{P_n}, \quad n = 1, ..., m \tag{B.6}$$

and m is the number of look angles measured. The cost of a scattering center expresses the likelihood that the calculated position of the possible scattering center is accurate. Those possible scattering centers with lowest cost should most accurately estimate the position of the actual scattering center. The estimated position of a possible scattering center which has low cost should therefore fall very close to the actual position if it is indeed free of corruption.

The next threshold to be set in the grouping process is on the allowed deviation in amplitude and position within a string. The thresholds on position and amplitude deviation should reflect the chosen cost threshold. If the threshold on cost is set low, then one would expect very small deviations in the positions and amplitudes of the scattering centers making up a string. For a low cost threshold, the thresholds on position and amplitude deviation within a string should be set low accordingly. A string produced under these criteria can be expressed as

$$\mathbf{S}_k = \{p_{(i,j)}\} \tag{B.7}$$

where

$$\begin{aligned}
\textit{Position threshold} &\geq |\textit{position}(p_{(i,j)}) - \textit{position}(p_{(k,l)})| \\
\textit{Amplitude threshold} &\geq |\textit{amplitude}(p_{(i,j)}) - \textit{amplitude}(p_{(k,l)})| \\
i &= 1, ..., m \\
k &= 1, ..., m \\
i &\neq k \\
j &= 1, ..., n_i \\
l &= 1, ..., n_k, \text{and}
\end{aligned}$$

$$p_{(i,j)}, p_{(k,l)} \subseteq \mathbf{T}_1.$$

The result of the first grouping is a set of data which includes a set of strings and possible scattering centers at each look angle. The strings resulting from the first pass through the data should be reliable estimates of the amplitudes and positions of actual scattering centers. After the first grouping though, there will be a large body of possible scattering centers which are not a part of a string. In order to include these possible scattering centers in a string, a second grouping of scattering centers must be performed. The second grouping will differ from the first grouping. In the second grouping, the thresholds defined in the last paragraph must be increased in order to include more possible scattering centers for consideration. For the second grouping, the cost threshold will be raised. The input to the second grouping includes strings as well as possible scattering centers. The possible scattering centers which are members of a string cannot be considered for membership in any other string. This requirement is stipulated because a possible scattering included in a string, under strict thresholds, is assumed to be best grouped with the members of that string rather than with strings that might be formed under less strict thresholds. This requirement implies the following relationship between the set of possible scattering centers for the second grouping and the set of strings:

$$\mathbf{S_i} \supseteq \mathbf{p_{(j,k)}} \quad \Rightarrow \quad \mathbf{T_2} \cap \mathbf{p_{(j,k)}} = \emptyset. \qquad (B.8)$$

In addition, a string can have a maximum of one possible scattering center from any given look angle. This restriction simply states that a scattering center is associated with at most one peak in the envelope of the impulse response of the target. Since there is a good chance that existing strings represent actual scattering centers, an attempt is made to first group the possible scattering centers in $\mathbf{T_2}$ which satisfy the cost threshold, with

existing strings. The possible scattering centers which fail to be grouped to an existing string are then considered for grouping with each other to create additional strings.

The result of the second grouping is again a set of data which includes a set of strings and a set of possible scattering centers. A process similar to that performed in the second grouping is performed in the third grouping. In this grouping, the same cost threshold and amplitude deviation are used as were used in the second grouping. The position deviation threshold though, is increased. The same grouping procedure is used: grouping to existing strings and then forming new strings. After the grouping process is completed, an attempt is made to merge strings which were created under the more strict position deviation threshold. Those strings which satisfy the current amplitude and position deviation thresholds are merged into one string. The fourth grouping is the same as the previous two, except that the amplitude deviation threshold is increased.

The second, third, and fourth groupings set a pattern of applying thresholds which is repeated several times. The process consists of raising the cost threshold, then raising the position deviation threshold, and finally raising the amplitude deviation threshold. This process results from observations associated with evaluating real data. It was seen that scattering centers with higher costs may still accurately estimate the position and amplitude of an actual scattering center despite their cost. In order to identify such cases, the cost thresholds were raised first without changing the thresholds for the position deviation or amplitude deviation. After those cases were accomodated, a great number of possible scattering centers were not included in a string. In order to include more scattering centers for consideration in the grouping process, the position threshold was increased. It was found that the estimated position of a scattering center was more likely to vary

from the actual position than its estimated amplitude. For this reason the amplitude requirements were raised last. This process was repeated until the maximum cost, position deviation, and amplitude deviation thresholds were reached.

Upon completing the graduated thresholding routine, one is left with a set of strings and a set of possible scattering centers which are not yet members of strings. From this information a decision must be made for each string as to whether it corresponds to an actual scattering center. The verification process for a string was discussed in Section 5.5, where it was shown that if a scattering center cannot be tracked over a wide enough angle, it may not be an actual scattering center. Rather, the possible scattering center may be a result of the distortions introduced by interference discussed earlier in Chapter 5. The second requirement for verification is that the scattering center must be present in a majority of the look angles spanning the minimum look angle. Often a string may have a number of look angles where a possible scattering has not been identified as a member of the string. These instances will be referred to as gaps. If a string has one or more large gaps within the section fulfilling the minimum angle requirement, the string may not be a scattering center but a result of a coincidence of errors. It may also represent an actual scattering center which may not be represented in a number of look angles due to distortion caused by interfering scattering mechanisms. Such distortion may lead to significant errors in the scattering center's estimated location. In either case, the scarcity of confirming information prevents the string from being considered as an actual scattering center.

If a string spans a minimum angle and has sufficiently small gaps throughout that span, then the string is verified and considered to correspond to an actual scattering center. The verification process still leaves several possible

scattering centers as either members of unverified strings or not members of strings at all. In order to increase the number of possible scattering centers which are members of a verified scattering center, two additional steps are taken. A verified string, although satisfying the requirements given above, may still have several gaps. Unless a scattering center changes drastically as a function of look angle, the scattering center still contributes to the RCS of the target even if it cannot be located. In order to account for the gaps, the actual scattering center corresponding to the verified string is rotated to the angle where the gap occurs. The down range position and magnitude of the scattering center at this look angle is determined. The down range position and magnitude of the scattering center is compared to the down range position and magnitudes of the set of peaks at the same look angle. If a peak can be found which matches the down range and magnitude specifications, and is not currently a part of a possible scattering center which is a member of a valid string, the scattering center is then considered a part of the valid string. The second way in which more possible scattering centers are included in valid strings is by trying to verify as yet unverified strings. The alternate method of verifying is to apply the gap filling technique just presented to unverified strings. If after applying the gap filling technique an unverified string fulfills the requirements for minimum angle span and maximum gap size, the string is then verified. It should be noted that a string verified in this manner may give a less reliable estimated position.

The last step in identifying scattering centers is to determine the position and amplitudes of scattering centers corresponding to verified strings. Each verified string is composed of possible scattering centers of varying costs and possible scattering centers included by the gap filling procedure. The confidence that one may place in the estimated position and amplitude of a possible scattering center is dependent on its cost. These varying de-

grees of confidence should be reflected in the position determination of the actual scattering center at each look angle. In Chapter 5 it was observed that the amplitude and position of a scattering center may change with look angle. In order to accomodate this possibility, a curve is fitted to the amplitude and position data as a function of angle. In order to accomodate the varying degrees of confidence that one has among the matches, a weighting is applied to the curve fitting routine. The possible scattering centers are weighted according to their cost. The functions include down range position as a function of angle, cross range position as a function of angle, vertical offset as a function of angle, and amplitude as a function of angle.

Bibliography

[1] N. Abramson, *Information Theory and Coding,* McGraw-Hill, New York, New York, 1963.

[2] K. L. Boyer and A. C. Kak, " Structural Stereopsis for 3-D Vision," *IEEE Transactions on Pattern Analysis and Machine Intellegence.*, vol 10, no. 2, pp. 144-166, March 1988.

[3] A. Dominek, T.J. Barnum, "The OSU Compact RCS Measurement Range," Internal Report, The Ohio State University, ElectroScience Laboratory, Columbus, Ohio, May 27, 1988.

[4] A. Dominek, "A Time Domain Technique for Mechanism Extraction,"*IEEE Transactions on Antennas and Propagation.*, vol ap-35, no 3, Mar. 1987.

[5] H. J. Scudder, " Introduction to Computer Aided Tomography," *Proceedings of the IEEE.*, vol 66, pp. 628-637, June 1978.

[6] Special issue on *Computer Tomography, Proceedings of the IEEE.*, March 1981.

[7] F. Natterer, *The Mathematics of Computerized Tomography,* John Wiley and Sons, New York, New York, 1986.

[8] Robert E. Kell, " On the Derivation of Bistatic RCS from Monostatic Measurements," *Proceedings of the IEEE.*, vol 53, no.8, pp. 983-988, August 1965.

[9] F.J. Harris, "On the Use of Windows for Harmonic Analysis with the Discrete Fourier Transform," *Proceedings of the IEEE.*, vol 66, no 1 , Jan. 1978.

[10] F.Y.S. Fok, "Space-Frequency Sampling Criteria for Electromagnetic Scattering of a Finite Object," MS Thesis, The Ohio State University, Department of Electrical Engineering, Columbus, Ohio, 1984.

[11] A. Papoulis, *The Fourier Integral and its Applications,* MacGraw-Hill Book Co., New York, New York, 1962.

[12] D.L. Mensa *High Resolution Radar Imaging,* Artech House, Inc., Dedham, MA, 1981.

[13] D.L. Mensa, S. Halevy, G. Wade, "Coherent Doppler Tomography for Microwave Imaging," *Proceedings of the IEEE.*, vol 71, pp. 254-261, February 1983.

[14] R.C. Rudduck, Y.C. Chang, "Numerical Electromagnetic Code - Reflector Antenna Code NEC-REF (version 2) Part I: User's Manual," TRN 712242-16,The Ohio State University, ElectroScience Laboratory, Columbus, Ohio, December, 1982.